Final Report EP-C-12-014 WA 3-01

Battery Durability in Electrified Vehicle Applications:

A Review of Degradation Mechanisms and Durability Testing

Prepared for Environmental Protection Agency:

Jeff Cherry
Assessment and Standards Division
2000 Traverwood Drive
Ann Arbor, Michigan, 48105

Submitted by Thomas Merichko:

FEV North America, Inc.
4554 Glenmeade Lane
Auburn Hills, MI 48326

August 7, 2015

ABSTRACT

FEV North America, Inc. has been tasked with conducting an extensive literature review on the subject of EV battery durability. The literature review is intended to inform the participants of the United Nations Economic Commission for Europe (UNECE) Electric Vehicles and the Environment Informal Working Group (EVE IWG) and their colleagues in developing and/or improving EV programs and policy, including the consideration of any GTRs needed to fill gaps related to EV regulation. All classes of Electrified Vehicles (xEVs) are considered, with these being BEVs, HEVs, and PHEVs. The review examines the electrochemical basis for the deterioration of batteries used in xEV applications along with testing activities performed on xEVs and automotive grade cells, battery packs, etc.

TABLE OF CONTENTS

LIST OF FIGURES

LIST OF TABLES

Definitions

Unless otherwise indicated, the definitions given here are derived from those given by the USABC Battery Test Procedures

cycle	The period commencing from the start of one charge/discharge to the start of the next charge/discharge where said period includes discharge time, open-circuit time, and charge time. The depth of discharge (or percentage of capacity) associated with each cycle must be specified.
cycle life	The number of cycles, each to specified discharge and charge termination criteria, such as depth-of-discharge, under a specified charge and discharge regime, that a battery can undergo before failing to meet its specified end-of-life criteria.

Introduction

We shall examine the types of electrified vehicles (xEVs), which includes Battery Electric Vehicles (BEVs) along with Hybrid Electric Vehicles (HEVs) and subset thereof, the Plug-In Hybrid Electric Vehicle (PHEV), which for the purpose of this document will be treated as a separate entity from HEVs. The design goals for xEVs drive the selection and utilization of battery technology, and as such we will also explore the various types of batteries used in xEV applications. It is also of value to note that the *end-of-life* (EOL) criteria is also driven by the xEV application.

As the basic building block of a battery pack is the cell, we shall examine the electrochemical degradation mechanisms which can occur in battery cells. As the purpose of this review is ultimately to provide recommendations for future development of testing methodologies for the evaluation of batteries in xEV applications, knowledge of the effects of various stresses on battery cells will help to relate vehicle-level tests to battery degradation and durability.

Additionally, we shall review tests conducted on xEVs which demonstrate a reduction of battery performance characteristics as well as tests conducted on battery packs along with individual cells. For each case, attention will be called to the electrochemical degradation processes at play. We shall examine, at the vehicle level, the effect of climate, battery cycling, charge and discharge regimens, drive cycles, and storage conditions, among other topics. Data from model-based tests will also be examined.

Due to the international nature of the EVE-IWG, the evaluation of standards associated with xEV testing and performance evaluation will be presented and compared.

According to several sources, HEVs and PHEVs, and BEVs are expected to sustain performance capabilities for 15 years and 10 years, or 30000 cycles and 20000 cycles, respectively [14, 15]. A direct result of such expectations is the oversizing of LiB packs when designing ESSs onboard vehicles to account for the estimated degradation [16]. Oversizing the ESS can lead to increased vehicle weight, decreased vehicle storage space, and increased costs. Therefore, it is desirable to understand the mechanisms behind battery degradation and how they affect battery lifetime.

Overview of xEV Architectures and Battery Technologies

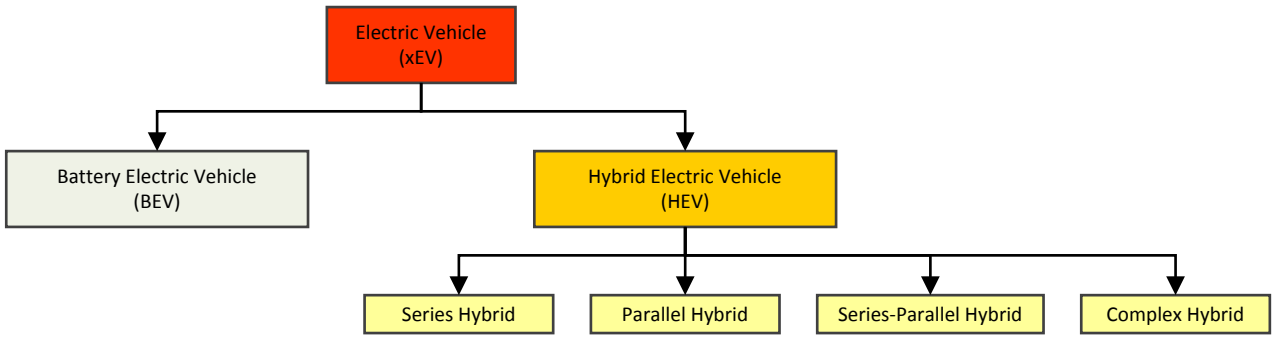

Figure 1 Classification of EVs according to the type(s) and combination of energy converters used (electric motor & ICE) [1]

Broadly speaking, electrified vehicles may be divided in to two subclasses: Battery Electric Vehicles (BEVs) or Hybrid Electric Vehicles (HEVs), with Plug-in Hybrid Electric Vehicles (PHEVs) distinguishing themselves in the sense that they are, like BEVs, capable of charging themselves from the grid. In this section we shall offer a brief overview of the architectures and operation modes used in xEVs.

Battery Electric Vehicles (BEVs)

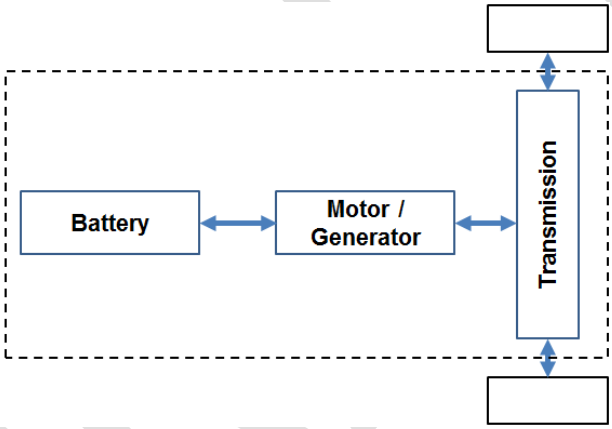

Figure 2 Basic Architecture of a BEV

BEVs (see Fig. 6) result when only the EM1 powertrain remains from the series–parallel hybrid architecture. Because the vehicle is powered only by batteries or other electrical energy sources, zero emission can be achieved. However, the high initial cost of BEVs, as well as its short driving range and long refueling time, has limited its use. Still, new BEV architectures have been proposed that use several energy sources (e.g., batteries, supercapacitors, and even reduced power fuel cells) connected to the same dc bus [27], which should eventually reduce the refueling time, expand the driving range, and drive down the price [2]

Hybrid Electric Vehicles (HEVs)

While BEVs are propelled by electric motors only, HEVs employ both ICE and electric motor in their powertrains. The way these two energy converters are combined to propel the vehicle determines to the three basic powertrain architectures: series hybrid, parallel hybrid, and series-parallel hybrid. Complex hybrid refers to architectures that cannot be classified as one of these three basic types.

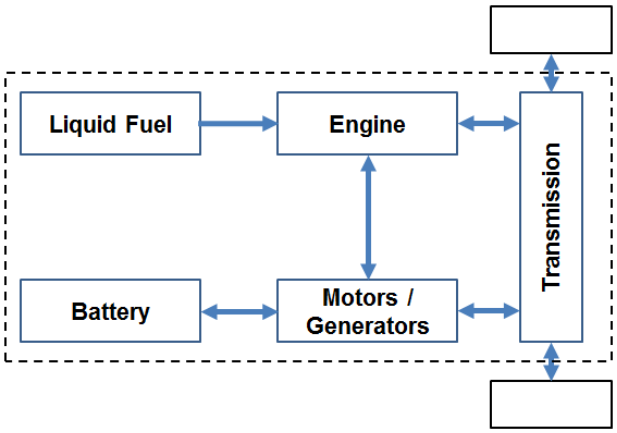

Figure 3 Basic Architecture of a Series-Parallel HEV

Series–Parallel HEVs: A Series-Parallel HEV has both Series and Parallel energy paths. As shown in figure 5, a system of motors and/or generators that sometimes includes a gearing or power split device couples allows the engine to recharge the battery. Variations on this configuration can be very complex or simple, depending on the number of motors/generators and how they are used. These configurations can be classified as Complex hybrids (such as the Toyota Prius and Ford Escape Hybrids), Split-Parallel hybrids, or Power-Split hybrids [3].

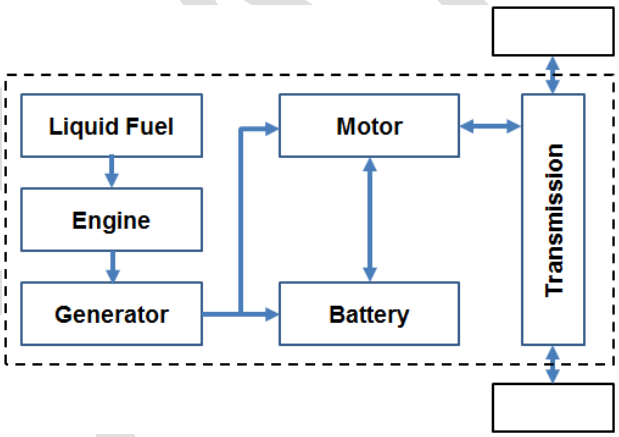

Figure 4 Basic Architecture of a Series HEV

Series HEVs: In series HEVs, all the traction power is converted from electricity, and the sum of energy from the two power sources is made in an electric node that is commonly in a dc bus. The ICE has no mechanical connection with the traction load, which means it never directly powers the vehicle. In series HEVs, the ICE mechanical output is first converted into electricity by a generator [2]. The ICE's role is charging (or recharging) the battery and supplying energy to the electric motor, always being operated at maximum efficiency [1]. The converted electricity can either charge the battery or directly go to propel the wheels via the electric motor and the transmission, thus bypassing the battery. [2]

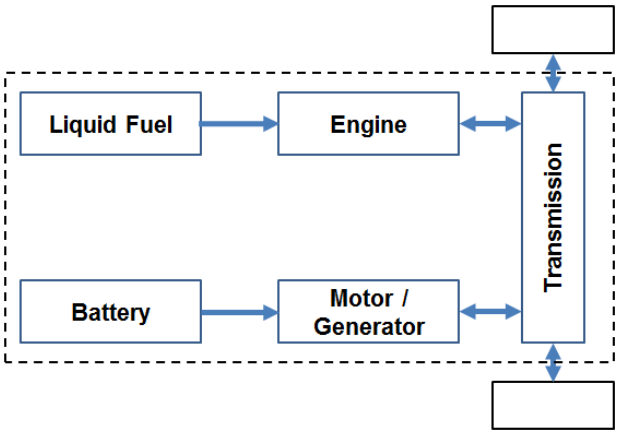

Figure 5 Basic Architecture of a Parallel HEV

Parallel HEVs: In a Parallel Hybrid, there are two parallel paths to power the wheels of the vehicle: an engine path and an electrical path, as shown in figure 4. The transmission couples the motor/generator and the engine, allowing either, or both, to power the wheels. Control of a Parallel Hybrid is much more complex that for a Series Hybrid because of the need to efficiently couple the motor/generator and engine in a way that maintains drivability and performance [3].

The previous HEV architectures provide different levels of functionality. These levels can be classified by the power ratio between the ICE and EMs.

Table 1 Different Functions of the Various HEV Architectures

	Micro HEV	Mild HEV	Full HEV	Plug-in HEV
Series-parallel			x	x
Series			x	x
Parallel	x	x	x	

1. **Micro Hybrid**: Micro hybrid vehicles use a limited-power EM as a starter alternator [30], and the ICE insures the propulsion of the vehicle. The EM helps the ICE to achieve better operations at startup. Because of the fast dynamics of EMs, micro hybrid HEVs employ a stop-and-go function, which means that the ICE can be stopped when the vehicle is at a standstill (e.g., at a traffic light). Fuel economy improvements are estimated to be in the range of 2%–10% for urban drive cycles.
2. **Mild Hybrid**: In addition to the stop-and-go function, mild hybrid vehicles have a boost function, which means that they use the EM to boost the ICE during acceleration or braking by applying a supplementary torque. The battery can also be recharged through regenerative braking. However, the electrical machine alone cannot propel the vehicle. Fuel economy improvements are estimated to be in the range of 10%–20%.
3. **Full Hybrid**: Full hybrid vehicles have a fully electric traction system, which means that the electric motor can insure the vehicle's propulsion. When such a vehicle uses this fully electric system, it becomes a "zero-emission vehicle" (ZEV). The ZEV mode can be used, for example, in urban centers. However, the propulsion of the vehicle can also be insured by the ICE or by the ICE and the EM together. Fuel economy improvements are estimated to be in the range of 20%–50%.

Plug-in Hybrid Electric Vehicles (PHEVs):

A plug-in hybrid-electric vehicle (PHEV) is a hybrid-vehicle with the ability to recharge from the grid. It is endowed with a modest electric driving range (on the order of tens of miles), and a small gasoline-powered

ICE. The PHEV offers a compromise between the drivability and affordability of the hybrid-electric vehicle (HEV), and the potential environmental and energy security benefits of the battery electric vehicle (BEV). Like the BEV, the PHEV possesses the capability to displace petroleum sourced energy with grid-sourced energy; and, like the HEV, the PHEV is not range limited in any meaningful sense [4].

Above a threshold minimum battery state-of-charge, the PHEV operates in "charge depleting" mode, in which it freely draws down the onboard battery to meet vehicle power demands. Once it reaches this minimum SOC threshold, the vehicle switches to "charge sustaining" mode (Figure 21). Charge-sustaining mode is functionally equivalent to vehicle operation in a conventional HEV. During this mode of operation, the vehicle maintains the SOC within a limited operating envelope (the overall SOC excursion during this mode of operation might be on the order of +/- 200 W-hr), using stored battery energy to optimize ICE operation, and recharging via either regenerative braking or an accessory-like loading on the engine. [4]

Battery Technologies for xEVs

Currently, xEVs are primarily using six battery technologies: lithium-nickel cobalt aluminum (NCA), lithium oxide cobalt (LCO), lithium-nickel-manganese-cobalt (NMC), lithium-manganese spinel (LMO), lithium titanate (LTO), or lithium iron phosphate (LFP). [5]

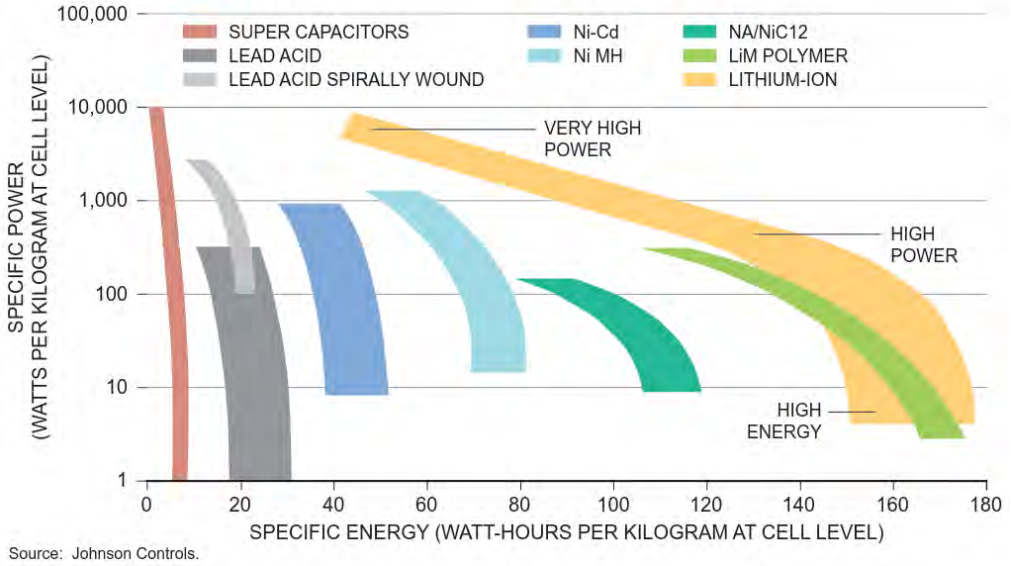

Source: Johnson Controls.

Cathode	Anode	Abbrev.	Energy Density	Power Density	Cycle Life	Safety*	Cost
Lithium Cobalt Oxide	Graphite	LCO	High	Fair	Fair	Fair	High
Nickel Cobalt Aluminum Oxide	Graphite	NCA	High	High	Fair	Fair	High
Lithium Iron Phosphate	Graphite	LFP	Low	High	High	Very good	Fair
Lithium Manganese Oxide	Graphite	LMO	High	High	Fair	Very good	Fair
Lithium Manganese Oxide Spinel	Graphite	LMO	High	High	Fair	Good	Low
Lithium Manganese Oxide Spinel Polymer	Graphite	LMO	High	High	Fair	Good	Low
Manganese Nickel Cobalt Oxide	Graphite	MNC	High	Fair	Low	Fair	High
Lithium Manganese Oxide Spinel	Lithium Titanate Oxide	LMO-LTO	Low	Low	High	Good	High
Lithium Nickel Oxide	Graphite	LNO	High	Fair	Fair	Fair	Fair
Lithium Manganese Nickel Oxide Spinel	Graphite	LMNS	High	High	Fair	Fair	Low
Lithium Manganese Nickel Oxide Spinel	Lithium Titanate Oxide	LMNS-LTO	Fair	High	High	Good	Low

* "Safety" refers to the thermochemical reactivity of the specific cathode/anode couples. Beyond this, (1) the reactivity with the electrolyte must be considered and (2) system-level safety is primarily determined by the battery management system, which includes thermal management.

Source: Shmuel De-Leon, "High Power Rechargeable Lithium Battery Market," presented at IFCBC Meeting, February 4, 2010.

Table 2 Comparison of Lithium-Ion Battery Chemistries Across a Sampling of Key Performance Attributes [6]

Vehicle OEM	Model	Battery Supplier	Drivetrain	Drivetrain Architecture	Battery Chemistry	Format	Thermal Management
Chevy (GM)	Volt	Compact Power/ LG Chem	PHEV	Series	LMO Spinel Polymer	Prismatic	Liquid
Nissan	LEAF	AESC (NEC/ Nissan)	BEV	Series	LMO	Prismatic	Air
Fisker	Karma	A123	PHEV	Series	LFP (Nanophos-phate)	Cylindrical (26650)	Liquid
Mitsubishi	"i"	GS Yuasa	BEV	Series	LMO-NMC/ Hard Carbon	Prismatic	Air
Prius (Toyota)	PHEV	PEVE	PHEV	Parallel/ Powersplit	NCA	Prismatic	Liquid
Smart (Daimler)	fortwo ED	Duetsche ACCUmotive (Daimler & Evonik)	BEV	Series	*	*	Liquid
Tesla	Model S	Panasonic Samsung	BEV	Series	LMO	Cylindrical (18650)	Liquid
Volvo	C30 EV	Enerdel/Ener1	BEV	Series	LMO-NMC/Hard Carbon	Prismatic	Air
BMW	ActiveE	S8 LI Motive (BMW, Bosch, Samsung)	BEV	Series	NMC	Prismatic	Liquid
Toyota	Rav4 EV	PEVE	BEV	Series	LMO Spinel Polymer	Cylindrical (18650)	Liquid
Scion (Toyota)	IQ-EV	PEVE	BEV	Series	LMO Spinel Polymer	Prismatic	Liquid
Ford	Focus	Compact Power/ LG Chem	BEV	Series	LMO Spinel Polymer	Prismatic	Liquid
Honda	Fit EV	GS Yuasa	BEV	Series	LMO-NMC/ Hard Carbon	Prismatic	Liquid
Coda Automotive	CODA	Lishen/LIO Energy Systems	BEV	Series	LFP	Prismatic	Liquid
Ford	C-Max Energi	Compact Power/ LG Chem	PHEV	Parallel/ Powersplit	LMO Spinel Polymer	Prismatic	Liquid
Fiat	500 EV	*	BEV	Series	*	*	*
Chevy (GM)	Spark EV	A123	BEV	Series	LFP	Prismatic	Liquid
Fisker	Nina	*	PHEV	Series	*	*	*
Honda	Accord	GS Yuasa	PHEV	Parallel	LMO-NMC/ Hard Carbon	Prismatic	Liquid
Tesla	Model X	Panasonic Samsung	EV	Series	LMO	Cylindrical (18650)	Liquid
BMW	I3	SB LI Motive (BMW, Bosch, Samsung)	(1) BEV (2) PHEV	Series	NMC	Prismatic	Liquid
BMW	I8	SB LI Motive (BMW, Bosch, Samsung)	PHEV	Series	NMC	Prismatic	Liquid
Ford	Transit Connect	Johnson Controls	BEV	Series	NCA	Cylindrical	Liquid
Azure	Balance	Johnson Controls	PHEV	Parallel	NCA	Cylindrical	Liquid

* Unknown or not available.
Note: Data current as of February 2012.

Table 3 Representative Subset of Battery Chemistries Considered by Current Automobile Manufacturers [6]

Positive/negative electrode material	Nominal cell voltage [V]	Specific capacity Positive/negative [mAh/g]

$LiCoO_2$ / graphite	3.7	120 / 370
$LiMn_2O_4$ (LMO) / graphite	3.7	100 / 370
$LiNiO_2$ / graphite	3.7	170 / 370
$LiFePO_4$ (LFP) / graphite	3.3	150-160 / 370
$LiCoNiMnO_2$ (NMC) / graphite	3.7	130-160 / 370
$LiNiMnCoO_2$ / graphite	3.7	200 / 370
$LiNiCoAlO_2$ / graphite	3.7	180 / 370
Graphite / $LiTiO_2$ (LTO)	2.2	175 / 160

Nickel-metal-hydride (NiMH) batteries are based on the release and absorption of hydrogen (OH-) by a nickel oxide anode and a metal hydride cathode [25]. In the past NiMH batteries were considered to be a good interim solution for BEVs, as lithium-ion batteries showed important safety problems [23,26]. However, with a specific energy of 50-70 Wh/kg they cannot deliver the specific energy of 150-200 Wh/kg demanded for BEVs [27]. Also, the high share of nickel in NiMH batteries (7-8 kg/kWh) might limit future cost reductions due to high nickel prices. [23,28,29]. Therefore, NiMH batteries are not seen as a serious candidate for large scale application in battery electric cars [29-31]. [7]

Lithium-ion (Li-ion) batteries represent the largest share of commercial batteries for BEV purposes. At present, these batteries provide commercial battery electric cars with a range of around 150 km [32-34]. Li-ion batteries have electrodes that intercalate lithium, i.e. the electrode materials are a host structure for lithium ions [35,36]. A range of cathode materials is being used, with varying strengths and weaknesses [2]. In all cases, however, further development of the technology is needed to improve performance levels as well as to decrease costs (700-1200 $/kWh), while safety is guaranteed [9,10,37,38,E. Kelder, personal communication, July 7, 2010]. Important aspects are the specific energy, which has now reached levels up to 125 Wh/kg, battery degradation and power capacity decline at low ambient temperatures [9,E. Kelder, personal communication, July 7, 2010].

High temperature or sodium-beta batteries are based on sodium ion transport between the cathode and anode. There are two variants: the sodium-sulfur (NaS) and ZEBRA battery. Both batteries have an anode that consists of molten sodium [25]. The NaS battery has a molten sulfur cathode, the ZEBRA battery has a transition metal halide cathode. The metal is either nickel or iron. The use of nickel chloride (Sodium-Nickel-Chloride battery) is the most common option [20]. To attain good ionic conductivity of the ceramic electrolyte, the internal operating temperature of these batteries lays between 300 and 350ºC [20]. Because of this temperature, application of ZEBRA batteries is currently only considered to be an option when they are used frequently, like in for example commercial and public transport vehicles [39]. The specific energy (115 Wh/kg) approaches that of Li-ion batteries, but the specific power has to be drastically improved from 180 to 400 W/kg [8,9]. Current costs are relatively low at a level of 600 $/kWh, but still substantially higher than the demanded 100-250 $/kWh [8,40]. NaS batteries are commercially available for stationary applications, but do not appear to be suitable for BEVs because of fundamental safety issues; damage to the ceramic electrolyte can lead to fire and explosion [20].

Lithium Metal Polymer (LMP) batteries are closely related to Li-ion batteries. Metallic lithium is applied instead of a lithium intercalation anode material; on charge, lithium ions migrate to the negative electrode and undergo a reduction reaction by which metallic lithium is formed [21]. The use of metallic lithium should have a positive effect on the specific energy. However, at a level of 100 Wh/kg, batteries that are to be used in electric cars show no performance advantage (yet) compared to Li-ion batteries. Their specific power (150-200 W/kg) lags behind, and LMP batteries do not seem to meet a cycle life of 1,000 cycles currently [28,41,42].

Also other lithium based battery technologies undergo research and development activities. Lithium-sulfur (Li-S) batteries have a sulfur cathode in which sulfur is typically paired with carbon [43]. For the anode, metallic lithium as well as other materials can be used [44]. In lithium-air (Li-air) batteries, lithium is applied as anode material and oxygen from ambient air acts as cathode material. Demonstrated specific energy levels at cell level are 350 and 260 Wh/kg for lithium-sulfur and lithium-air batteries respectively, compared to about 150 Wh/kg for Li-ion [9,45-48].
However, other aspects like specific power, efficiency, and lifetime need more attention [9,44,49-54].
Next to lithium, other materials like zinc, aluminum and iron can be used as anode material in metal-air batteries. Of these concepts, zinc-air (Zn-air) batteries get most attention. Their stage of development is significantly ahead of other types, and it is believed that they could reach the cost levels required for BEVs [9,36,55]. For BEV purposes, a zinc-air flow battery is being developed by ReVolt; the anode is a liquid zinc slurry which flows through tubes that function as air cathode [55].

Aluminum-air and iron-air technologies were widely considered in the past, but interest declined as interest in and expectations of other battery types grew [36].

Conversion, organic, nickel-lithium and lithium-copper batteries are all based on the migration of lithium ions. In conversion batteries, conversion instead of intercalation takes place; a new lithium-oxide matrix is formed in which metallic particles are embedded [37,56]. The organic lithium battery is made from organic materials [56]. The nickel-lithium battery consists of a metallic lithium anode and a nickel hydroxide cathode [57]. In the lithium-copper battery, a metallic copper cathode is applied [58].

Because of the high operating temperature of current sodium-ion batteries, research also focuses on developing ambient temperature sodium-ion batteries, i.e. batteries that can operate at room temperature [18,20]. Magnesium-ion batteries are based on transport of magnesium ions between the electrodes [59]. The all-electron battery is a concept in which electrons are used instead of ions to store energy [60,61].

Conversion, magnesium-ion and all-electron batteries are believed to have the potential to attain higher specific energy levels compared to state-of-the-art Li-ion batteries [18,61,62]. In the personal view of Tarascon [18], organic lithium and ambient temperature sodium-ion batteries can reach specific energy levels comparable to present Li-ion batteries. The reduced use of non-renewable resources in the first battery type, and the safety of the latter, together with the abundance of low cost sodium, are considered to be great virtues [18,20,63]. [7]

Lithium ion batteries [8]

Lithium-ion batteries are secondary cells typically constructed with a lithium metal oxide positive electrode, carbon negative electrode, and an organic electrolyte with lithium salts. Here, we focus primarily on batteries with a LiCoO2 cathode and graphite anode, yielding a nominal cell voltage of 3.7V. We also study lithium-ion cells with a LiCoO2-nickel manganese cobalt oxide composite cathode, which similarly has a nominal voltage of 3.7V. The electrolyte/anode interface is inherently unstable, but the electrolyte decomposes to form a passivating solid electrolyte interphase (SEI) layer which conducts ions but limits further degradation [88]. The battery is charged and discharged following an intercalation process in which lithium is inserted into the graphite electrode on charging and extracted on discharging and inserted into the positive electrode.

Lithium-ion capacity fade ranges from approximately 12-24% after 500 cycles [93]. Different processes contribute to aging in the anode and cathode in lithium-ion cells. Anode degradation occurs primarily at the surface [104]. Although the SEI plays an important role in protecting the graphite anode and electrolyte from further degradation, decomposition of the electrolyte continues slowly during cycling and parasitic consumption of lithium by the growing SEI decreases the amount of cyclable lithium in the system. SEI growth increases

impedance both because of increased thickness and loss of contact. The SEI can also reduce the surface area of available active material in the electrode, reducing capacity. SEI growth and gas evolution are accelerated by high temperatures and high SOC [13, 104]. Additional degradation mechanisms include plating of lithium on the anode surface induced by low temperatures and high rates [13]; degradation of the current collector caused by low SOC and overdischarge; binder decomposition at high SOC and high temperature; and solvent co-intercalation, which further passivates some of the active material and can led to mechanical stresses in the electrode [104]. Changes in anode volume during charge and discharge, which are greatest during high DOD cycling, can also result in mechanical stress which may lead to contact loss in the electrode or with the current collector [14, 104].

Like in the anode, volumetric changes in the cathode during cycling increase stress and can result in micro-cracking and contact loss within the electrode and with the current collector. Mechanical stress may be increased by phase changes in the electrode. High voltages can cause slight dissolution of the LixCoO2 electrode as well as increase interfacial impedance [104]. Surface films may grow on the cathode surface due to side reactions, including electrolyte decomposition and gas evolution.

Nickel Metal Hydride batteries [8]

NiMH batteries are composed of a nickel oxyhydroxide positive electrode and a rare earth-based metal hydride alloy negative electrode, which absorbs hydrogen during charge, mediated by an alkaline electrolyte. The nominal operating voltage is about 1.2 V. NiMH batteries suffer from relatively high self-discharge, with the effect strongest immediately after full charge [92]. While some of this capacity can be recovered, storage of NiMH batteries for a long period causes some irreversible capacity loss as well. Self-discharge can result from loss of active material in the positive electrode, degradation of the separator, and migration of metal ions to the opposite electrode, some of which is irreversible [92].

NiMH can typically withstand over 500 cycles before reaching 80% capacity. Aging is accelerated by high temperature, overcharge and overdischarge, high charge and discharge rates, and deep discharge [89]. Positive electrode damage is reported to result from mechanical stresses induced by volumetric changes during charge, which can cause a loss of connectivity between particles; overcharge magnifies this effect [85]. The negative electrode degrades due to corrosion during cycling [60]. Impedance growth due to loss of electrolyte to either gassing or corrosion on the negative electrode contributes to NiMH power fade [60]; this effect also is accelerated in overcharge conditions.

Charging strategies for NiMH cells include using high current at the beginning of charging to speed up the charging process and increase efficiency [52] and incorporating a discharge pulse to reduce overpotential [31]. Zhang et al. has also found that pulse charging reduced pressure and overpotential in NiMH cells and increased cycle life; 5s pulses followed by 1s rest showed better results than longer pulses [111].

Lithium iron phosphate batteries [8]

Lithium iron phosphate batteries are a type of lithium-ion battery with a $LiFePO_4$ cathode and, typically, a graphite anode and organic electrolyte, yielding a nominal cell voltage of 3.2V. While their volumetric energy density is lower than their LCO counterparts, they are remarkable for their long lifetimes, typically greater than 1000 cycles.

Degradation in lithium iron phosphate batteries appears to primarily be a function of loss of cyclable lithium [36, 83] and some loss of active material in the graphite anode [68, 83]; the cathode has not been found to contribute much to capacity loss, but the growth of interfacial resistance is hypothesized to contribute to power fade at high rates [55]. Over time, parasitic reactions in the SEI lead to consumption of the cyclable lithium,

decreasing capacity; increase in resistance appears to be minimal [54, 68]. Changes to the SEI have been observed in cells that have been stored uncycled [54, 83], but volumetric changes to the graphite anode during cycling are hypothesized to add stress to the SEI and contribute to crack formation, exposing additional graphite which consumes lithium while forming an additional passivating layer [33, 68]. The graphite anode may also degrade and suffer loss of contact with the current collector [68]. Aging is accelerated by high temperatures [33, 83]. Storage at 100% SOC is also found to contribute to more rapid capacity fade than storage at lower SOC [83].

Aging studies on LFP batteries in studies mimicking electric vehicle or vehicle-to-grid use seem to have slightly mixed results. Safari et al. only found higher degradation in LFP cells (as a function of throughput) under complex discharge cycling than constant discharge when performed at high temperature, and measured less than 10% capacity loss after 2000 cycles at room temperature [83].

Few studies have focused on complex charging cycles for LFP cells, but Savoye et al. found that the overpotential in LFP cells during charging increases with pulse length and range of current distribution (as measured in the root mean square of the current), reducing efficiency and available charge capacity [86]. A similar trend in overpotential is seen in utility-mimicking pulse charge tests [48].

Existing Definitions of Battery Durability and End-of-Life Criteria

In 2010, the German National Platform for Electromobility [9] published a study regarding the future of standards for electrified vehicles. At the time, studies on battery durability were given as a potential research area but no pressing need for standards on the topic was identified [9]. Even today, the European Commission does not have any battery durability requirements in place [10]. We therefore turn to available literature in order to find other definitions used for durability which we may use to synthesize into a definition of durability which is applicable toward xEVs.

Boulos et al. [9] from Ricardo-AEA conducted a study into the definition of durability for products as part of an initiative from the European Commission – DG Environment. Specifically, the purpose of the study was to identify two priority products and develop a methodology for measuring their durability. To this end, the authors of [9] have compiled together a number of durability definitions from other works. It should be noted, however, that these definitions relate to a variety of products which are neither related to batteries nor to automotive applications. Nevertheless, these definitions shall assist us in formulating our own definition of durability as it specifically relates to xEV battery durability. These definitions are shown in Table 4.

From these definitions, the authors of [9] conclude: it becomes clear that the terms ‘product lifetime’ and ‘product durability’ are inextricably linked and that the terms are frequently used interchangeably.

The key practical aspect that must be considered when exploring the implication of durability for products, if product durability is to be taken forward as a single element to be improved in its own right through the application of European Product Policy measures, is testing:

- Any definition of durability needs to be able to be tested – i.e. a test method must exist or be developed that enables repeatable and replicable testing to be performed.
- Testing under normal conditions is the usual method to give the anticipated lifespan, for example, testing under typical ambient conditions (temperature and humidity) and typical frequency of use.
- Further testing can be done under ‘challenging’ conditions, which use foreseeable conditions that are more challenging than typical use patterns, such as higher temperatures, increased humidity, increased frequency of use. Other examples of testing under more challenging conditions could include cyclic corrosion testing, salt spray testing, thermal aging, thermal cycling or thermal shock, vibration – random or shock. The specific testing carried out will depend on the type of product and the range of potential conditions it may be subjected to during its lifetime.
- The lifetime of a product needs to be defined, as does the point at which a first lifetime ceases and a potential second lifetime begins, for example if the product is remanufactured.

Report/Paper Title	Definitions relating to product durability	Reference
Further steps towards a quantitative approach to durability design	Definition: The durability design objective is to keep the probability of failure within a specified time interval (or service life) below a certain threshold value that depends on the consequences of failure of the component or system.	Lounis et al., 1998
Design for environment: a method for formulating product end-of life strategies	Definition: Wear-out life: the length of time until the product no longer meets the original function(s). Product is obsolete when it is no longer able to perform its intended function; e.g. because of failure of key components or it is outmoded.	Rose, 2000
Timber – Design for Durability	Definition: The capacity of a timber product, component, system, building or structure to perform for a specified period of time, the function for which it was intended – be it aesthetic, structural or amenity.	National Association of Forest Industries, 2003
Durability and the Construction Products Directive (now repealed) together with the Guidance Paper issued in 2004	Definition: Durability of a product is the ability of a product to maintain its required performance over a given or long time, under the influence of foreseeable actions.	EC, 2004
The durable use of consumer products	Definition: Product life (or durability) is the product's actual life in use. It should be differentiated among the product's economic life (determined by the opportunity cost) and product's technical life (determined by the duration of the product's ability to fulfill its technical function).	Kostecki, 1998
Design for Durability	Definition: The concept of durability in design embraces longer lasting products that focus on a better use of finite resources through, for example, combining functionality, opportunities for secondary lives, and increasing overall lifespan and product information.	Monteiro de Barros et Dewberry, 2006
Life cycle, sustainability and the transcendent quality of building materials	Definition: Durability is the characteristic of those objects or materials that maintain their properties over time.	Mora, 2007
Longer Product Lifetimes	"the expected lifetime of a product under a typical consumer use profile"; "the number of years that the product is designed to last, or number of product uses"; "Increasing product design life is defined here as measures which seek to replace shorter life products with products with different specifications which are purposely designed to last longer."	ERM for Defra, UK, 2011
MEErP, Material efficiency module	Lifetime considerations form part of the non-energy related product considerations, and will be given as per year of use, as well as whole lifespan. The product lifetime can refer to: • The technical lifetime is the time that a product is designed to last to fulfill its primary function (technical lifetime). • The actual time in service is the time the product is used by the consumer (service lifetime). The actual time in service is not a typical parameter in industry and depends more on the user than on the manufacturers of the product design.	European Commission

Table 4 Definitions of durability in the literature [11]

The definition arrived at by Boulos et al. was: *Durability is the ability of a product to perform its function at the anticipated performance level over a given period (number of cycles – uses – hours in use), under the expected conditions of use and under foreseeable actions. Performing the recommended regular servicing, maintenance, and replacement activities as specified by the manufacturer will help to ensure that a product achieves its intended lifetime* [11].

For determining definitions of durability with respect to xEVs, we may turn our attention toward the requirements which are set for vehicle End-of-Life (EOL). A number of parameters which are to be met upon reaching EOL conditions are defined by the USABC (United States Advanced Battery Consortium). The requirements for HEVs, PHEVs, and BEVs are given for year 2018 and 2020 commercialization. These requirements are shown in Table 17 - Table 19 in the Appendix. If we treat battery durability as being intrinsically linked to battery life

These USABC standards established battery EOL for BEVs as: (1) "the net delivered capacity of a cell, module, or battery is less than 80% of its rated capacity when measured on the DST (Reference Performance Test); or (2) the peak power capability (determined using the Peak Power Test) is less than 80% of the rated power at 80% DoD." EOL conditions are therefore based upon performance metrics. But, returning to the EOL goals, we are left with limiting factors such as a calendar life of 15 years for all xEVs [12] [13] [14] and cycle life goals of 75000 cycles for HEVs, 5000 cycles for PHEVs, and 1000 cycles for BEVs. Therefore, a component of our definition of durability needs to ensure that the rated capacity and rated power are greater than or equal to the associated values specified in the EOL criteria.

Strictly speaking, durability is defined as "The ability to withstand wear, pressure, or damage" [15]. However, we shall make distinctions with the formal English definition of durability when considering existing types of tests of xEV batteries. Durability, insofar as we should be concerned, should not be confused with Abuse, or that is to say, damage inflicted upon the battery which is liable to cause outright, if not catastrophic, failure. ISO-12405 has provisions for Performance, Reliability, and Abuse testing. SAE J2464, for example, consists entirely of Abuse tests [16].

We therefore set out to define xEV Battery Durability as such:

"The ability of an electrified vehicle battery to withstand degradation of functionality such that power & energy performance targets are met during typical drive cycles, consumer usage, and storage conditions without exceeding its end-of-life cycle and calendar life specifications."

In testing for battery durability using the above definition, xEVs and their battery systems will be subjected to drive cycles featuring various charge and discharge scenarios along with storage such that a vehicle will be able to (using USABC BEV goals [14] as an example) achieve either ≥ 15 years of calendar (storage) life or continue operating beyond 1000 cycles while maintaining ≥ 80% of its rated capacity and power.

Electrochemical Degradation Mechanisms of xEV Batteries

Introduction

In order to gain a better understanding of the degradation of batteries used in xEVs, we shall examine the electrochemical factors occurring at the battery cell level. Such an investigation is worthwhile as the battery packs which comprise the RESS of an xEV consist of these cells, and effects seen at the vehicle level are a direct result of degradation occurring within the cells of a battery pack. In this section, we shall investigate some of the chief causes of capacity and power fade in batteries.

The various battery components undergo different aging mechanisms; the binder and electrolyte decompose, the current collector corrodes, the separator melts and corrodes, and the cathode undergoes structural disorder and metal dissolution.

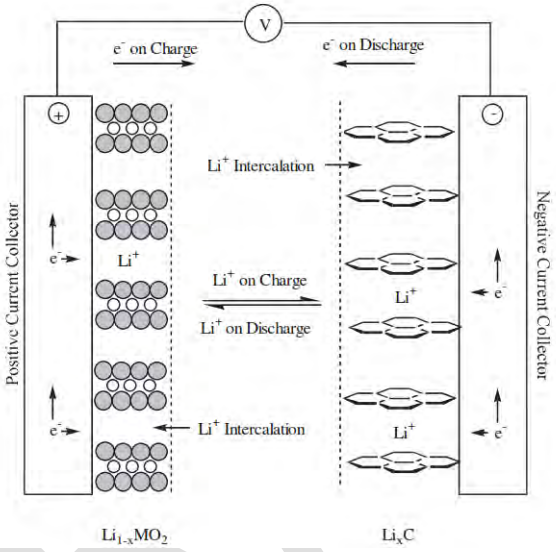

Figure 6 Schematic of the electrochemical process in a Li-ion cell. [14]

Physical Degradation Mechanisms

Degradation of the Anode

Formation of Passivated Surface Layer [15]

Graphite is one of the common anode materials for lithium ion batteries operating in organic electrolytes, such as $LiPF_6$, with co-solvents like ethylene carbonate (EC), dimethyl carbonate (DMC), diethyl carbonate (DEC), methyl ethyl carbonate (EMC)). The reaction of the anode with the electrolyte solution in the formation stage results in the formation of the *solid electrolyte interphase (SEI).* Anion contaminates, such as F−from HF and PF_5, readily react with lithium to form insoluble reaction products which are non-uniform, electronically insulating, and unstable on the surface of the graphite particles [7–11]. In addition, the dissolution of the cathode electrode metal from the lattice into the electrolyte due to the disproportionation of Mn^{3+} (into Mn^{2+} and Mn^{4+}) by traces of hydrofluoric acid (HF) in the electrolyte, resulting in the deposition of contaminateson the anode electrode surface [12].

At higher battery potentials, during the intercalation of lithium ions into the anode lattice structure, the graphite anode oxidizes. At this potential, electrolyte co-solvents, such as EC, which is highly reactive, react with the lithium ions which leads to growth on the anode surface [13,14]. The presence of these reaction products on the surface retards the intercalation kinetics of the carbon anode [15]. The surface layer grows in thickness as the decomposition reaction continues [16–22]. The layers become unstable and crack due to expansion and contraction of the graphite lattice during the insertion and de-insertion of the lithium ions [26–28]. This allows further surface reaction at these sites that may eventually isolate the graphite particles from the current collector. Figure 1 shows a typical surface film morphology and cracking of the layer (e.g., [26,27]). The surface crack formed on the surface does not typically travel to the carbon electrode [26]. The formation of this surface film layer is the predominate source of lithium ion loss in lithium ion battery during storage conditions [25]. It also leads to an increase in the charge transfer resistance, impedance, and clogs pores on the carbon anode electrode [29–31], which limits accessibility of lithium ions to the anode surface leading to an increase in irreversible capacity [32–34]. The growth of this surface layer on the anode electrode is prevalent in the electrolyte system with EC as the co-solvent compared to those with DEC or DMC as co-solvents [35–38].

Anode Impedance [15]

The growth of the passive surface layer on the anode creates resistance to lithium ion flow, which results in a rise in the charge transfer resistance and the impedance of the anode [39,40]. This increase in anode impedance is said to increase with charge rate, cycle number, temperature, and anode material particle size [41–43]. However, at temperatures in the range of 10–30 °C and with a low charge rate (C/20), the anode electrode contribution to the overall battery impedance is low. This is attributed to the small amount of the surface film formed on the electrode surface [44]. The low charge rate limits the amount of excess Li+ that is not intercalated into the electrode to react with the electrolyte [45,46]. A typical SEM micrograph of anode covered with products of electrolyte decomposition reaction products is shown in Figure 2. (e.g., [38,39,44,46,47]). Common surface reaction products formed on the anode surface include Li-alkyl carbonates, lithium carbonate species and fluorinated products. These products affect the intercalation and de-intercalation kinetics of the anode, and thus result in an increase in anode electrode impedance relative to the cathode [47–49].

Degradation Due to the Loss of Recyclable Lithium Ions [15]

The irreversible lithium ion loss is generally attributed to two phenomena, namely: (i) solid electrolyte interface (SEI) layer formation via electrolyte decomposition at the formation stage; (ii) side reaction of lithium ion with

decomposed electrolyte compounds and water (e.g., 10–1500 ppm) in the electrolyte at the later stage of the battery operation [50]. The loss and/or consumption of recyclable lithium ions at the anode by the passive layer is a major cause of the reduction in the reversible capacity of the lithium ion battery [51,52]. As the layer grows, lithium is consumed in the reaction and the increased thickness inhibits Li+ transfer, thus the lithium ions must tunnel through the layer. This phenomenon is the main degradation mechanism in fully charged batteries at storage conditions [52–55], where the electronic insulating surface layer formed clog the pores and isolate graphite particles. The irreversible lithium ion loss is also a function of the specific area of the graphite particles, since an increase in area increases the volume of reaction products [56,57]. For a graphite anode with low specific area, the charge loss is low. The electrolyte additive, vinylene carbonate (VC) is one that increases the lithium ion loss rate at the anode for the Li/coke electrode during storage (ambient temperature conditions). Because it increases the rate of SEI formation reaction at ambient temperature conditions to increase the SEI thickness. However, its beneficial effect is seen at higher temperature (35–50 °C) and higher voltages >0.4 V for Li/coke, electrode as it slows down the side reaction rate and undergoes reduction and polymerization to form poly alkyl Li-carbonate species that suppress both solvent and salt anion reduction on the anode electrode. Similarly, in batteries stored at voltages greater than 3.6V, electrolyte oxidation at the cathode can also induce surface reaction deposits that cover the active cathode electrode area. These covered areas are insulating, which could result in a non-homogeneous local current distribution in the cathode electrode.

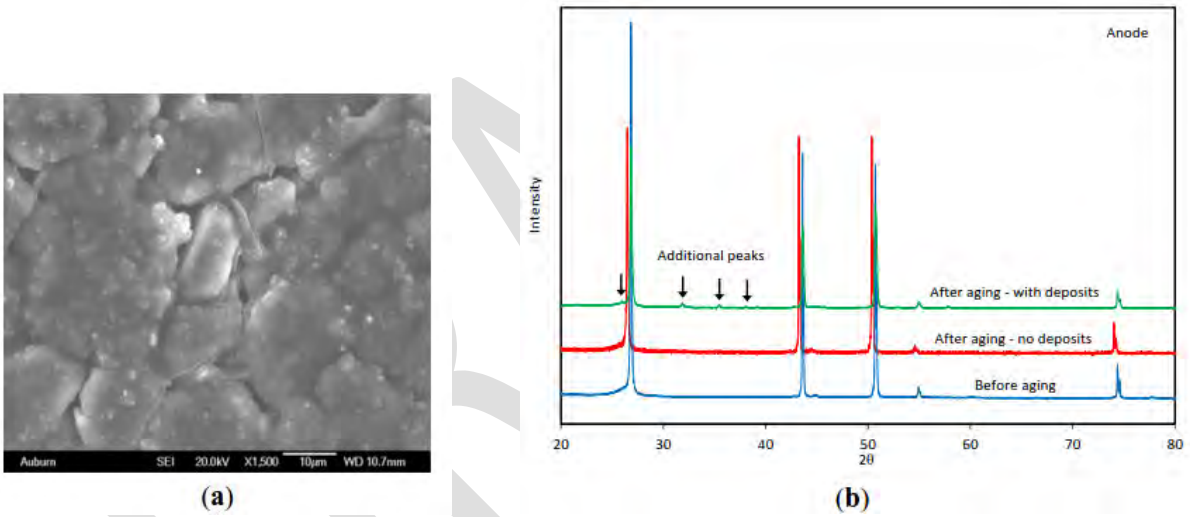

Figure 7 Structural changes on the anode electrode from degradation. (a) Surface cracks on the surface of aged anode electrode; (b) XRD spectra of aged anode electrode showing change in crystal structure (new phases). **[15]**

Metallic Lithium Plating on the Anode

The usage of well-ordered carbon and non-graphitizable carbon have gradually replaced lithium metal as the preferred anode material for the lithium ion battery due to benefits in capacity, cyclability, low electrode potential relative to Li^+/Li, and a lower susceptibility to lithium plating [15]. Nevertheless, metallic lithium deposits remain a factor in anodes.

There are several factors that initiate the formation of metallic lithium on the surface of the anode electrode, some of these include: (1) the nature of the electrolyte (i.e., electrolyte formulations with high EC content exhibit lithium plating); (2) the ratio between anode and cathode capacities (i.e., low anode/capacity ratio will polarize the anode and promote lithium plating); (3) the operating temperature and the charge rate [i.e., low temperature (−20 °C) coupled with a high charge rate] all influence plating on the anode [81,83]. These factors affect the anode kinetics and the lithium ion diffusion rate, such that lithium plates on the surface of the electrode rather than intercalating into the lattice of the carbon.

The formed metallic lithium deposits on the graphite anode are affected by the degree of random orientation of the particles in the crystal structure in the anode material and the non-uniformity of the current distribution which is a function of diffusion and current density [84,85]. This subsequently results in the formation of moss-like deposits and dendrites [15]. These moss-like deposits and dendrites grow as a function of the temperature and current density between the polymer separator and the anode. As the temperature and charge rate increases, the reaction rate also increases and metallic lithium is deposited on the graphite at overcharge. Dendrites can cause the separator to disconnect and become isolated from the electrolyte and in some instances pierce through the separator. These dendrites can cause a short circuits and consequently to thermal runaway situations. Lithium plating can typically be identified by a voltage plateau on the discharge voltage profile and a low columbic efficiency [15].

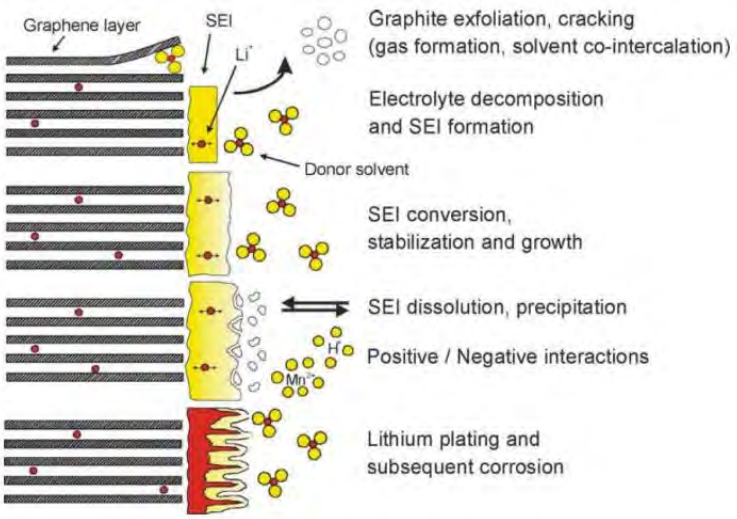

Figure 8 Degradation Methods for the Negative Electrode **[18]**

Regarding the anode, Vetter et al. [18] concluded that SEI formation and growth leads to an impedance rise at the anode. Usually, SEI formation takes place mainly at the beginning of cycling. SEI growth proceeds during cycling and storage and is favored by elevated temperatures. The rise in impedance which comes as a result of this growth can be directly linked to power fade. Furthermore, in parallel to SEI growth, corrosion of lithium in the active carbon takes place, leading to self-discharge and capacity fade due to loss of mobile lithium. The formation and growth of the SEI leads to gradual contact loss within the composite anode, and thus, increases the impedance in the cell. Lithium metal plating might occur at low temperatures, at high rates and for inhomogeneous current and potential distributions. The Li metal reacts with the electrolyte, which may contribute to accelerated aging. A strong influence of the specific cell components on the aging mechanism can be observed. Although the general mechanisms presented here hold true for most of the lithium-ion systems they may be pronounced differently for each particular system [18].

Cause	Effect	Leads to	Reduced by	Enhanced by
Electrolyte decomposition (→SEI)(Continuous side reaction at low rate)	Loss of lithium Impedance rise	Capacity fade Power fade	Stable SEI (additives) Rate decreases with time	High Temperatures High SOC (low potential)
Solvent co-intercalation, gas evolution and subsequent cracking formation in particles	Loss of active material (graphite exfoliation) Loss of lithium	Capacity fade	Stable SEI (additives) Carbon pre-treatment	Overcharge
Decrease of accessible surface area due to continuous SEI growth	Impedance rise	Power fade	Stable SEI (additives)	High temperatures High SOC
Changes in porosity due to volume changes, SEI formation and growth	Impedance rise Overpotentials	Power fade	External pressure Stable SEI (additives)	High cycling rate High SOC
Contact loss of active material particles due to volume changes during cycling	Loss of active material	Capacity fade	External pressure	High cycling rate High DOD
Decomposition of binder	Loss of lithium Loss of mechanical stability	Capacity fade	Proper binder choice	High SOC High temperatures
Current collector corrosion	Overpotentials Impedance rise Inhomogenous distribution of current and potential	Power fade Enhances other aging mechanisms	Current collector pre-treatment (?)	Overdischarge Low SOC
Metallic lithium plating and subsequent electrolyte decomposition by metallic Li	Loss of lithium (loss of electrolyte)	Capacity fade, power fade	Narrow potential window	Low temperature High cycling rates Poor cell balancing Geometric misfits

Table 5 Lithium-ion aging – causes, effects, and influences. Reproduced from Vetter et al. **[18]**

Lithium Titanate (LTO) anodes

Although much of the focus has been on graphite and carbon anodes, Morales et al. [16] investigated $Li4Ti_5O_{12}$ (LTO) as an anode material coupled with a lithium-iron phosphate cathode. It was shown that LTO permitted allowed for high rate capabilities but is a particularly poor conductor. This sentiment was echoed by Etacheri et al. [17], who observed that LTO is inferior to graphite due to its low capacity and high voltage which in turn leads to poor energy density. One thing to note is that LTO features no passivation phenomena on account of its high reduction voltage. This gives LTO excellent low temperature performance [17].

Degradation of the Cathode

Vetter et al. [18] offered three basic principles for the aging of the cathode:

- Structural changes during cycling;
- Chemical decomposition/dissolution reaction;
- Surface film modification

An overview of these mechanisms are shown in **Figure 9**

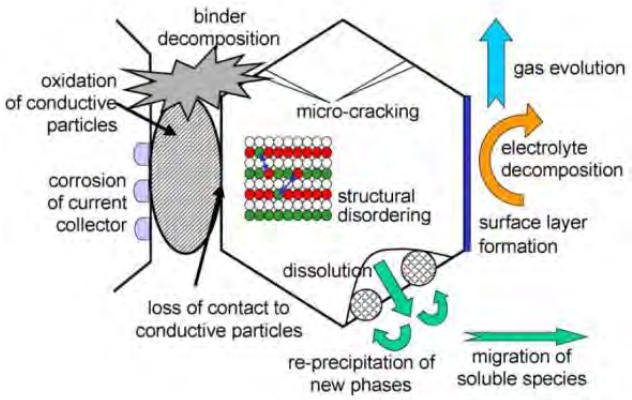

Figure 9 Degradation mechanisms for the positive electrode **[19]**

Kubiak et al. [20] offer a review of some of the aging mechanisms of the various chemistries used for automotive-grade batteries:

Manganese Spinel Electrode $LiMn_2O_4$ (LMO)

Cite [18]

$LiMn_2O_4$ is noted to have features at high (4.5V) and low voltages (3.3V) which are detrimental to its cyclability. These features are associated to phase transitions, which occur during cycling. A result of these transitions is a loss of electrical contacts. Although a composition of $Li_{1.05}Mn_{1.95}O_4$ can improve performance with respect to capacity retention, the usage of this particular composition demonstrates poor performance at high temperature and after storage at a low SOC [18].

The dissolution of Mn has been identified as the main cause of the capacity loss seen in LMO electrodes, and is also at the origin of the increase in the polarization through the contamination of the electrolyte and deposition on to the negative electrode. The limited high temperature performance of $LiMn_2O_4$ is attributed to failure mechanisms which vary depending on whether or not the cell is in a charged or discharged state [20].

When in a charged (high potential) state, electrolyte degradation occurs such that reactions with the SEI layer of the Li_xC_6 electrodes occur. The product of this reaction is LiF, which accumulates over time or upon cycling and contributes to irreversible capacity loss as the lithium used to form LiF is no longer available for subsequent cycles. [20]

In the discharged state (low potential), capacity fading is also associated with an irreversible loss of lithium which is linked to reactions on the positive electrode. In this case, the reasons for capacity loss are the

dissolution of Mn into the electrolyte following a disproportionate distribution of Mn^{3+}. This results in soluble Mn^{2+} species + Li^+ + H_2O which react with PF_6 salts thereby creating hydrofluoric acids, starting the destructive process again. [20]

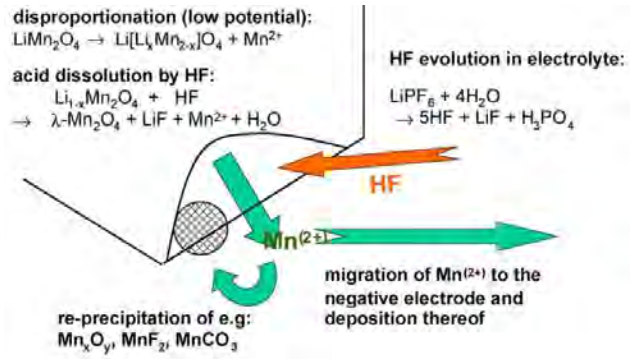

Figure 10 Dissolution of lithium manganese spinel **[18]**

The basic concept of reducing Mn dissolution lies in minimizing the surface of the spinel in contact with the electrolyte. This was first performed by minimizing the surface area of the powder. To further improve the capacity retention at high temperature, researchers have altered the surface through encapsulation methods. Two types of coating have been optimized: one based on Li2CO3 obtained by combustion of acetylacetone previously grafted on the top of the particles and a second one based on B2O3 treatment [74]. In both cases, improvements have been obtained. It is worth noting that LiCoO 2 coating can also protect the Mn spinel particles even at high temperature [75].

Cationic and anionic substitution has also been intensely studied by researchers [76,77]. Briefly, manganese substitution by aluminium has improved the aging mechanism with the best composition being LiAl0.2Mn1.8O4. However, this substitution induces an increase in the tetravalent manganese in the starting material. Thus, a price is paid in terms of initial capacity. Very good cycling properties have been obtained by Ariyoshi et al. [78]. To increase the initial capacity, while maintaining the good storage properties at high temperature, Amatucci et al. have considered the anionic fluorine substitution and studied the effect of fluorine substitution on the chemical and structural stability of the spinel Li1+xMn2-xO4-zFz (LAMOF) [76,77]. Through a careful s ystematic study of the double substitution, an initial discharged capacity of 118 mAh g-1 has been reached with really lengthy cycle life even at high temperature.

However, even if LAMOF composition appears to be suitable for cycling at high temperature, Mn dissolution has not been totally suppressed, and large quantities of LAMOF do not seem to be produced by powder producers. Moreover, it has been discovered in 2001 that mixing LiMn2O4 with LiN i0.8Co0.2O2 (NEC) [79] or with LiN i1/3Mn1/3Co1/3O2 (Sanyo) [80,81] has a strong influence on the Mn dissolution at high temperature and even suppresses this dissolution. It has been established that the addition of layered materials can suppress the hydrogen concentration in solution, and the amount of required addit ives depends on its specific surface area. The main advantage of the addition of these specific additives is that they also act as active materials so high density positive electrodes can be obtained.

3.2 $LiFePO_4$ electrode (LFP)

Use: [5] [21] [8] [22] [23]

$LiFePO_4$ has recently attracted a significant interest as a cathode material for Li-ion batteries because it's a low cost material with excellent safety characteristics and also it has the potential of providing a long cycle and calendar life [82–89]. However, $LiFePO_4$ is an insulating material, which seriously limits its rate capability

[82–84]. Extensive works have been conducted to enhance the electronic conductivity of $LiFePO_4$ by coating it with carbon [85–89] or by cationic doping [88,90]. Although $LiFePO_4$ shows good stability, traces of moisture in the $LiFePO_4$ material could be detrimental to its long-term storage since $LiFePO_4$ dissolution in the electrolyte was observed at high temperature [91]. In 2005, K. Amine and al. studied the high-temperature storage and cycling characteristics of prismatic Li- ion cells with carbon-coated $LiFePO_4$ cathodes, MCMB graphite anodes and a $LiFP_6$/EC-DEC electrolyte [67]. The cells showed a significant capacity fade when cycled at 37°C and 55°C and interfacial impedance of the graphite electrode increased significantly during high-temperature cycling. Carbon-coated $LiFePO_4$ electrodes were found to release iron ions into the electrolyte when aged at these temperatures. The observed impedance rise of the graphite electrodes and the consequent capacity fade of the cells were attributed to the formation of interfacial films that were produced on the graphite electrodes as a result of possible catalytic effects of the metallic iron particles. To understand the origins of the iron dissolution, LiFeP O4 was investigated in various electrolyte solutions [92-94]. LiFePO4 electrodes demonstrated higher stability at elevated temperatures, in solutions that contain no acidic or protic contaminants. The capacity loss due to iron dissolution does not result from bulk changes but rather to surface reactions [95]. A systematic study of a series of $LiFePO_4$ samples containing different amount of Fe^{3+} impurities showed that the most contaminated sample exhibited the highest level of iron dissolution and consequently the lowest electrochemical performance [96]. A mechanism for iron dissolution and capacity fading has been proposed where iron dissolution is linked to the reaction between acidic species in electrolyte and Fe3+ impurities present in the positive. The dissolved iron ions migrate to the negative electrode and are reduced into metallic iron. This causes an increase of the thickness of the SEI layer on the graphite electrode and consequently to an impedance rise, causing a strong capacity fading and a loss of power. The deposition of metallic iron can lead to the growth of iron dendrites which may penetrate through the separators and causes short-circuit and the failure of the cell [96,97].

Using water- free electrolyte [56] or electrolyte additives [98,99], coating of the LiFePO4 active material [100 - 103] or surface modification of the negative electrode [104] have been proposed to overcome iron dissolution. Although considered among the most stable intercalation materials for lithium- ion secondary batteries, olivine exhibits a dramatic atmospheric reactivity dependent on time even for ambient temperature. Exposure to humid air or directly to water affects the purity of the LiFePO 4 material [105-108]. The regeneration of pure LiFePO4 can be obtained by an appropriate thermal treatment under inert atmosphere [109].

In addition to the iron dissolution, one has to consider the Li insertion/extraction mechanism in LiFePO4/FePO4. It is highly anisotropic and involves the coexistence of a Li-rich and a Li-poor phases and [110-113]. The presence of cracks in the bc plane can also be observed [114-115]. These cracks may be caused by high internal strain a long b-axis upon Li-extraction/insertion. They lead to increased polarization of electrode and poor electric contact between active particles and conductive additives or aluminium foil current collector. This can be considered as one of the reasons for capacity fading for pure LiFePO4.

Stability and very high performance of $LiFePO_4$ electrodes can be achieved by the appropriate choice of synthetic mode, processing conditions, and uncontaminated solutions [116]. Thus, it is strongly recommended to store LiFePO4 under dried atmosphere. Recent reports of commercial batteries based on LFP positive electrodes show that physical degradation of the carbon negative and loss of active lithium are the dominating mechanisms responsible for cell capacity loss [117-118]. The instability of the negative resulted in the instability of the SEI layer which accelerated losses of active lithium and cell capacity.

3.3 $Li_{1+x}(Ni_{0.8}Co_{0.15}Al_{0.05})O_2$ electrode (NCA)

Cite from [20] [24] [25]

The class of layered oxides based on $LiNiO_2$ has been considered as a good candidate for replacement of $LiCoO_2$ in positive electrode material of Li- ion batteries because of its lower cost and higher capacity compared to $LiCoO_2$ and better environmental compatibility. $LiNiO_2$ adopt the α-$NaFeO_2$ structure with consecutive alternating N iO2 and Li layers. However it is difficult to synthesize stoichiometric LiN iO2 and cation disorder has important consequences on Li transport and leads to rapid decrease in capacity. Therefore the substitution of Ni^{3+} by Co^{3+} has been proposed in order to stabilize the oxidation state and reduce N i2+ formation.

Further improvements have been obtained with by Al (and other metal) doping [119 -121], and hence $Li(Ni_{0.8}Co_{0.15}Al_{0.05})O_2$ has seen tremendous commercial success. However electrodes based on NCA materials still suffer from deterioration of properties such as capacity fading and increase in impedance by cycling or by aging at elevated temperature (Fig. 6)

The increase of interfacial resistance at the positive has been reported to be the main reason behind the capacity decay and the power fade of the battery [122-131]. Many studies on positive electrodes have been conducted to explain the structural changes that result from cycling or aging. Several changes such as the formation of N iO-like surface layer of active material [132,133], the loss of connectivity between particles [134], the formation of a solid electrolyte interface (S EI) at the surface of the positive electrode [135-137], the corrosion of aluminium current collector [138] or an increase in electronic contact resistance between electrode components within the positive electrode [137,139] were reported for degraded positive electrodes:

The quantitative relationship between the deterioration of electrochemical properties and structural/chemical changes of the positive electrode is still unclear. Although no structural changes have been observed in the bulk structure of the NCA positive electrode, [140] a lower valence of Ni was observed after cycling or aging at high temperature [141]. The combination of electrochemical, spectroscopic and electron microscopy methods provided new insights on the capacity fading and impedance rise of batteries based on NCA positive electrode material. Inactive N i ions with lower valence than expected are present in the NCA active material. The estimated fraction of inactive Ni ions provides a suitable quantitative explanation for the measured capacity fade of the positive electrodes. The Ni-O phase was found to be located at grain boundaries in the primary/secondary particles [142]. Its formation occurs during Li extraction and leads to subsequent oxygen loss.

In addition to its structural instability, the use of NCA cathode material can lead to thermal runaway. The contributions of delithiated NCA sample and electrolyte on the overall thermal runaway mechanism were evaluated by different methods and a mechanism has been proposed. XRD and DSC analysis show that the exothermic reaction of the delithiated cathode occurs at temperatures close to the onset temperature of structural changes in the delithiated cathode [143,144]. High electrochemical performance with excellent stability of NCA electrodes can be achieved [145]. As the cycle life of NCA/graphite cells strongly depends on the positive electrode, it is recommended to carefully control both the end of charge as well as the working temperature.

Jungst et al. [43] studied the decrease in the capacity of LIB the size 18650 with the positive electrode of $LiNi_{0.8}Co_{0.15}Al_{0.05}O_2$ and the negative electrode of graphite MAG-10, which were intended for powering an electric vehicle. The batteries with the SOC of 60, 80, and 100% were stored at 25–55°C and their impedance was periodically measured. The LIB impedance steadily increased with the storage duration [26].

3.4 $Li_{1+x}(Ni_{1/3}Co_{1/3}Mn_{1/3})_{1-x}O_2$ electrode (NMC)

The layered $LiNi_{1/3}Co_{1/3}Mn_{1/3})_{1-x}O_2$ (NMC) is another alternative to the commonly used $Li(Ni_{0.8}Co_{0.2})O_2$ and could offer longer calendar life for the HEV applications. The metals Co, Ni and Mn can be accommodated in the layered metal structure to give a range of composition $Li(Ni_xCo_yMn_z)O_2$, where x+y+z = 1. It possesses the same α-NaFeO2-type structure as $LiMn_{0.5}Ni_{0.5}O_2$ with Ni, Co and Mn adopting valence states of 2+, 3+ and 4+ respectively [146-148].

The $Li(Ni_{1/3}Co_{1/3}Mn_{1/3})O_2$ composition (NMC) has shown very promising electrochemistry and intriguing structural behavior [149]. The stability of the NMC material has been explained by its low degree of cation disorder (1-6%) [150-155] and its low volume change during (1-2% for $Li_{1-x}(Ni_{1/3}Co_{1/3}Mn_{1/3})O_2$,where $0<x<0.7$ Li insertion/extraction [150,153,156,157]. Moreover it possesses excellent safety properties compared to $Li(Ni_{0.8}Co_{0.15}Al_{0.05})O_2$ at high state of charge [158 -161]. The electrochemical stability of NMC depends on the upper cut-off voltage in charge and the material shows rapid capacity decay when charged at high voltage [162 -164]. Over-lithiation has been proposed to improve the stability of the NMC at high voltage due to the lower volume change of the layered structure at high level of Li extraction [165-169]. A plateau in the high voltage region (>4.5 V vs. Li/Li+) is observed during the first charge. It leads to an irreversible capacity loss proportional to the degree of over- lithiation but the capacity can be recovered by a deep discharge [170]. The high- voltage plateau is explained by structural changes due to oxygen loss from the NMC during Li extraction [172,173]. F inally it has been proven that over-lithiation stabilize s the structure during delithiation and thus improves the cycling stability (Fig. 7).

Structural rearrangements of delithiated NMC have been observed after aging at 70°C for 60 days. They were attributed to oxygen release and cation rearrangement [174]. Moreover, changes in the stoichiometry of the transition metals have been reported in aged NMC materials. Thus, the ratio Ni/Mn and Ni/Co became much greater than 1 near the surface of the NMC particles [175]. It appeared that NMC particles present a strong reactivity towards electrolyte solution. Electrolyte additives such as lithium bis(oxalate)borate (LiBOB), vinyl ethyl carbonate (VEC), and lithium difluoro(oxalato)borate (LiDFOB) or $LiC_2O_4BF_2$ have been already proven to be effective in improving the cycling stability of NMC/graphite cells [176-178].

Lithium Cobaltite $LiCoO_2$ electrode (LCO)

Aurbach et al. [27] performed a study on the electrochemical behavior and surface chemistry of $LiCoO_2$ cathodes as a function of cycling and storage at 25, 45, and 60°C and showed that, during prolonged storage and/or cycling at elevated temperatures in an electrolyte containing $LiPF_6$, positive electrodes based on lithium cobaltite undergo noticeable degradation. The major reason for the degradation of a battery as determined by the authors of [27] is not so much the change in the composition of the active mass of the positive electrode so much as the processes occurring on its surface. These processes are caused by the formation on a cobaltite electrode of a film of LiF, which forms as a result of interaction of lithium cobaltite with traces of hydrofluoric acid. This film leads to an increase in the impedance of the positive electrode, thereby impeding lithium ion migration through the SEI.

Lithium cobaltite may find itself subjected to chemical dissolution, which leads in particular to the formation of Co^{2+}. The Co^{2+} ions can then undergo discharge at the surface of the negative electrode. The authors of [104] in [26] reported on a direct link between the amount of metallic cobalt at the surface of the negative carbon electrode and the decrease in the capacity of LIB that had been charged to a voltage in excess of 4.2 V (considered here to be an overvoltage). The value of the decrease in the capacity of LIB with a positive electrode based on lithium cobaltite depends on the technology of the preparation of the latter, in the first place, on the character of thermal treatment during the synthesis of the active material [26].

The authors of [61, 62] in [26] showed that the decrease in the capacity of LIB during their cycling could have been caused by the disordering of the layered crystalline structure of $LiCoO_2$, resulting in deactivation of a fraction of lithium ions in the cathode, and by the emergence, in the $LiCoO_2$ particles, of a large number of cracks and pores that hindered the free solid-phase diffusion of lithium ions in the electrode material. The increase in the thickness of the passive film at the surface of the negative carbon electrode as a result of the electrolyte electroreduction also plays a substantial role in the capacity decrease.

Degradation of the Separator

Degradation of the Electrolyte

A standard modern electrolyte for LIB is manufactured chiefly based on lithium hexafluorophosphate ($LiPF_6$).

In moistened electrolytes, $LiPF_6$ readily undergoes hydrolysis with the formation of acidic products (POF_3, HF); it is at equilibrium with PF_5 ($LiPF_6 = LiF + PF_5$) [137], which actively reacts with the solvent. In particular, EC reacts with PF_5 and undergoes polymerization with the evolution of carbondioxide [142]. Hydrofluoric acid easily enters reactions with the material of the positive electrode, especially with lithium–manganese spinel [143].

The electrolyte decomposition as a result of electroreduction on the negative electrode leads as a rule to a decrease in the capacity and cycle life of the LIB as a consequence of the irreversible decrease in the content of salt and solvent. On the whole, the process of electroreduction of various carbonate electrolytes on the negative carbon electrode obeys the same regularities as on metallic lithium, due to the closeness of potentials of lithium and completely lithiated carbon [26][159]. In either case, the electroreduction of the electrolyte leads to the formation of a carbonate film of a solid electrolyte at the electrode surface and the evolution of gaseous products (propylene, ethylene) [26].

Similarly to the negative electrode, the electrolyte decomposes at the positive electrode/electrolyte interface [8] [18]. The compounds found in the electrolyte oxidize on the surface to produce a thin film depending on the operating conditions. Contaminants within the electrolyte can catalyze polymerizations or produce gaseous products that develop or damage the SEI film, respectively [105]. Gases can also cause damage to the active material. This SEI formation is difficult to detect because the positive electrode potential is much higher than that of the negative electrode [104]. The SEI formation depends on temperature, SOC, and voltage as with the negative electrode [15] [105]. For storage potentials greater than 3.6 V, the decomposition of the electrolyte is accelerated [15].

Effects of Temperature on Degradation Mechanisms

Broussely et al. [28] performed a comprehensive analysis of the degradation of the capacity of LIB with different depths of discharge (monitored from the LIB voltage), which had been stored for a long time at 15–60°C. A year's storage at 60 and 30°C led to a capacity loss of 15–20 and 7–8%, respectively, as shown in Figure **11**. No unambiguous dependence of the degradation on the depth of discharge was discovered.

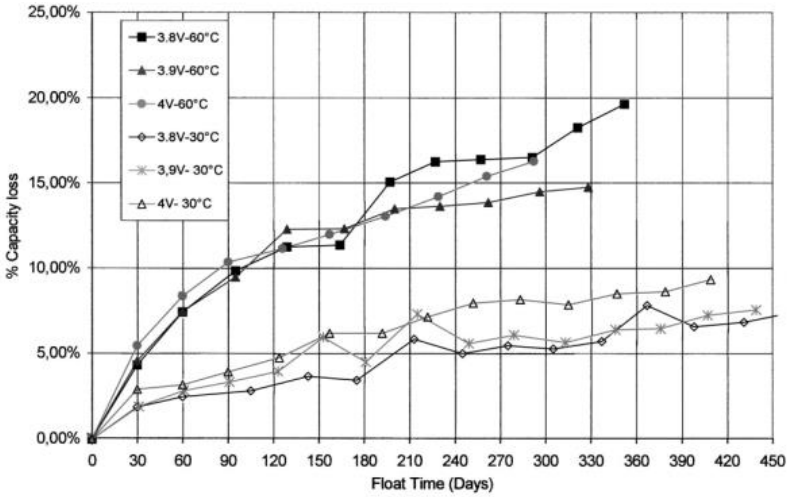

Figure 11 Capacity loss on cells measured at 30°C – C/3, during storage at 60 and 30°C under various voltages **[28]**

In a presentation dealing with Electric Vehicle Battery Thermal Issues [44], Rugh et al. show how at low temperatures the relative resistance and relative capacity of Li-Ion batteries show worsening characteristics as temperature decreases, with resistance sharply spiking around -40°C and capacity also demonstrating a steep dropoff after freezing.

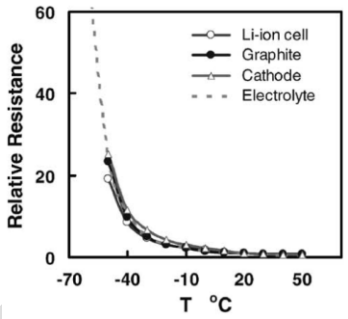

Figure 12 Li-Ion Battery Resistance Increases with Decreasing Temperature **[44]**

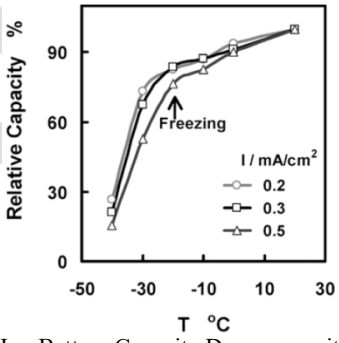

Figure 13 Li-Ion Battery Capacity Decreases with Decreasing Temperature **[44]**

An increase in the activation resistance of the process of discharge of lithium ions and the concentration polarization by lithium ions at low temperatures makes the electrode potential noticeably more negative, which eventually leads to electrodeposition of metallic lithium (lithium plating, as discussed in Degradation of the Anode) on the carbon surface. The electrolyte reduction on the freshly formed surface of metallic lithium is responsible for the change in the structure (an increase in the density and thickness) of the solid-electrolyte film on the negative electrode, which is accompanied by an increase in its ohmic resistance, which in turn gives rise to an additional increase in the polarization. Such changes in the surface films lead to a gradual irreversible decrease in the capacity ([166] from [26]). While the discharge capacity changed during cycling to the 15th cycle following a relatively small decrease in the temperature (to –10°C) by no more than 5%, the capacity drop at −20°C amounted to 35%. Returning to room temperature did not lead to restoration of the initial state of the battery: the discharge capacity amounted to a mere 85% of the initial value.

The stability of negative electrodes is also negatively affected by the LIB storage at temperatures in excess of 40°C. The capacity decrease of fully charged carbon electrodes during storage is always smaller than that of

fully discharged electrodes ([105] from [26]). The reason for this phenomenon is thought to be the destruction of the surface film of a solid electrolyte, which leads to continuous delithiation of the bulk of the electrode with a subsequent interaction of lithium atoms with the electrolyte, i.e. to irreversible self-discharge of LIB.

To evaluate the contribution made by the negative electrode to the self-discharge of LIB in a three-electrode cell with a lithium counter electrode and a lithium reference electrode, Yazami et al. [169] investigated the decrease in the capacity of a carbon electrode subjected to a tenfold cycling and then stored at 70°C. For the electrolyte they employed 1 M $LiPF_6$ in an EC–DMC mixture. Based on the impedance investigations (the electrode impedance perceptibly increased after storage) and charge–discharge characteristics (the electrode capacity dropped by 1.5–2.5 times as a function of the storage duration), the authors of [169] make the conclusion that, during storage at an elevated temperature, lithium that was intercalated into carbon diffuses out of the space between graphene planes towards their external surfaces, thus making it easier for the chemical reactions between lithium and electrolyte and its impurities to occur. The deposition of the products of these reactions at the electrode surface is responsible for the impedance increase, which in turn compromises the discharge characteristics [26].

The effect of elevated temperatures during storage on the negative carbon electrode was investigated in [170]. In new condition, the prepared electrode contained no noticeably pronounced film, whereas after storage at 50°C to 75°C, the surface was covered by a solid-electrolyte film of varying, non-uniform thickness (40 to 200nm). After 40 days in storage, the measured impedance of the negative carbon electrode increased by 8, 28, and 35% respectively, whereas reversible capacity decreased by 5, 12, and 18% respectively for storage temperatures of 50°C, 65°C, and 75°C [170] from [26].

The degradation of LIB and the decrease in the their capacity after storage at elevated temperatures (up to70°C) may be caused not only by destructive processes on negative electrodes but also by quite a number of processes occurring on positive electrodes.

Amine et al. [16] were studying the conservation of the capacity and stability of LIB the size 18650 with the chemical composition of graphite–$LiNi_{0.8}Co_{0.2}O_2$ along with an electrolyte of $LiPF_6$ in an equimolar mixture of EC and DEC, which was then stored at temperatures ranging from 40 to 70°C. The observed degradation of the LIB (in the first place, the decrease in the discharge capacity) was accompanied by a considerable increase in the impedance of the positive electrode, which was connected, in opinion of the authors of [16], with an excessive increase in the thickness of the solid-electrolyte film on the electrode. The correctness of this assertion is confirmed by the results obtained in [172, 173], whose authors used a variety of methods to investigate the properties and composition of surface films on the positive electrode based on LiNi0.8Co0.2O2 after a sufficiently long storage at elevated temperatures in an electrolyte based on $LiPF_6$. It was established that after storage the solid-electrolyte film contained a large amount of LiF; in so doing, the weight of the film after storing LIB at 70°C was greater than that after storage at 50°C by 10%.

During storage at elevated temperatures and when discharged by high currents, when the temperature inside LIB may exceed 80°C, there can occur a phase transformation of cobaltate and a disproportionation of $Li_{0.5}CoO_2$ to $LiCoO_2$ and Co_3O_4 [26][175].

When stored in conditions of an elevated temperature, a lithium–manganese spinel also may be subjected to disproportionation ($2Mn^{3+} \leftrightarrow Mn^{4+} + Mn^{2+}$) [80, 94].In the presence of hydrofluoric acid, which forms as a result of hydrolysis of $LiPF_6$, at an elevated temperature the spinel undergoes dissolution via the reaction $2LiMn_2O_4 + 4H^+ \rightarrow 3\lambda\text{-}MnO_2 + Mn^{2+} + 2Li^+ + 2H_2O$ [18][109, 169]. Water generated in this reaction accelerates the electrode degradation and the capacity sharply decreases [26].

Jungst et al. [29] performed a study wherein Li-ion cells were stored at 40, 50, 60, or 70°C for times of 2-8 weeks for the calendar and cycle life aging studies. Some cells were maintained at a single SOC (60 or 80%) for the calendar life tests, while others were cycled at a defined ΔSOC of 3, 6, or 9%. The chemistry used in the high-power cells was a mixed metal (Ni/Co) oxide cathode material, a graphite carbon anode, and an ethylene carbonate / diethyl carbonate (DEC) electrolyte containing 1M $LiPF_6$ salt. Here, it was shown that the total impedance is significantly increased after aging and that most of the change occurs in the cathode interfacial impedance.

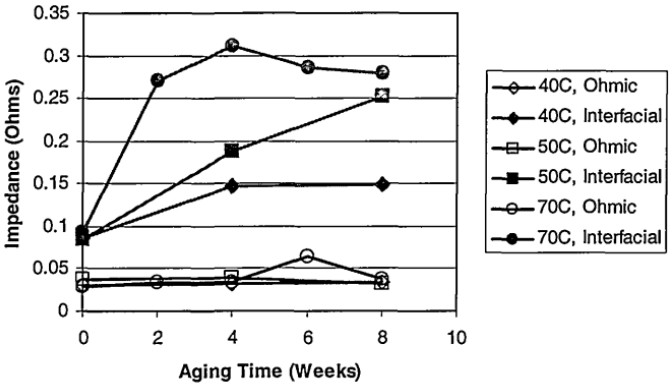

Figure 14 Changes in Interfacial Impedance and Ohmic Resistance after Aging at Different Times and Temperatures. **[29]**

Interfacial impedance and ohmic resistance values were compared at high SOC. Figure 14shows these results for three different aging temperatures. The largest step increase in the interfacial impedance occurs after the first aging interval at 40 or 70°C and thereafter it nearly levels off. At 50°C, the interfacial impedance continues to increase for at least 8 weeks. The total increase is largest at the highest temperature [29].

Effects of Cycling on Degradation Mechanisms

The majority of the SEI forms during the first cycle of the battery, and this continues to grow slowly over the remainder of the battery's lifetime. During this first cycle, reduction reactions of the electrolyte additives occur on the surface of the active material. The chemical reduction reactions for ethylene carbonate (EC), propylene carbonate (PC), dimethyl carbonate (DMC), and diethyl carbonate (DEC) are described in Eqs. (4.1) – (4.12) in [21].

Effect of Fast Cycling

A study at Sandia National Laboratories was conducted in order to observe the effect of cycling on $LiCoO_2$ [30]. In addition to the cathode for this study being $LiCoO_2$, the anode material selected was mesocarbon microbeads (MCMB).

Cycling at two different rates, C/2 ("fast") and C/5 ("slow"), was performed, and the entropy profiles of the cycled electrodes in half-cells were subsequently measured. Cycling results (capacity vs. cycle number) for half-cells cycled at C/2 (the "fast" rate) are shown in Figure 15. The first five cycles are formation cycles, in which the charging rate was C/5 and the discharge rate was C/2. Only a small number of cycles were studied at this fast rate, so the cycling was performed in half-cells without concern for lithium dendrite formation at the anode. As shown in Figure 15, cycling capacity after 20 cycles was 20% lower than the initial discharge capacity. This represents a significant amount of cycling-induced degradation. The loss in capacity is wholly attributable to the $LiCoO_2$ electrode because the molar amount of lithium at the lithium metal electrode was in great excess of that at the $LiCoO_2$ electrode**.** Any lithium lost to side reactions at the cathode (electrolyte decomposition and electrochemical formation of passivating surface layers) would be readily replenished upon discharge with lithium from the anode. Thus, the loss in capacity at the $LiCoO_2$ cathode was due to changes in

the composite electrode or the $LiCoO_2$ itself and not simply to a depletion of electroactive lithium in the cell. The OCP and entropy (as dE/dT in mV K-1) of $LiCoO_2$ electrodes after cycling at C/2 rate are shown in Figure 16. The full ~140 mAh g^{-1} capacity was recovered during the performed thermodynamics measurements on account of the cells being charged at such a slow rate (one-hour charging steps at C/20 with open-circuit rest periods of 20-24 hours between steps, for an effective rate of ~C/500). In that case, there were only minor changes in full cell OCP after 1000 cycles at C/2 despite ~30% losses in cycling capacity. In the view of the authors of [30], the loss in cycling capacity at the C/2 rate is purely due to kinetic effects and not to a fundamental change in the thermodynamics or structure of $LiCoO_2$. Examples of kinetic degradation effects are the continued growth of the passivating layer on the cathode (which would cause increasing ohmic and transport barriers) and particle breaking or cracking (which would increase ohmic resistance and create electrochemically inaccessible regions of $LiCoO_2$).

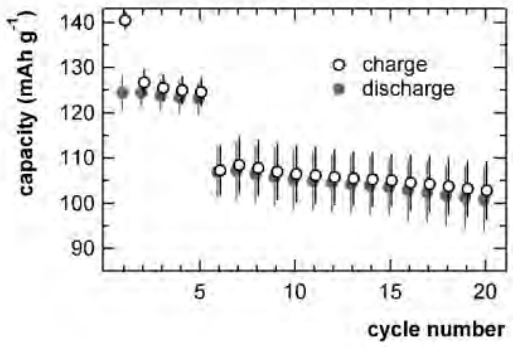

Figure 15. Specific (gravimetric) capacity of galvanostatically cycled half-cells containing $LiCoO_2$ cathodes and lithium anodes. Cycling rate was C/5 (charge) and C/2 (discharge) for the first five cycles and C/2 (charge and discharge) thereafter. [30]

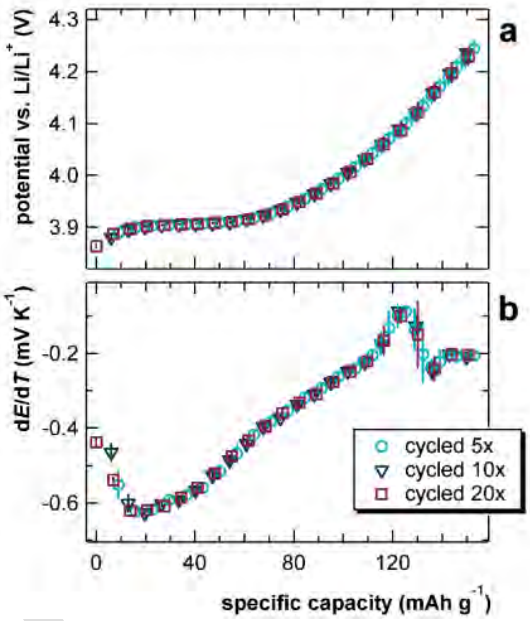

Figure 16. (a) Open-circuit potential and (b) dE/dT of half-cells containing $LiCoO_2$ cathodes and lithium anodes after cycling according to the conditions in Figure 15 (C/2 rate). **[30]**

Furthermore, Aurbach et al. [27] concluded that capacity loss in $LiCoO_2$ electrodes resulting from cycling or storage was due to surface phenomena and not structural changes. The effect of particle cracking or breaking was previously observed using transmission electron microscopy (TEM) on $LiCoO_2$ particles that had been cycled 50 times at C/5 rate or 286 times at 1C rate. Thus, the previous reports and the results reported here are all in agreement that kinetic degradation effects are a significant contributor to cycling-induced performance losses in cells with $LiCoO_2$ cathodes. [30]

Effect of Slow Cycling

For longer-term cycling experiments, a slower rate of C/5 (relative to $LiCoO_2$) was used. Capacity data for full cells ($LiCoO_2$ vs. MCMB) cycled at C/5 (the "slow" rate) are shown in Figure 17. The first five cycles are formation cycles, in which the charging rate was C/10 and the discharge rate was C/5. The use of full cells is a closer representation of commercial, rechargeable, lithium-ion batteries and allows high amounts of cycling

without concern for dendrite formation. As shown in Figure 5.5, cycling capacity after 500 cycles was 46% lower than the initial discharge capacity. The loss in capacity in these full cells is not readily attributable to either the $LiCoO_2$ electrode or the MCMB electrode because the capacities of both electrodes were roughly matched. Any lithium consumed in side reactions (electrolyte decomposition and electrochemical formation of passivating surface layers) would be irreversibly lost and at least partially responsible for the loss in cycling capacity.

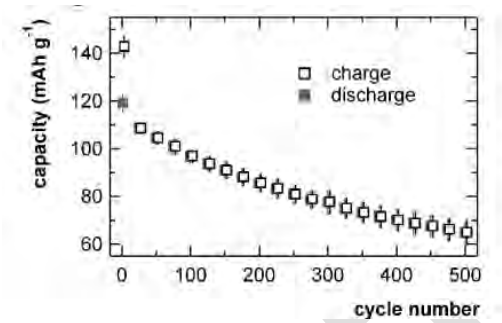

Figure 17 Specific (gravimetric) capacity of galvanostatically cycled cells containing $LiCoO_2$ cathodes and MCMB anodes. Cycling rate was C/10 (charge) and C/5 (discharge) for the first five cycles and C/5 (charge and discharge) thereafter. Markers and error bars are the average and standard deviation, respectively, of measurements from three identically prepared cells.

Studies of commercial LIB cells previously demonstrated that the $LiCoO_2$ cathode was largely responsible for voltage fade, and the graphitic anode was largely responsible for capacity fade. However, both electrodes experienced both types of performance degradation to some extent. After cycling at C/5 to the designated number of cycles (5, 200, or 500), the full cells were disassembled. The cycled LiCoO2 electrodes were rinsed in EMC and transferred to half-cells with new lithium counter-electrodes for entropy measurements. The OCP and entropy (as dE/dT) of these $LiCoO_2$ electrodes after cycling are shown in Figure 18. The OCP and entropy profiles of electrodes that were cycled five times (Figure 5.6) match those of uncycled electrodes (Figure 5.2) very closely. As shown in Figure 18, electrodes that were cycled 200 and 500 times lost a significant amount of capacity. They did not reach the 140 mAh g^{-1} full capacity even at this low effective rate of ~C/500. This suggests that a significant amount of the loss in cycling capacity of the full cells was due to degradation of the $LiCoO_2$ cathode. Some of the capacity loss could also be due to a slight loss of material in transferring the electrode from a spent, full cell to a new half-cell. Regardless of the latter possibility, $LiCoO_2$ electrodes that were cycled 500 times at C/5 and re-assembled into new half-cells had severe rate limitations. This suggests that the kinetic effects discussed above (surface resistance and particle cracking) were also a significant contributor to the performance losses of $LiCoO_2$ electrodes cycled at the slower rate of C/5. [30]

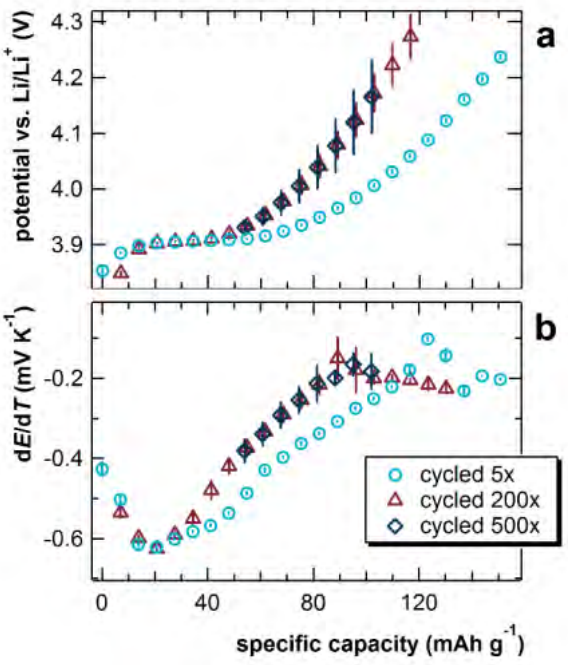

Figure 18 (a) Open-circuit potential and (b) dE/dT of half-cells containing $LiCoO_2$ cathodes and lithium anodes. The $LiCoO_2$ electrodes were cycled in full cells (vs. MCMB) according to the conditions in Figure 17 (C/5 rate), removed from the full cells, and then placed in new half-cells for the measurements in a and b. Markers and error bars are the average and standard deviation, respectively, of measurements from three identically prepared cells [31].

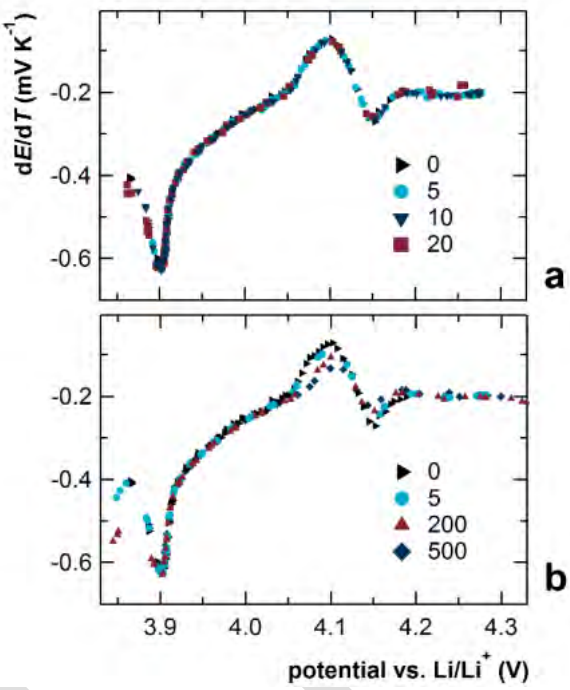

Figure 19. Thermodynamic data for LiCoO2 from Figure 16 and Figure 18 expressed as dE/dT vs. OCP (entropy vs. Gibbs free energy). The $LiCoO_2$ electrodes were cycled at (a) the "fast" rate of C/2 and (b) the "slow" rate of C/5, and the number of cycles is shown in the legends. All of the data points from three identically prepared cells for each condition (cycling rate and number of cycles) are shown individually [31].

The OCP profiles and entropy profiles of $LiCoO_2$ electrodes that were cycled 200 and 500 times appear to have retained the same general shape as those of uncycled electrodes. However, the loss in capacity with cycling resulted in a loss of resolution in the OCP curves and entropy profiles, as shown in Figure 5.6. Furthermore, the samples that experienced high amounts of cycling exhibited larger amounts of error. These factors make it difficult to determine whether there were any real changes in the thermodynamic quantities of LiCoO2 after cycling or whether the observed changes were primarily due to a loss in capacity. The two dependent variables have a unique relationship because OCP changes monotonically with the independent variable, gravimetric capacity. Thus, any changes in the thermodynamics can be observed clearly and independently of changes in total capacity. Furthermore, each replicate data point can be plotted separately (as entropy vs. OCP for an individual sample cell) rather than plotting averages of replicate samples. This results in higher-resolution data as the slight OCP variations among repeat samples result in a more continuous entropy curve. Both fast-rate and slow-rate data are presented in this manner in the following section. [30]

A study by Zhang [31] was performed to assess the effect of the charging protocol on the cycle life of a commercial 18650 Li-ion cell using three methods: (1) constant current (CC) charging, (2) constant power (CP) charging, and (3) multistage constant current (MCC) charging. These patterns are shown in **Figure 20**. Fast charging resulted in an accelerated capacity fading due to the loss of Li+ ions and the related growth of a surface layer, which was associated with metallic lithium plating onto the anode and a high polarization at the electrolyte–electrode interface. Analyses of the cell electrochemistry showed that use of a reduced current to charge the initial 10% capacity and near the end of charge, respectively, was favorable for long cycle life.

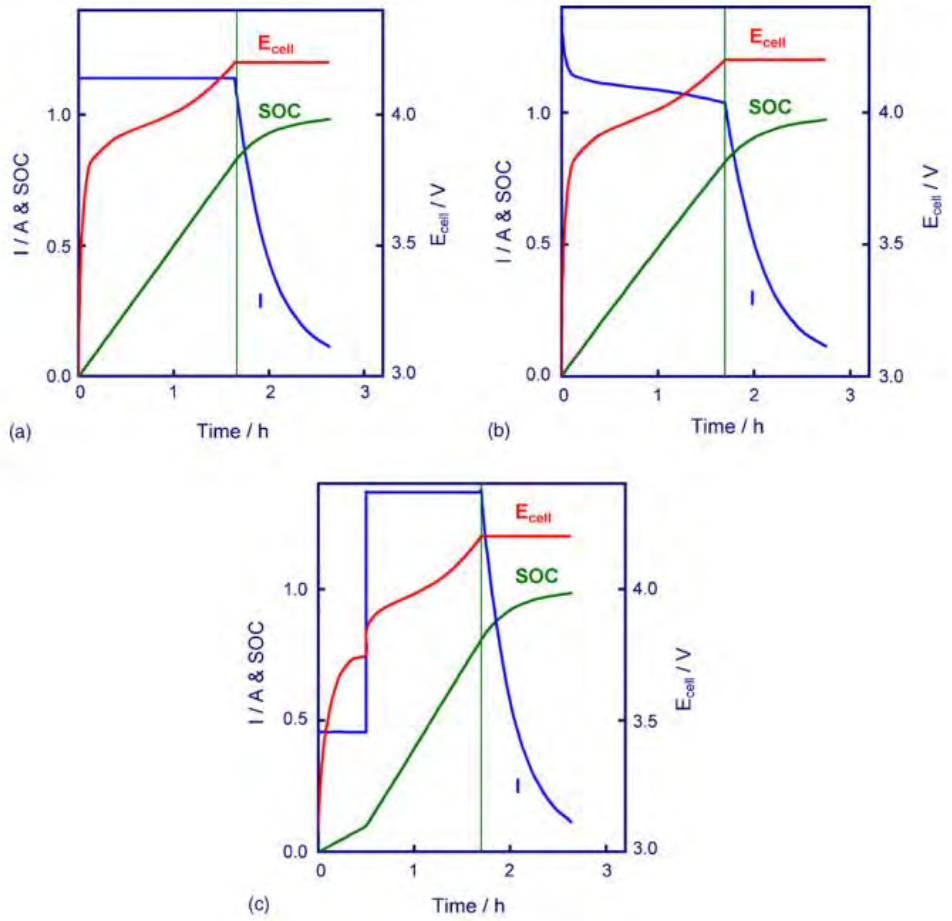

Figure 20. Characteristics of the charging protocols for a commercial 2.4Ah 18650 Li-ion cell using an averaged charging rate of 0.5C (a) Constant Current-Constant Voltage (b) Constant Power-Constant Voltage and (c) Multistage Constant Current – Constant Voltage. **[31]**

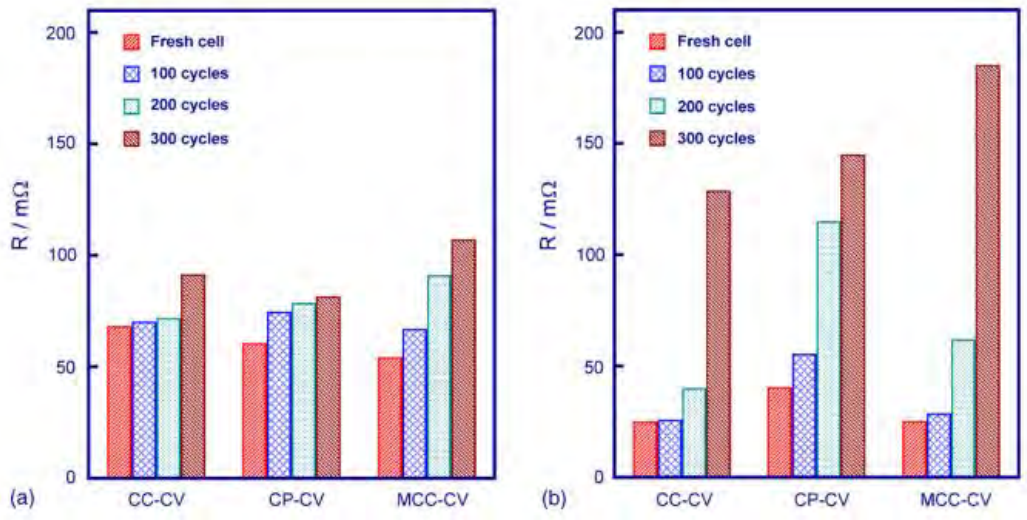

Figure 21 Comparison of the ohmic resistance (a) and charge-transfer resistance (b) for 18650 cells by different charging protocols. **[31]**

From the results of this work, it may be concluded that cycle life of Li-ion cells is significantly affected by the charging protocol even if the same charging rate is applied. A good charging protocol should strictly follow the cell chemistry. Impedance analysis shows that the cell with a low SOC (<0.1) has a much higher resistance, which suggests that a low charging rate be desirable for charging the initial 10% capacity. Potential monitoring

indicates that due to electric polarization, the potential of the graphite anode may fall to below 0 V versus Li^+/Li near the end of charging so that metallic lithium plating can occur on the anode. Although the plated metallic lithium can continue to intercalate into the graphite, it inevitably reacts with the electrolyte solvents, which not only reduce charging efficiency but also promote progressive growth of the resistive surface layer. Therefore, a low charging rate is favorable for healthy charging near the end of charging. It is shown that the capacity loss of a Li-ion cell during cycling is associated with increased cell impedance and reduced charging efficiency relating to metallic lithium plating on the anode. [31]

Effects of Depth-of-Discharge on Degradation Mechanisms

Shim et al [24] performed tests using $LiNi_{0.8}Co_{0.15}Al_{0.05}O_2$/graphite lithium-ion pouch cells which were cycled over 100% DOD at both room temperature and 60°C so as to investigate the effect of high temperature degradation mechanisms. For the cells used in their experiments, they were subjected to a formation cycle by charging and discharging at a rate of C/25, which allowed for the initial SEI layer to form smoothly. Following this procedure, the cells were charged to 4.1V and held at this voltage until current dropped below C/20 or for two hours, whichever came first. Discharging was performed with a constant current until 3.0V was reached, considered to be 100% DOD.

Cycling of the cells was conducted as follows: 10 cycles at C/5, C/2, C, and 2C. Following cycling at these rates, the cells were subjected to 100 cycles at a rate of C/2. Each cell underwent a total of 140 cycles. The capacity losses are shown in Figure 22.

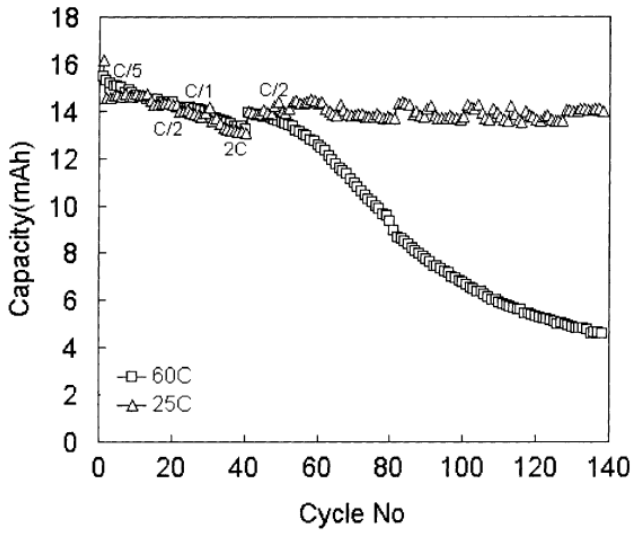

Figure 22 Cycling performance for pouch cells at 25 and 60°C. Cut-off voltage 3.0-4.1V [24]

As much as 65% of the initial capacity was lost after 140 cycles at 60°C. The authors of [24] concluded that the loss of cycling capacity and the rise in impedance in the cathode of the cell which was cycled at 60°C was due to a low-conductivity SEI layer forming on the cathode.

Effects of Overcharging and Overdischarging

The overcharge of lithium-ion batteries of all types leads to some undesirable processes, which result in irreversible degradation of lithium-ion batteries and a subsequent decrease in the capacity and energy density [26].

As a result of overcharge of the negative carbon electrode there occurs the deposition of metallic lithium onto it. The main reason for the said process is, as a rule, an exceedingly great excess of lithium in lithium-ion battery at the expense of unbalanced initial ratio between weights of positive and negative electrodes. When such an unbalanced lithium-ion battery is being charged, the potential of the positive electrode fails to reach its normal state and remains far more negative. As the control parameter for the polarity change and for the passing to a regime of discharge is the potential difference between positive and negative electrodes, and this difference of potentials in the case of electrodes unbalanced with respect to lithium is below nominal, the charging process still continues after the negative electrode reached a state saturated with respect to lithium. Another reason for overcharge of the negative electrode is a forced charging, which leads in some cases to overpolarization of the negative electrode ([67] from [26]).

The lithium that was deposited on the negative carbon electrode rapidly reacts with the solvent to form on the surface of the negative electrode a film covered by a film of salt (Li_2CO_3 and LiF [68] from [26]) and other products. The film blocks the pores in the carbon electrode and diminishes the magnitude of its working surface area, which leads to a decrease in the activity of the negative electrode and to the capacity degradation.

The number of electrochemical and chemical reactions that proceed on an overcharged positive electrode is quite large. The reactions depend on particular conditions: the electrode material, the electrolyte composition, the temperature, and so on. An overcharge may lead to the capacity loss because of the formation of an inert material, for example, Co_3O_4 in the case of a cathode of lithium cobaltite [69] from [26]; $LiNi_2O_4$, in the case of a cathode of $LiNiO_2$ [69] from [26]; and a compound of di-or tetravalent Mn in the case of a cathode of $LiMn_2O_4$ [70] from [26].

The high potentials (sometimes in excess of 4.5 V),which are realized in conditions of overcharge on positive electrodes, may lead to exothermic reactions of oxidation of organic solvents with the formation of gaseous and insoluble solid products (in particular, Li_2CO_3) which block the electrode pores [71]. The combination most stable against the oxidation happens to be a mixture of EC with dimethyl carbonate (DMC) [72].

Leising et al. ([15] from [26]) were analyzing the behavior, in conditions of overcharge, of model cells of three types, specifically, graphite/$LiCoO_2$, Li/$LiCoO_2$, and Li/graphite. Comparing the heat evolution in the said cells, the said authors established that the main source of the heat evolution in LIB is the reactions that proceed on the positive electrode (in this particular case, based on lithium cobaltite).

Overcharge and overdischarge (voltage reversal) of rechargeable batteries can occur if the control electronics of the charging station or the battery pack control electronics in the BMS malfunction or if severe cell imbalance occurs in a battery pack. [67]

Overcharge and overdischarge of rechargeable cells and batteries can occur due to charger failure or cell imbalance within a series/parallel connected battery. During charge, if several cells are connected in series and one has a higher SOC than the others do, it will reach full charge before the others. If the charger is designed to charge series strings (rather than individual cells), as the string reaches full charge, the cell will be overcharged. If overcharge occurs, a cell becomes more unstable and creates additional safety problems because it will have poorer thermal stability compared to un-abused cells (see Figure 28). Modern sophisticated BMS instrumentation can be programmed to detect and avoid this condition. Likewise, during discharge of a battery pack, if one cell has a slightly lower beginning voltage or lower capacity than the others do, it will reach full discharge before the others. If the string is then forced to continue discharging—a situation that can occur if system electronics are not sufficiently smart to identify the condition—it will discharge below 0.0 V into a state of “overdischarge” or “voltage reversal.”63 This will usually highly degrade the battery’s ability to be recharged. Prolonged exposure to this condition (depth of reversal) can lead to safety problems, such as evolution of hydrogen and oxygen gases in large amounts sufficient to cause cell venting or metal plating on the

cathode. In systems where multiple cells are used, a common quality-control standard condition is to use cells that have been matched to within ±5% cell capacity.

The ability to withstand overcharge depends strongly on the current level (low charging current is more likely to result in benign failure) as well as the chemistry of the battery. Aqueous electrolyte systems (e.g., lead-acid, nickel/cadmium, and NiMH) are relatively insensitive to overcharge because after 100% SOC is reached, additional current drives the electrolysis of water (which produces hydrogen and oxygen) and limits the maximum voltage that the cell experiences. Cells with an aqueous electrolyte may contain catalysts to recombine the H2 and O2 evolved during overcharge to reform water, which will minimize the accumulation of potentially explosive gas mixtures. However, this feature is not widely used in commercial lead-acid batteries and the prevalence of lead-acid battery explosions during charging is the major contributor to more serious injuries attributable to batteries.

Li-ion and Li-polymer cells have poor response to overcharge abuse when compared with aqueous electrolyte cells because they do not have the protection of water electrolysis as an energy sink. In part, this poor response results from the higher energy content, more reactive electrode materials, and flammable electrolytes that create the potential for thermal runaway during the overcharge event.

The response of cells and battery packs during overcharge depends on overcharge parameters (current, maximum voltage), thermal environment, and cell materials and is a complex function of several failure mechanisms.65 Extended overcharge can result in cell heating that initiates internal decomposition reactions of the electrodes and electrolyte that lead to thermal runaway.

In addition, increased cell temperatures can result in melting of the separator material and subsequent internal shorting of the cell. This behavior is particularly problematic for shutdown separators that result in high-cell impedance at shutdown. For a single cell or a series configuration of cells, the charging power supply will apply the full compliance voltage across the single cell after separator shutdown occurs. Many separator materials have been observed to fail immediately or within a short time after shutdown in this condition, as shown in Figure 10. [67]

The thermal response of Li-ion cells during overcharge is largely determined by the cathode chemistry. During the charge cycle, lithium is removed from the cathode oxide material. Different cathode oxide chemistries have different levels of lithium when fully charged, varying from $Li_{0.5}CoO_2$ to $Li_{0.0}FePO_4$ at 100% SOC. Overcharging continues to remove lithium from the structure, resulting in permanent crystallographic changes and increased oxidation potentials. Measurements of heat flow from the cells and cell skin temperature during overcharging has shown that there is a rapid increase in heat generation when all of the lithium has been removed from the cathode.

If the stability of the cathode becomes sufficiently good, other problems can become the determining factor in cell stability. For example, cells made with lithium iron phosphate cathode materials have the best thermal stability and overcharge stability. $LiFePO_4$ is thermally stable up to 250°C and does not evolve oxygen. The lithiated anode is still a significant source of energy. At high temperature, the SEI protective layer decomposes, exposing the lithiated carbon to the electrolyte. Reduction of the electrolyte can generate sufficient heat to cause a thermal runaway reaction with associated gas generation, venting, and possible fire. The electrolyte itself breaks down above 160°C, generating sufficient gas volume to cause cell venting.

Yamaki and coworkers demonstrated that overcharge response of a lithiated graphite (LiC_6)/$LiMn_2O_4$ cell depended on charge current; at low current, overcharge test results were benign, but at high current levels, the cells entered thermal runaway. Lithium plating on the anode is a possible failure mode during fast charge at low temperature. Lithium plating has the potential to create a finely divided lithium powder within the cell that may

become electronically isolated from the anode. In addition, dendrites of lithium may grow from the anode through the separator, possibly resulting in an internal short circuit. This situation, if it arises, creates a safety vulnerability that could persist after the overcharge event terminated. [67]

Conclusions

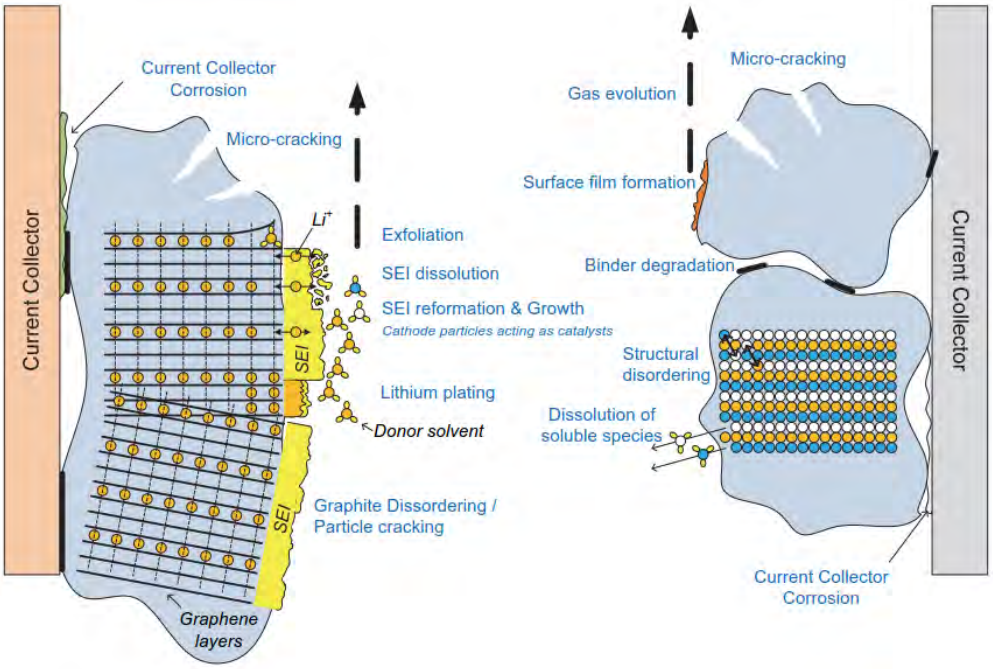

Figure 23 Aging mechanisms occurring at Li-ion battery electrodes **[32]**

The aging of Li-ion batteries is complex and determined by the operating conditions. In some cases it is possible to assign the observed capacity and power fade to a certain aging process. This is typically the case when the battery is used under extreme conditions such as elevated temperatures, high rate charging, or high SOC levels. However, in most applications where the conditions are controlled to optimize the total life the observed performance fade is the result of several processes of which some are coupled and others can be regarded as independent.

Generally, the capacity fade of Li-ion cells is due to a combination of three main processes:

- Loss of Li / loss of balance between electrodes
- Loss of electrode area
- Loss of electrode material / conductivity

The loss of cyclable lithium is in turn due to side reactions such as corrosion, Li-plating and solid electrolyte interface (SEI) formation at the graphite anode.

Since the graphite anode is the most widely used in present Li-ion batteries this study has set a particular interest in this electrode material. In contrast the aging properties of the cathode electrodes must be discussed from case to case depending on the particular cell design.

In addition, aging mechanisms that reduce capacity may also lead to changes in surface properties such as porosity and tortuosity. In this reasoning it is important to state that the available capacity might be reduced further by an increased voltage drop due to a rise in cell impedance that prevents the battery from being fully discharged (or charged) at a specific current. In most cases the capacity fade and impedance rise are clearly

correlated. The aging processes are further complicated by the fact that many of the studied mechanisms are coupled to a rise in cell impedance, leading first and foremost to a notable reduction in maximum cell power.

An overview of the most significant mechanisms for power fade / impedance rise is summarized by the following bullets and Figure 2.4:

- Surface film formation of both electrodes with low conductivity
- Loss of electrode area and electrode material leading to a higher local current density
- Lower diffusivity of lithium ions into active electrode particles and slower kinetics (increased charge transfer resistance) due to surface films
- Reduced conductivity between particles due to both surface films and degradation of binders, possibly in combination with a binder-Li reaction

A summary of the main electrode aging mechanisms, mainly described by Vetter et al. [18], is presented in **Figure 23**. Here, aging mechanisms can be categorized into mechanical changes (particle cracking, gas formation), surface film formation (SEI, lithium plating), bulk material changes (structural disordering), and parasitic reactions (binder degradation, localized corrosion).

The aging mechanisms at the electrodes are directly dependent on the choice of the electrode material. However, there are several similarities between different electrode materials.

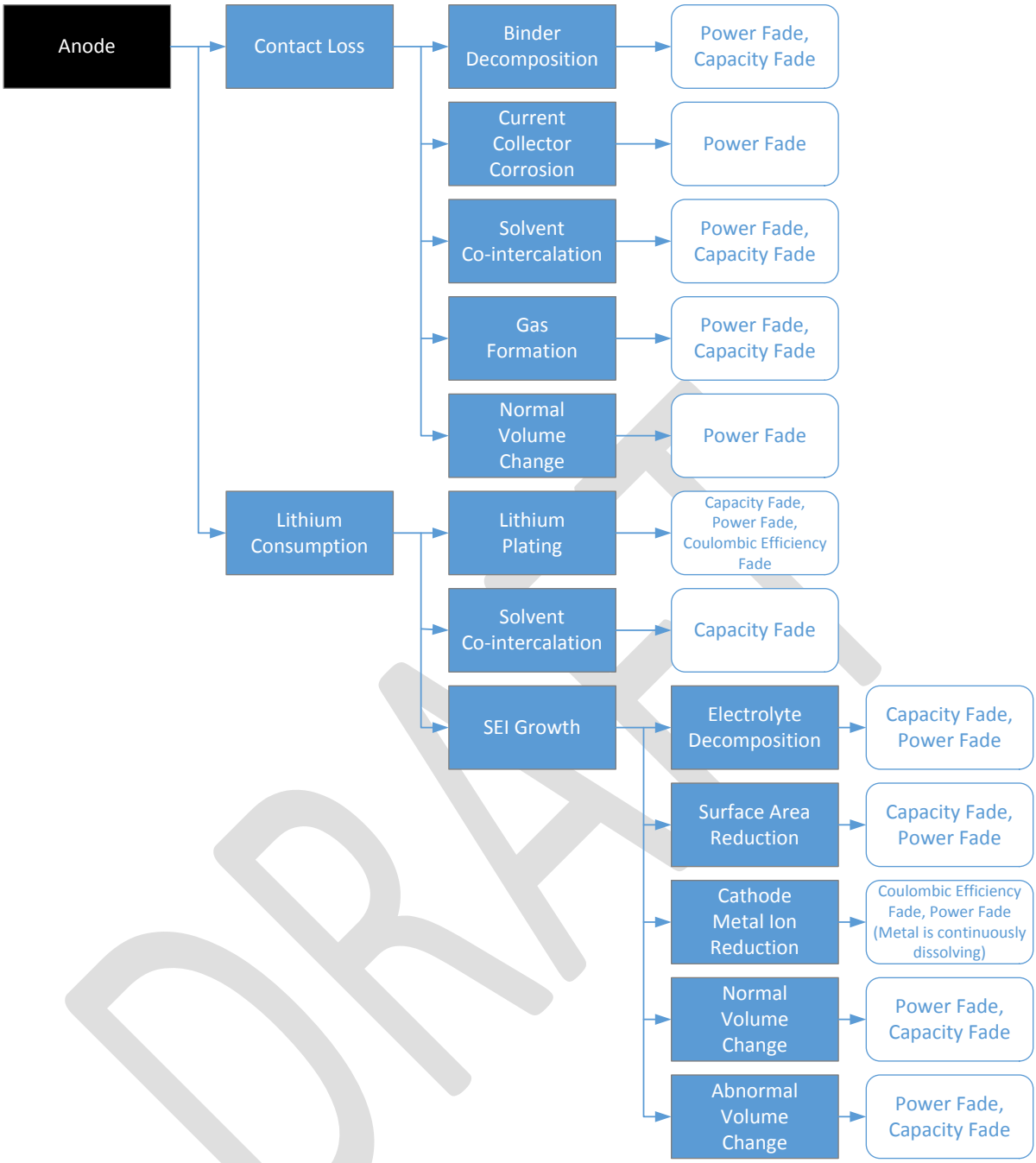

Figure 24 Degradation Mechanisms of the Anode **[21]**

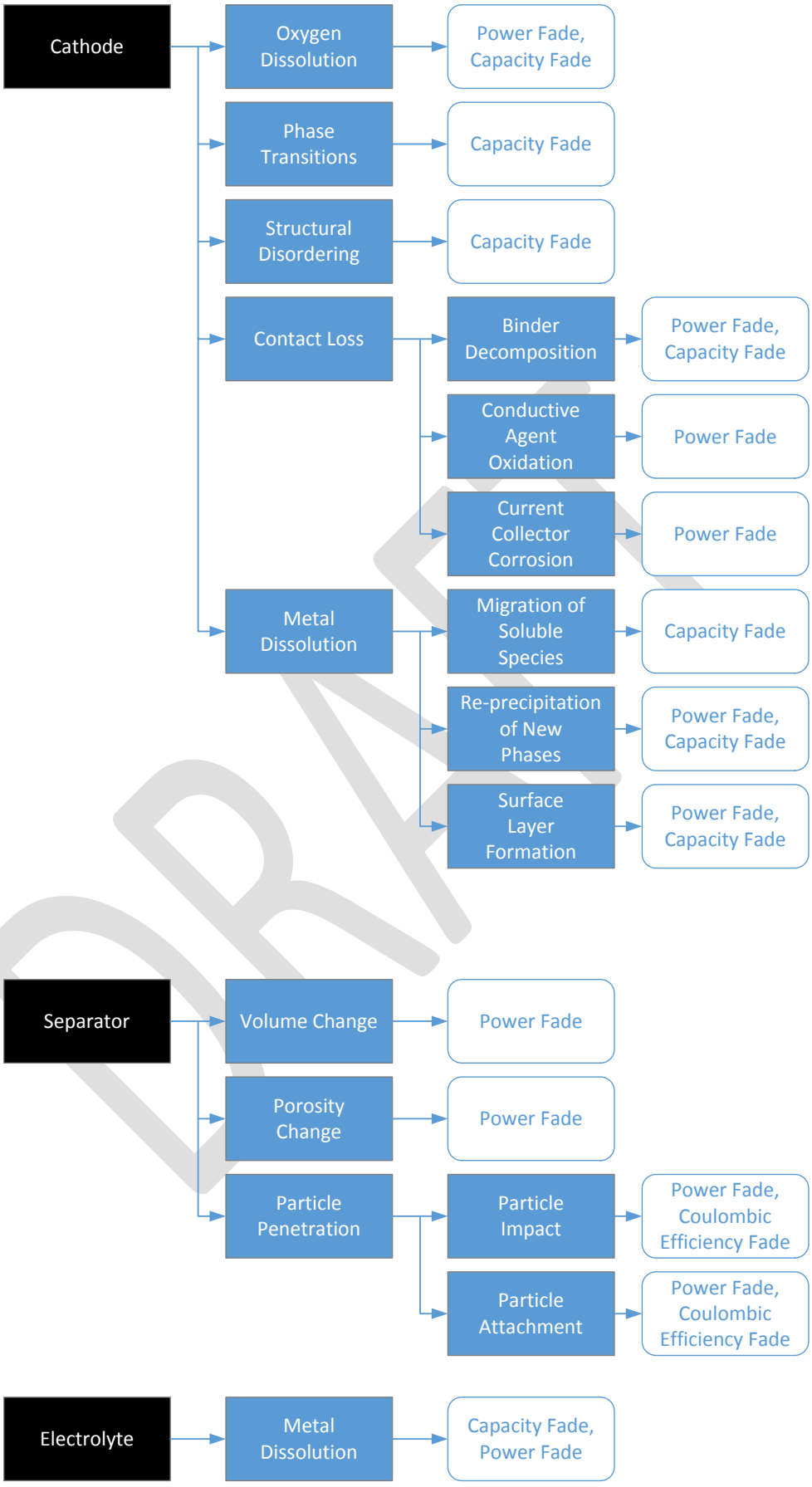

Figure 25 Degradation Mechanisms of the Cathode, Separator, and Electrolyte **[21]**

Testing Activities and Methodologies for Evaluating xEV Battery Durability

Introduction

In the previous section we have examined some of the electrochemical degradation mechanisms which affect battery durability in the various chemistries utilized for xEV applications. Although the studies from which such information comes involve testing, we now will focus on testing and evaluating durability at a vehicle-level or under vehicle-like conditions. In addition to road and dynamometer tests of vehicles, we shall also investigate laboratory tests of xEV batteries subject to simulated load conditions and model-based studies using vehicle and battery models derived from physical, empirical, and semi-empirical data.

We attempt to show here studies grouped by critical factor, whether it be charging patterns, cycling, depth-of-discharge, or climate and thermal effects. However, none of these factors may be treated as wholly independent of one another due to the nature of the batteries being evaluated. Some studies are multi-variate, changing charging rates and temperature to

Charge Patterns and Optimization

A study carried out by the University of Toledo [33] utilized a Li-ion battery model (as described by Eq.'s (8) – (15) in [33]) for evaluating Level 3 or Fast Charging on PHEVs with electric ranges of 10 and 40 miles.

Level	Location	V and I	Power (kW)	Approx. time to charge
1	Residential	110V, 15A	1.4	18 Hours
2	Residential / Public	220V, 15-30A	3.3	4-8 Hours
3	Commercial	480V, 167A	50-70	20-50 Minutes

Table 6. Charging Topologies **[33]**

Lacey et al. [34] examined charging under three scenarios: uncontrolled charging, delayed charging, and V2G. These are described thusly:

- Under uncontrolled charging, the EV is charged up to 80% SOC upon being connected to charging at 6:00pm. The battery then holds this SOC until 8:00am on the following days.
- Under a delayed charging scenario, the EV remains at 40% SOC from 6:00pm until the time when it needs to charge for the next trip at 8:00am.
- In a V2G scenario, the EV is discharged to the grid from the point in time in which it is connected to the grid (6:00pm) until its SOC reaches 10%. It remains at this minimum until it is charged for the next trip at 8:00am. The resting SOC is therefore 10%.

	Charge only (3kW)	Delayed charge (3kW)	Charge only (7kW)	Delayed charge (7kW)	V2G (3kW)	V2G (7kW)
Average SOC	56.5%	51.6%	54.2%	34.6%	32.2%	27.2%
Change in SOC	40%	40%	40%	40%	70%	70%
C/D rate (A)	7.50	7.50	17.50	17.50	7.50	17.50
Degradation after 1000 cycles (%)	4.54%	4.46%	8.00%	7.71%	4.19%	7.63%
Degradation after 8 years (%)	13%	13%	23%	23%	12%	22%
Lifetime (years)	12.1	12.3	6.8	7.1	13.1	7.2

Table 7 Degradation factors for the different scenarios **[34]**

The effect of degradation due to fast weekly fast charging coupled with uncontrolled slow charges of 3kW or 7kW is shown in Table 8.

Battery charging pattern				Degradation	
Home charging per week		Fast charging per month		After 1000 cycles	Time (years) to 80% of new capacity
3kW	7kW	23kW	50kW		
6	0	0	0	1.5%	13.77
6	0	4	0	3.3%	6.09
6	0	0	4	5.7%	3.52
0	6	0	0	2.5%	8.01
0	6	4	0	4.3%	4.62
0	6	0	4	6.7%	2.97

Table 8 Effect of weekly fast charging on battery degradation in comparison with uncontrolled domestic charging **[34]**

The results from [34] demonstrate the effect of fast charging on battery degradation and lifetime. Even in **Table 7** we see that charging at 3kW leads to a lifetime in excess of 10 years, going as far as to be in excess of 12 years for each of the 3kW cases, whereas with 7kW charging the battery lifetime is approximately 7 years or less. With fast charging at 23kW or 50kW, degradation is markedly faster, with the worst case shown being a combination of 7kW home charging with weekly fast charging of 50kW, resulting in a lifetime of less than 3 years [34].

Bashash et al. [35] examined the problem of charge pattern optimization with PHEV applications for the purpose of optimizing energy cost and battery life. Specifically, they sought to simultaneously minimize (i) the total cost of fuel and electricity and (ii) the total battery health degradation over a 24-h naturalistic drive cycle.

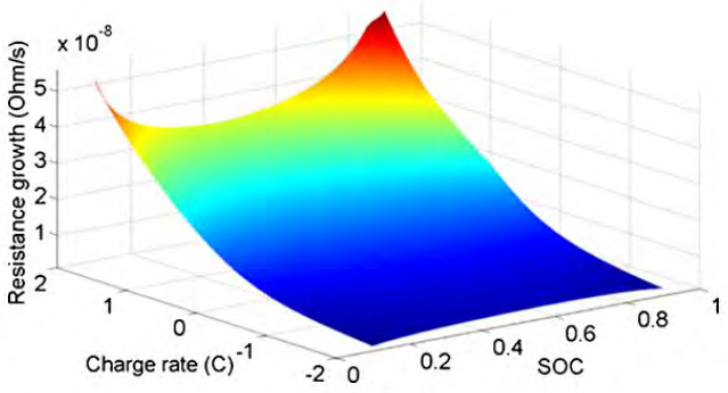

Figure 26 Battery degradation map **[35]**

To analyze degradation characteristics, the authors of [35] initialized their model at different SOC levels and applied currents at different rates to charge and discharge the battery. Average resistance growth is monitored. Figure 26 depicts the obtained map for an SOC range of 10–90% and a charging rate of −2C to 2C, with negative sign indicating discharge. The degradation map shows that at the low and high SOC ends the battery tends to degrade faster, especially when it is subject to high-rate charging. Additionally, battery degradation takes place at a slower pace during charge depletion, compared to charging or storage. [35]. The optimization procedure is performed using the NSGA-II genetic algorithm. Some of the optimized solutions are shown in Figure 28.

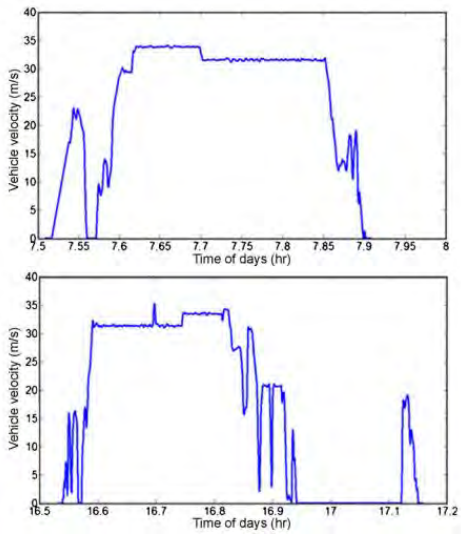

Figure 27. A sample suburban naturalistic drive cycle with two half trips, one in the morning and one in the afternoon (vehicle velocity is zero during the rest of the day) [35]

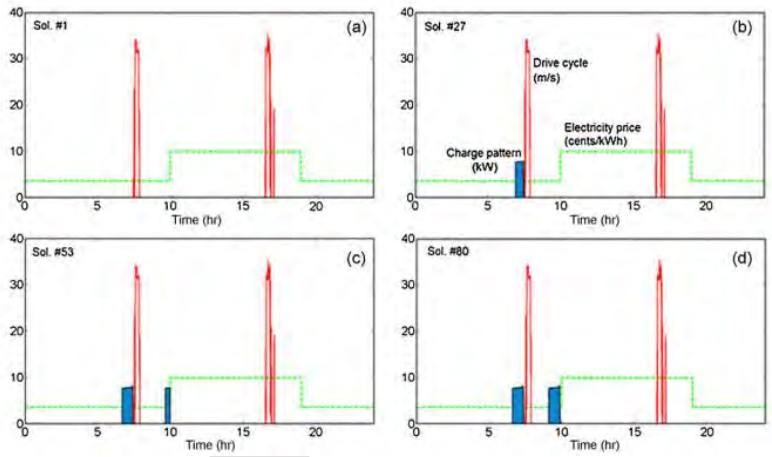

Figure 28. Four sample optimal PHEV charge patterns corresponding to: (a) Sol. #1 (least battery degradation), (b) Sol. #27, (c) Sol. #53, and (d) Sol. #80 (least energy cost). The red drive cycle spikes represent the drive cycles described in Figure 27 **[35]**.

The authors of [35] describe their obtained solutions thusly:

- The first solution shown, depicted in Figure 28(a) corresponds to the least battery degradation solution. There is no charge added to the battery, and thus, the SOC remains at the lowest limit for all time. The battery receives no external charge, and the PHEV operates as a conventional HEV.
- The second selected solution, i.e., Sol. #27, trades off the energy cost and battery health objectives with more preference towards battery health. As depicted in Figure 28(b), a charge amount of about 50% is added to the battery before the first trip only, and the charging is delayed until before the start of the trip. The reason for this delayed charging is to avoid the unnecessary degradation due to storage at high SOCs, and the best way to achieve this is to deplete the battery soon after charging.
- Solution #53 also trades off the optimization objectives, but with more weight on energy cost. As seen from Figure 28(c), both trips include charging, with the first trip receiving full charge (65%) while the second one receiving about 30% added charge. The first charging is delayed until the first trip departure time, while the second charging is delayed until the time of transitioning to on-peak electricity pricing. Therefore, PHEV charging takes place during off-peak hours only.
- The last solution, i.e., Sol. #80, corresponds to the charge pattern that results in the least energy cost. The only difference between this solution and Sol. #53 is that the PHEV receives full charge before both trips.

In another study by Hoke et al. [36], the focus on charging optimization was strictly on extending battery lifetime. The charge optimization method seeks to minimize the effects of three factors that lead to battery degradation: temperature profile, daily charge cycling (depth of discharge), and state of charge profile. To obtain driving data, a typical driving week for a Toyota Prius PHEV was sampled at 1Hz. This included five days of commuting 26-40 km (16-25 miles) round-trip, one longer trip of 65 km (40 miles), and one day on which the vehicle was not used [36]. Five charging scenarios are considered:

1. Full nightly charging at 6.6 kW (SAE level 2) to 90% SOC upon plug-in, without regard for battery degradation.
2. Full nightly charging to 90% SOC, with charge power profile optimized to reduce battery degradation.
3. Partial nightly charging as needed to provide for the next day's driving, optimized to reduce battery degradation. An ideal ability to perfectly predict the next day's energy requirement is assumed.

4. Partial nightly charging as needed to provide for the next day's driving with 16 km (10 mi) spare range, optimized to reduce battery degradation.
5. Partial nightly charging as needed to provide for the next day's driving one hour before departure and with 16 km spare range, optimized to reduce battery degradation.

The state of charge profiles for these scenarios are shown in **Figure 29**.

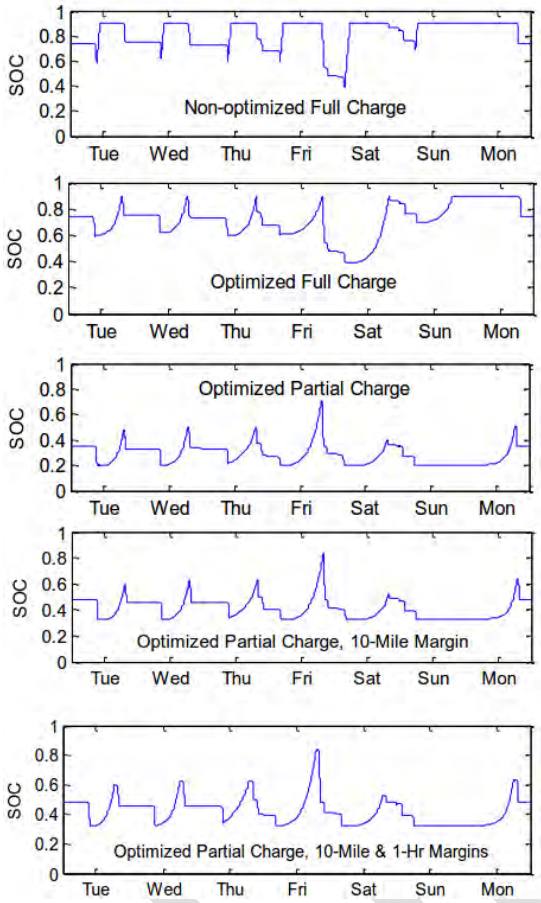

Figure 29 Weekly SOC profiles for the four charging methods. Horizontal axis labels indicate the beginning (midnight) of each day. **[36]**

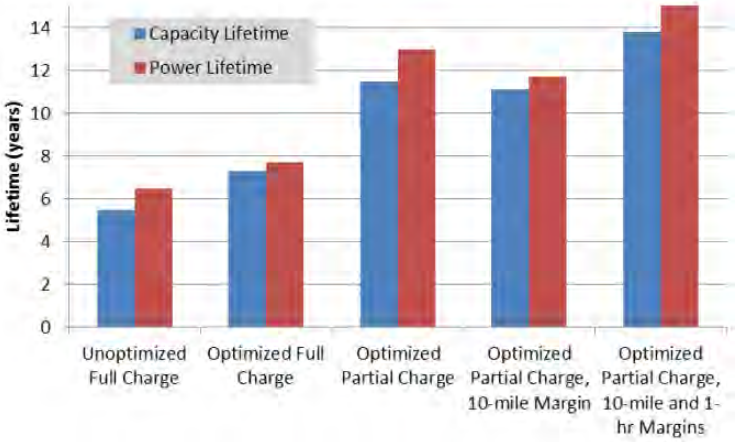

Figure 30 Comparison of battery energy and power lifetimes under the five charging scenarios. One power lifetime result over 15 years is truncated. **[36]**

As part of a NREL study, Neubauer and Wood [37] sought to assess the impact of realistic fast charging scenarios on BEV batteries, including thermal and degradation effects. The model-based experiment was conducted over a simulated 10 years of battery simulators for 180 driving profiles with added conditions for Level 2 home charging and Fast Charging station availability in two different climates (Seattle, WA and Phoenix, AZ). Additionally, the effects of battery thermal management systems were evaluated in three grades: passive cooling, high-power liquid cooling (active during driving), and high-power liquid cooling (active during both driving and charging).

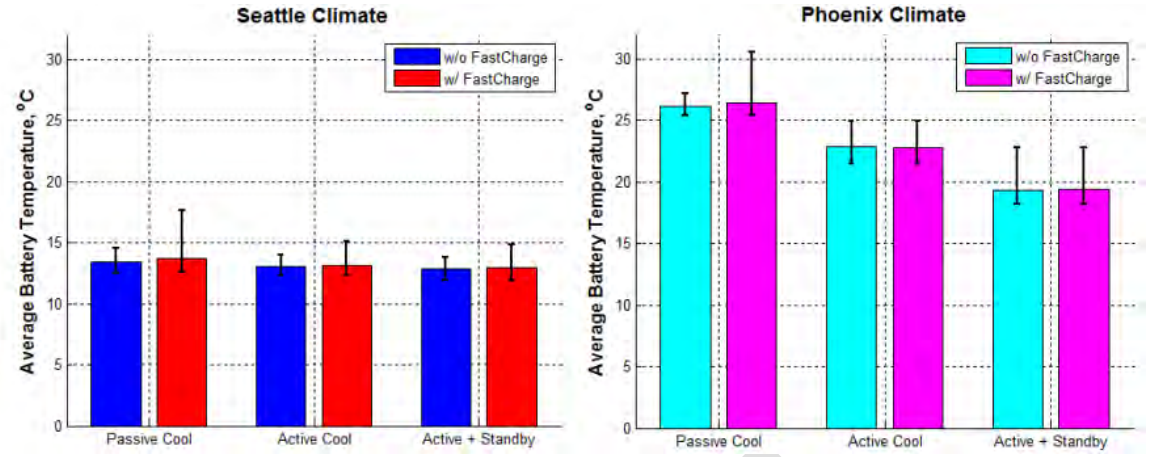

Figure 31 Effect of DCFCs and BTMSs on average battery temperature in Seattle (left) and Phoenix (right) **[38]**

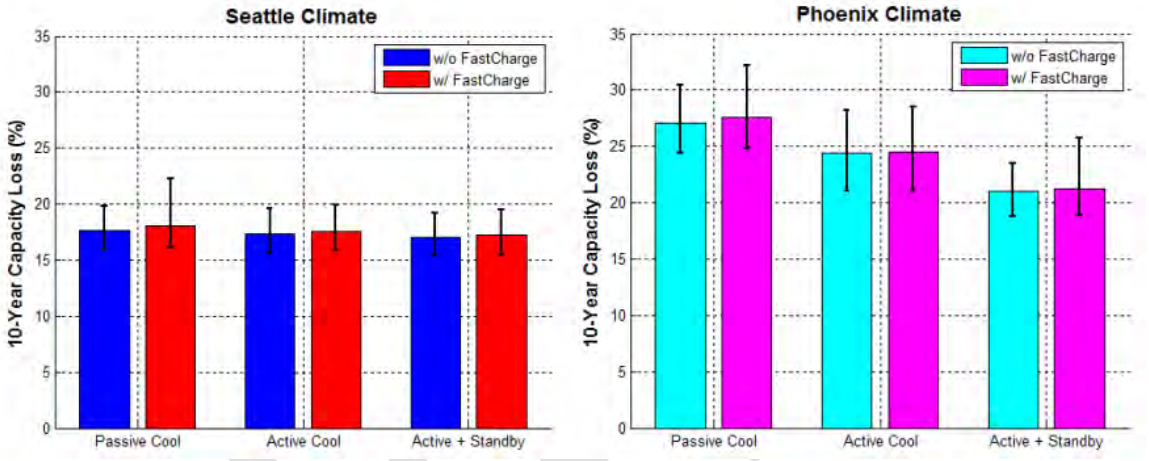

Conclusions from the study were that aggressive active battery cooling is important for constraining maximum battery temperatures, particularly for long fast-charge-enabled tours in hot climates, active battery cooling can also positively impact battery lifetime in hot climates when utilized while parked at a charger in addition to while driving [37]

A study by Krieger [8] presents a comparison of lead-acid, LCO-NMC, LCO and LFP cell degradation when charged with a wind-based current profile to evaluate the impact of variability on cell aging and consider alternative battery chemistries for off-grid renewable projects. Despite the goal of the author to apply these methods toward off-grid renewables, the effects observed here are nevertheless of relevance to automotive applications and offer comparisons of a wide range of battery chemistries utilized in automotive applications.

To perform a study on battery aging under variable conditions, Krieger [8] used the wind profile of a 150W wind turbine to collect 600 seconds worth of output current data with a resolution of 1s. The output sequence ranged from 0A to 6A with an average of 1.4A, as shown in Figure 32a. For the study, this pattern was scaled such that the average charging current was C/5 for any cell, with the maximum current pulse being roughly 0.8C. This pattern was repeated until the battery was fully charged.

This wind profile is modified for the assessment of the impact of degradation as shown in Figure 32b. This is the same profile as in Figure 32a, but with 10s sampling as opposed to 1s, thereby creating what Krieger refers to as a low-frequency wind profile. This effectively becomes the drive cycle for this study.

Additional profiles are created by using sampling steps of 0.1s, shown in Figure 32c and a smoothed profile using a 5s moving average of the wind turbine output current, shown in Figure 32d, to replicate the smoothing from an ultracapacitor. The reasoning behind these modifications to the profile is in order to determine whether or not capacity fade is affected by the frequency of the oscillations, the power distribution, or both.

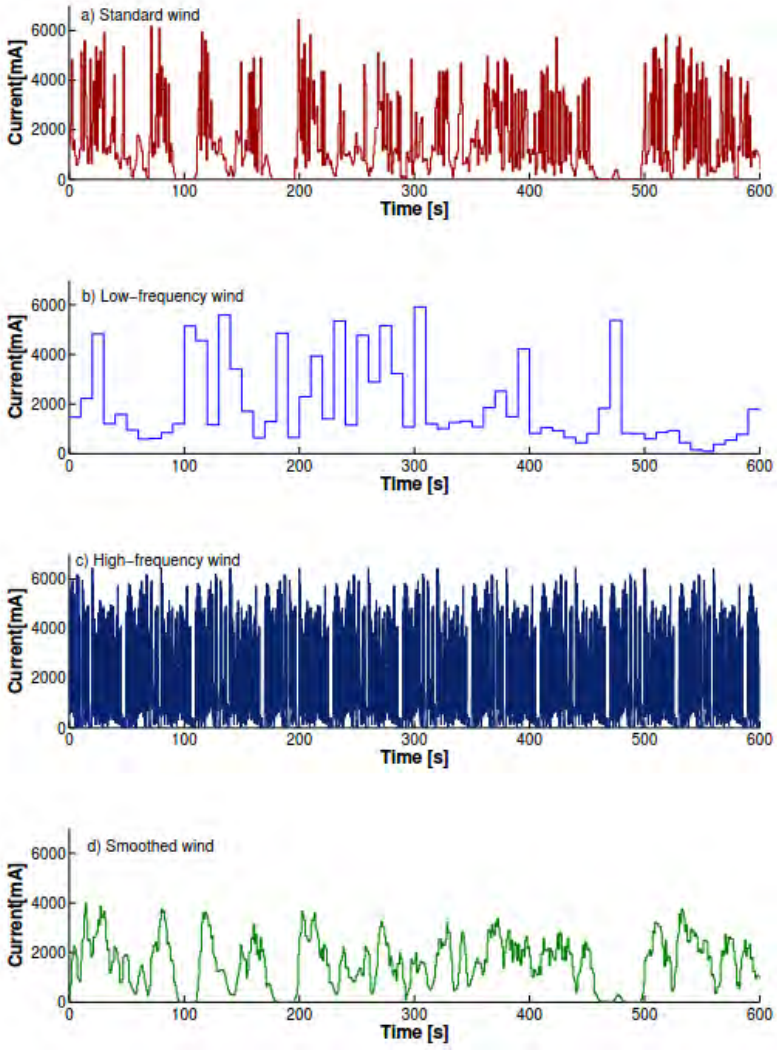

Figure 32: 600s data series of the a) standard wind, b) low-frequency wind, c) high-frequency wind, and d) smoothed wind current profiles, derived from the output current of a 150W wind turbine **[8]**.

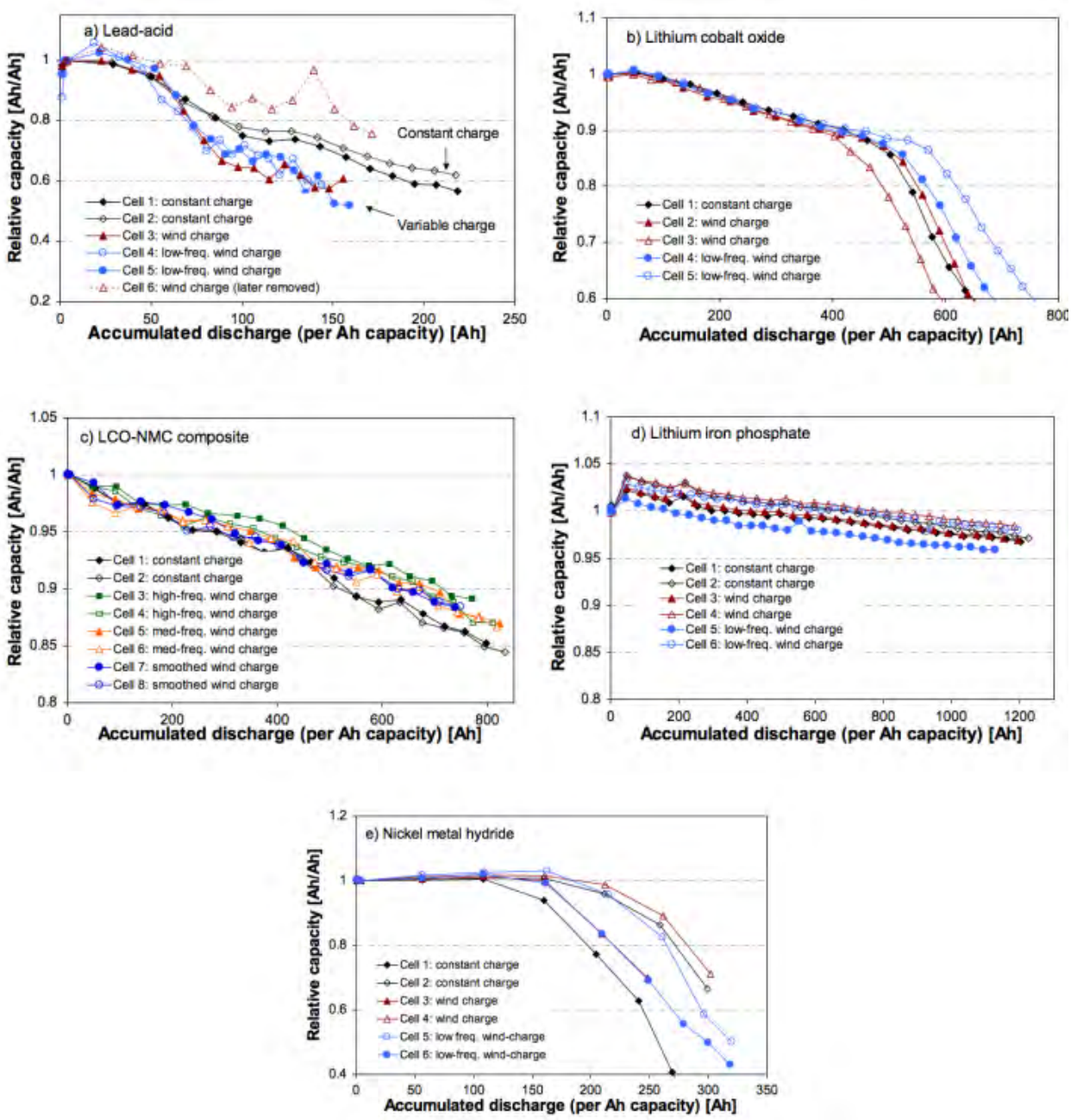

Figure 33. Capacity fade as a function of normalized discharge throughput in a) lead-acid, b) LCO c) LCO-NMC d) LFP cells and e) NiMH cells. **[8]**

Capacity fade in the lead-acid cells as a function of normalized accumulated discharge Ah is given in Figure 33a. The cells demonstrated a significant amount of variation, which the author of [8] attributed to both internal characteristics as well as fluctuations in ambient lab temperature. One cell charged with the standard wind profile exhibits erratic behavior and, while plotted in Figure 33a, was not considered in subsequent analysis. The cells charged at a constant rate show less degradation per processed Ah than the cells charged at a variable rate with the wind and low-frequency wind profiles.

Unlike the lead-acid cells, the LCO and LCO-NMC cells showed no aging benefit from the constant-charge profile. In Figure 33b, LCO cells charged with the low-frequency wind profile showed the least capacity fade, but these results may be within the noise of the system. In Figure 33c, the LCO-NMC cells charged at a

constant rate appear to lose capacity faster than those charged with any of the wind-based profiles, but the degradation trends have yet to fully differentiate after only 15% capacity loss. [8].

The LFP cells, shown in Figure 33d, show little aging after over 1200 cycles and nearly 1000 processed Ah per installed Ah. Capacity fade ranges from 1% to 3% loss from initial capacity. While the cells vary in total measured capacity fade, Krieger notes that this variance does not appear correlated with charge protocols and occurs primarily over the first fifty cycles; after this point, the degradation rate of all cells are similar. No variation in capacity fade between charge protocols could be identified from these plots.

The results of the capacity fade tests in the NiMH cells, seen in Figure 33e show no clear trends. After approximately 150 cycles, three of the batteries begin to rapidly lose capacity, and three maintain their capacity longer, but there is no correlation with battery charge profile. Krieger hypothesizes that the charging protocol for the NiMH results in overcharge, which is known to contribute heavily to NiMH degradation [39], due to the difficulty of ascertaining "end-of-charge" in these cells. Variations in the degree of overcharge due to the difficulty of test procedure standardization may result in the irregular degradation rates observed.

The discharge voltage curves for the standard wind-aged lead-acid, LCO, and LCO-NMC batteries are shown in Figure 34 along with a medium-frequency wind charged LCO-NMC cell, whose protocol most resembles the standard wind profile for this chemistry; the data plotted in these curves is collected following a full charge from a capacity test. The evolution of these curves highlights the relative aging mechanisms of these cells. Active material loss in all lithium-based cells is likely attributable to loss of cyclable lithium.

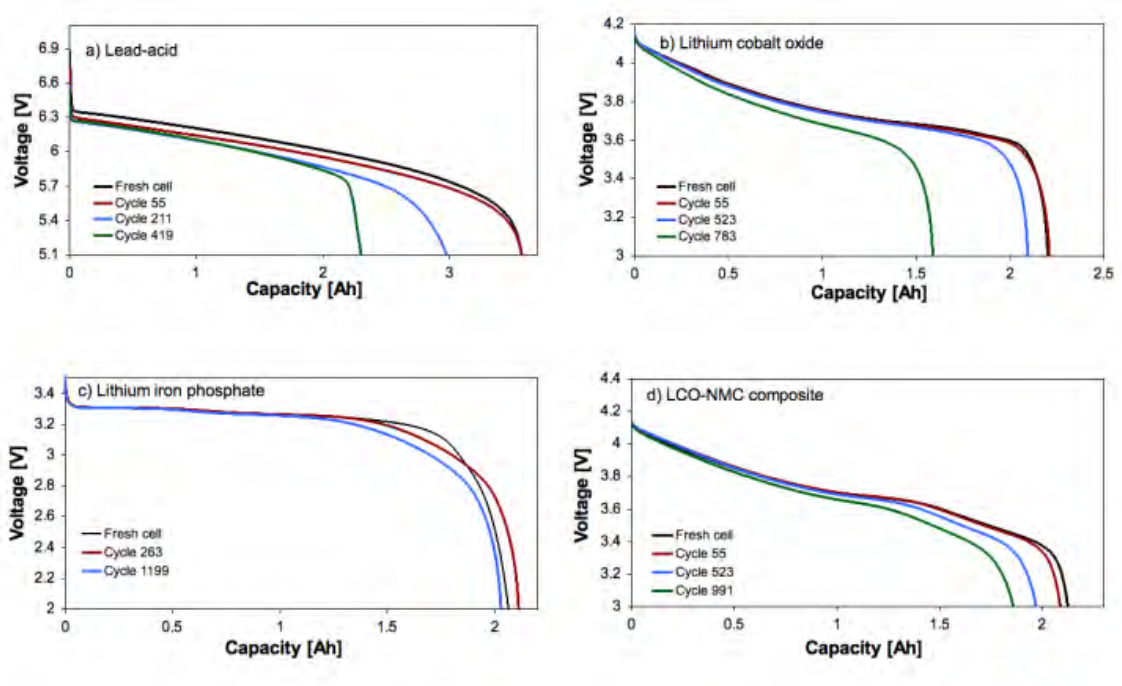

Figure 34 Discharge voltage curves after capacity tests in wind-aged a) lead-acid, b) LCO c) LFP and d) medium-frequency wind-charged LCO-NMC cells (Figure 4.2 from source) **[8]**.

The lead-acid cells studied show rapid capacity fade characterized by an increase in internal resistance and loss of active material, with more rapid degradation in wind-charged cells than constant-charged cells. The lead-acid cells are also subject to severe partial charging when charged with a variable current; this latter effect is greater for longer pulses and reflects the poor pulse charge acceptance of these cells. Even though much of this capacity fade is reversible, it greatly affects the operational performance of these cells. The LCO cells show better overall charge acceptance and, while variable charge results in greater partial charging, the frequency of the

variability does not affect charge acceptance. Variability does not increase capacity fade in the LCO cells. The LCO-NMC cells degrade slower than the LCO cells, and constant charge cells show initial signs of faster degradation than variable charge cells, which may be the result of incomplete charging limiting the side reactions induced by high SOC. Degradation in the LCO-NMC cells appears to be initially due to loss of active material, but ultimately shows an increase in resistance as well. The LFP cells show very little degradation under all charging protocols. No increase in resistance is seen, and the slight reduction in capacity observed appears to primarily stem from the loss of cyclable lithium. Partial charging in these cells does depend on pulse frequency, and 1s pulses are found to have greater charge acceptance than 10s pulses.

	Lead-acid	**LCO**	**LCO-NMC**	**LFP**
Characteristic cycle life	Poor	Good	Very good	Excellent
Effect of variability on lifetime	Decreases lifetime	No measured effect	Neutral or positive effect	No measured effect
Pulse length dependence of charge acceptance	Short pulses better than longer pulses	No measured effect	No measured effect	Short pulses better than longer pulses
Incomplete charge is a stressor	Yes	No	No	No
Charge power fade observed	Yes	Yes	Yes	No

Table 9 Summary of battery response to variable charging **[8]**

Climate and Thermal Effects

Smith et al. [40] performed a study wherein they sought to analyze battery degradation in various geographic environments and driving scenarios. In exploring this topic, the authors apply a semi-empirical life model of the graphite / nickel-cobalt-aluminum (NCA) lithium-ion chemistry which is subjected to battery charge and discharge profiles from plug-in hybrid electric vehicles. 782 single-day driving cycles taken from a Texas travel survey are used to provide the drive cycle information. This work done in [40] specifically considers aging scenarios for plug-in hybrid electric vehicles (PHEVs) with 10 and 40 mile (16 and 64 km, respectively) nominal electric ranges.

To obtain geographic temperature distribution information, data was gathered from PHEV sales distributions within the United States, and the study was conducted around the median and hottest climates of the top 100 cities which exhibit a high likelihood for PHEV ownership. [40]

In addition to the above, three cases are considered:

- Battery aging under storage
- Aging at variable temperature, constant SOC
- Aging at variable temperature and variable SOC

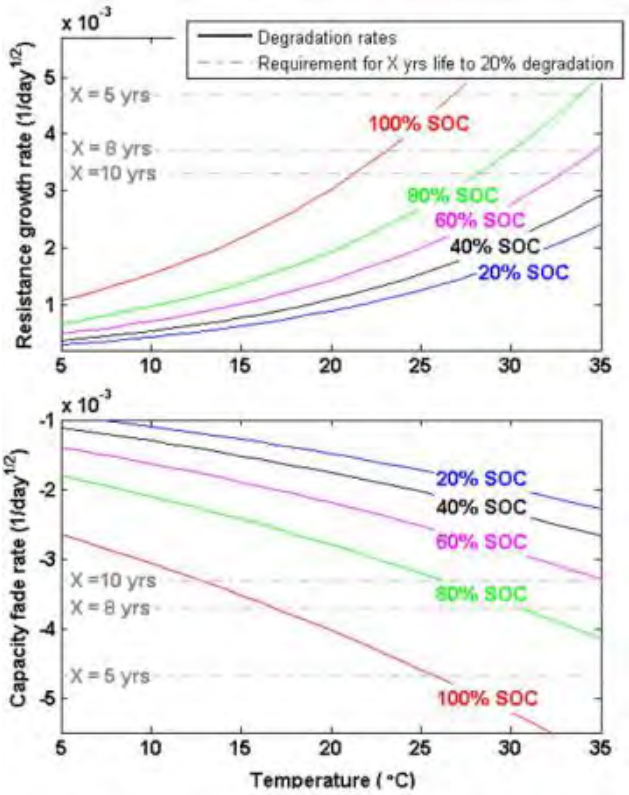

Figure 35 Typical graphite/NCA degradation rates for storage at constant SOC and temperature (solid lines). Dotted lines show maximum allowable degradation rates for example end-of-life requirements of 20% resistance growth and 20% capacity fade. [40]

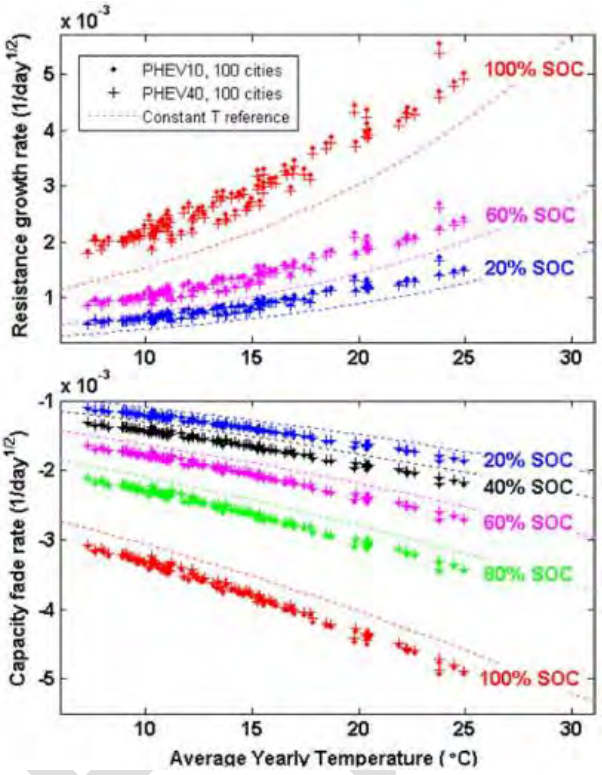

Figure 36 Resistance growth and capacity fade rates under storage at constant SOCs. Reference lines show results for constant temperature. Symbols show simulated results for PHEVs using hour-by-hour TMY ambient temperature and solar radiation data for 100 U.S. cities **[40]**

For the study conducted by Smith et al., the model did not take in to account degradation mechanisms such as fast charge-rates (with the exception of temperature rises as a result thereof), the effect of extreme temperatures (>50°C, < 0°C), damage done as a result of exceeding typical operating conditions, cell-to-cell manufacturing variations, and long term degradation effects which may manifest beyond 10 years of service life [40].

Subsequent analysis compares metrics of the Texas cycles to UDDS, HWY, and US06 standard drive-cycles. To achieve an appropriate mix of CD and CS operation, either four or five repetitions of the UDDS, HWY and US06 standard drive cycles are simulated so that each cycle's daily travel distance falls as close as possible to the Texas average of 38.9 miles/day. These UDDS, HWY, and US06 cycles are weighted with appropriate rest days such that the annual mileage of each is 12,375 miles/yr. The United States Advanced Battery Consortium (USABC) cycle-life test protocol is also simulated [23]. The PHEV10 USABC cycle simulated here uses both the CD and CS portions of the test protocol. The PHEV40 USABC cycle uses only the CD portion of the test. This is to keep the implied daily travel distance as close as possible to the Texas drive-cycle average.

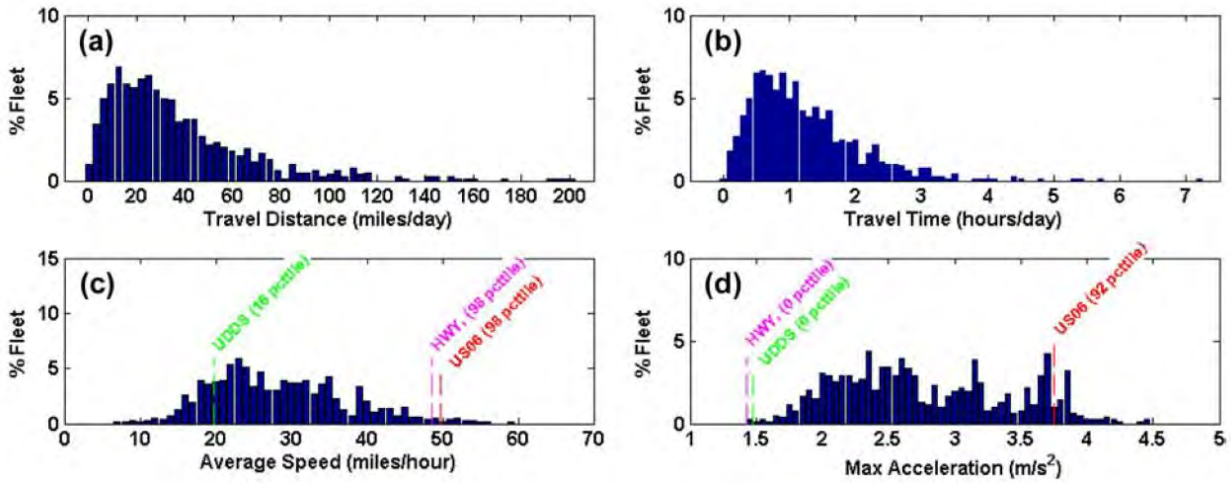

Figure 37 Drive-cycle metrics (a) distance-traveled per day, (b) travel time per day, (c) average speed while driving, and (d) maximum acceleration. Blue histograms represent 782 drive-cycles from Texas survey **[40]**.

Figure 37 shows histograms representing the 782 drive cycles used from the Texas survey. Averages speeds and maximum acceleration figures are compared against UDDS, HWY, and US06 drive cycles. Daily travel distance results (Figure 37a) show 66% of the Texas driving trips are less than 40 miles per day and 14% of drive cycles are less than 10 miles per day [40].

The authors of [40] assume resistance growth and lithium capacity loss to be proportional to the square-root of time, as this factor is typical of diffusion-limited film growth processes. At SOC $\geq$ 80% there is a greater sensitivity to temperature [40] shown in

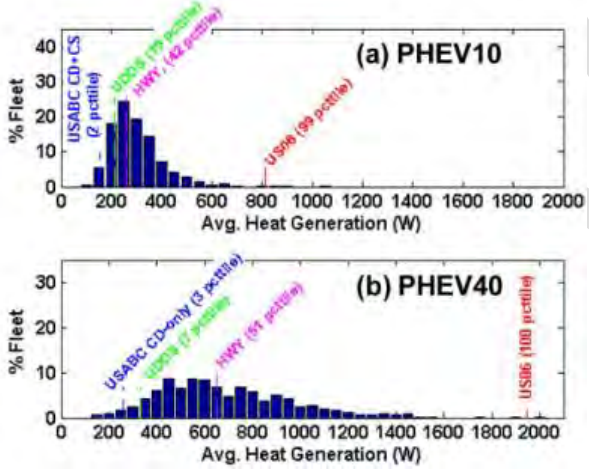

Figure 38 Model-predicted 100% DOD-equiv. cycles per day. [40]

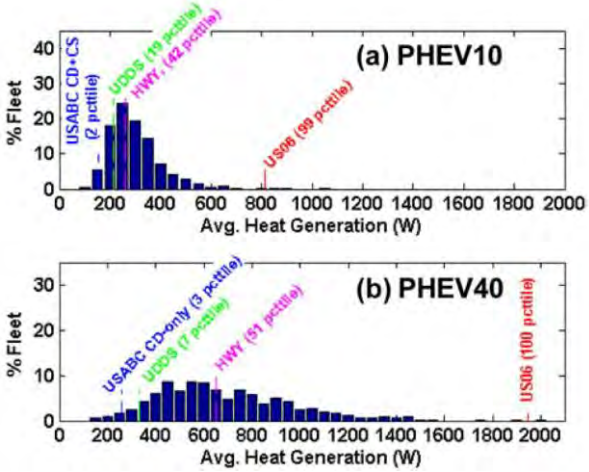

Figure 39 Model-predicted average heat generation rate during driving **[40]**

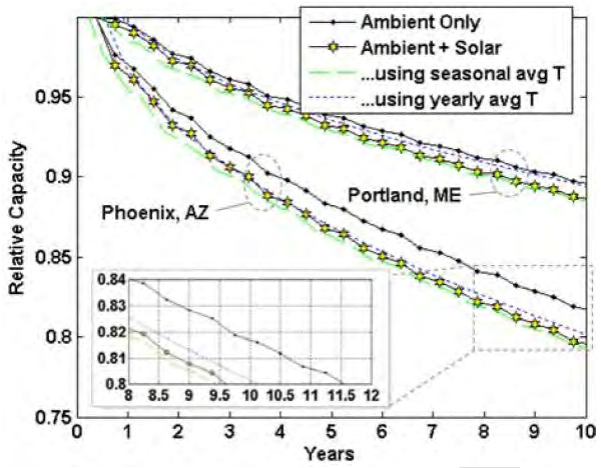

Figure 40 Capacity fade under storage at 90% SOC for two geographic locations with and without impact of solar loading on the parked vehicle **[40]**

The results of the study in [40] suggest that storage degradation in worst-case temperatures is negatively affected by high SOC. Therefore, part of a worst-case durability testing procedure should combine high SOC with high temperature in order to observe faster degradation. Furthermore, analysis of cycling-related degradation by comparing attributes of UDDS, HWY, US06 and USABC cycles to 782 single-day drive-cycles demonstrate the importance of factors such as the charge/discharge cycles and heat-generation as a by-product of such. Worst-case PHEV driving and charging patterns are those with high utilization of charge-depletion mode of operation.

Similar testing was conducted on the Nissan Leaf at Argonne National Laboratory, with testing being performed in a thermal chamber at temperatures of 20°F, 72°F, and 95°F (-7°C, 22°C, and 35°C respectively) [41]. For these thermal tests, the vehicles were operated using drive cycles such as UDDS, HWY, and US06. Data showing the impact of temperature on energy consumption and range are shown in Figure 41 and Figure 42 respectively.

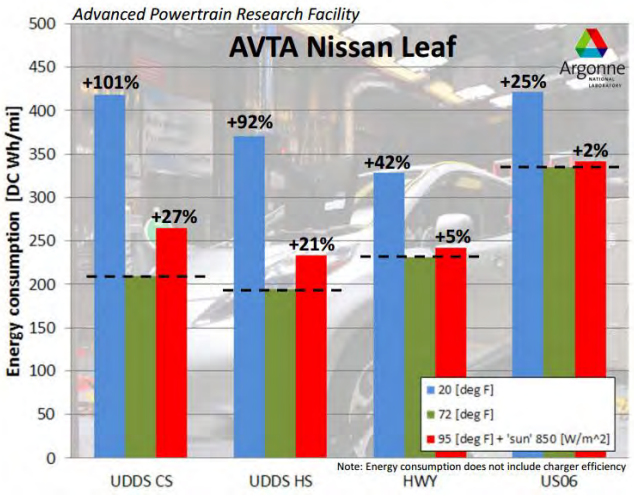

Figure 41 Impact of Temperature on Energy Consumption **[41]**

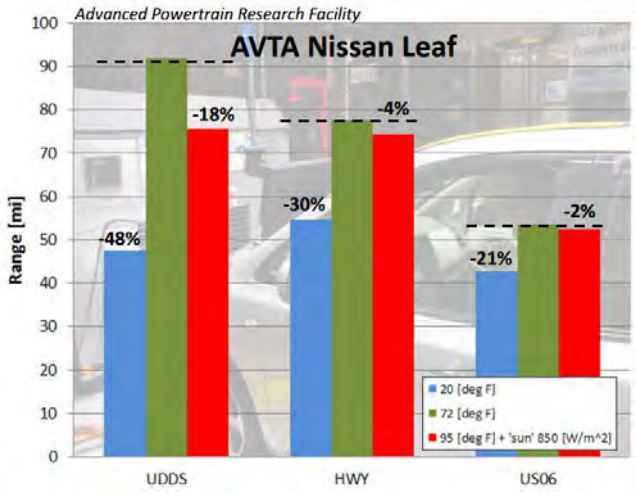

Figure 42 Impact of Temperature on Range **[41]**

It should of course be noted that in the cases of the 20°F and 95°F tests that the vehicle's cabin climate control was set to 72°F [41]. Such an approach in vehicle testing is warranted as it assumes the desire of the vehicle occupants to maintain a comfortable climate. Due to the Leaf being a BEV, the energy consumed to power heating contributes directly to the increased energy consumption and lower range [41].

Song et al [42] examined the impact of pre-heating a battery in low temperature climates on the performance and lifetime of the battery. Four cases were considered:

1. a reference test fixed at room temperature (+25°C)
2. preheating to +25°C (from the minimum of -20°C)
3. preheating to +10°C (from the minimum of -20°C)
4. no pre-heating at low temperature (fixed at -20°C)

A 6.9 kWh, 20Ah lithium polymer battery pack was connected to a battery HIL which was using a mid-sized BEV model supplied by Argonne National Laboratory. After the temperature soak, the battery was subjected to three UDDS cycles. The results of each of the cases are shown in Table 10:

	Case 1	Case 2	Case	Case 4
Remaining capacity (Ah)	7.47	7.32	7.26	6.82
SOC(%)	36.10	35.45	35.16	33.03
Room temperature contrast ratio(%)	-	0.73	1.02	3.15

Table 10 Comparison of remaining capacity for temperature profiles **[42]**

The results of [42] demonstrate that in a low temperature environment, the battery is able to retain greater capacity under a preheat / preconditioning scenario.

Barnitt et al. [43] performed a study similar to that of [42], showing effects for temperature pre-conditioning at both low and high temperatures. Here, three simulated vehicle types are considered:

1. PHEV15—a blended PHEV with an approximately 15-mile (23.4-km) all-electric range (AER) under certain usage conditions.
2. PHEV40s—a series PHEV designed to provide up to 40 miles (64 km) of AER, then operate in charge-sustaining (CS) mode using a range-extending gasoline engine.
3. BEV—a BEV designed to provide up to 100 miles of AER.

Additionally, the following scenarios for these vehicles are considered:

Climate Control Scenario	**Ambient Temp.**	**Thermal Preconditioning**	**Initial Battery Temp.**
A/C on (hot)	35°C	Yes	26.7°C
		No	35°C
Heat on (cold)	-6.7°C	Yes	1.7°C
		No	-6.7°C
Neither A/C nor heat on	20°C	N/A	20°C

Table 11 Climate Control, Temperature Scenarios **[43]**

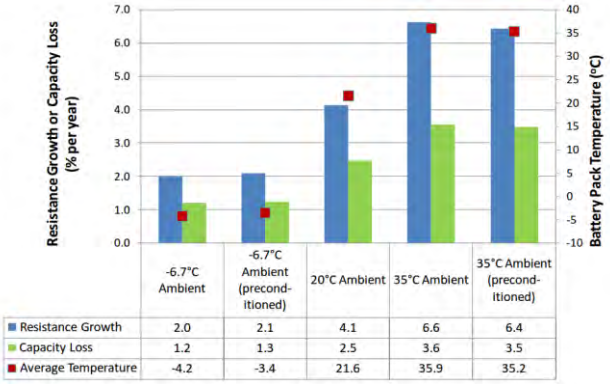

Figure 43 PHEV15 battery degradation rates (left axis) and average temperature (right axis) **[43]**

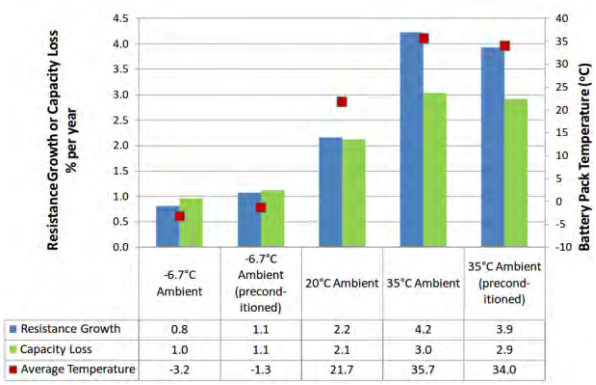

Figure 44 PHEV40s battery degradation rates (left axis) and average temperature (right axis) **[43]**

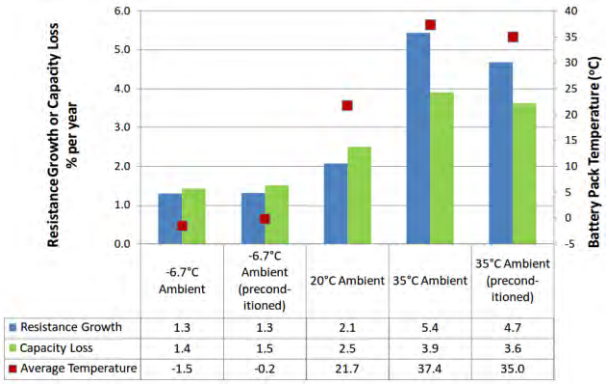

Figure 45 EV battery degradation rates (left axis) and average temperature (right axis) **[43]**

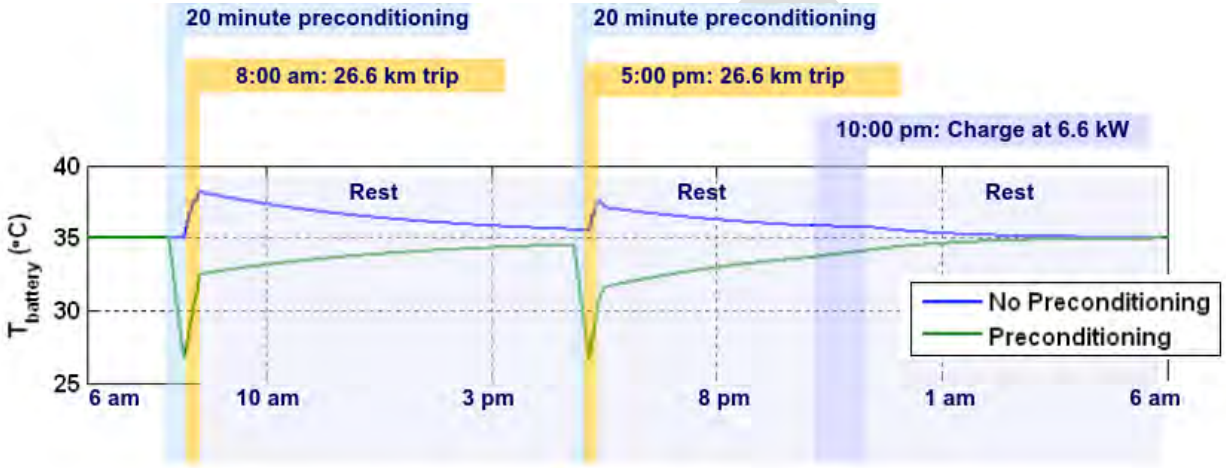

Figure 46 Battery temperature and SOC profiles for PHEV40s, 35°C ambient temperature, with and without thermal preconditioning **[43]**

From figures **Figure 43** to **Figure 45** we are able to observe the battery degradation results. From these results, pre-cooling of electric-drive vehicle batteries is predicted to reduce capacity fade by 2.1% to 7.1% and resistance growth by 3.0% to 13.8% in hot (35°C) ambient conditions when compared to the baseline configuration of no pre-conditioning [43].

A summary of the fuel consumption and CD range impact is given in Table 12.

EDV Platform (Climate Control)	Fuel Consumption Impact	CD Range Impact
PHEV15 (heat)	-1.4%	+19.2%
PHEV15 (A/C)	-0.6%	+5.2%
PHEV40 (heat)	-2.7%	+5.7%
PHEV40 (A/C)	-1.5%	+4.3%
BEV (heat)	N/A	+3.9%
BEV (A/C)	N/A	+1.7%

Table 12 Impact of thermal preconditioning as compared to scenarios without thermal preconditioning **[43] [44]**

As can be seen in Table 12, the effect of thermal preconditioning of the battery is able to offer benefits to both fuel consumption and to range, in addition to extending battery life as shown in Figures Figure **43** - Figure **45**.

A study performed by Vatanparvar and al-Faruque was conducted to develop an automotive climate control methodology which manages the vehicle's HVAC power consumption so as to improve battery lifetime and

driving range. In effect, the lifetime-aware HVAC system decreases power consumption of the HVAC when electric motor power consumption is high, and when the electrical motor is consuming less or generating, the HVAC may consume more in order to maintain the temperature and precool/preheat the cabin. [45]. The other methodologies examined where those of On/Off management and a fuzzy-based methodology. The modeling of these methodologies is outside of the scope of this review, but may be referenced within [45].

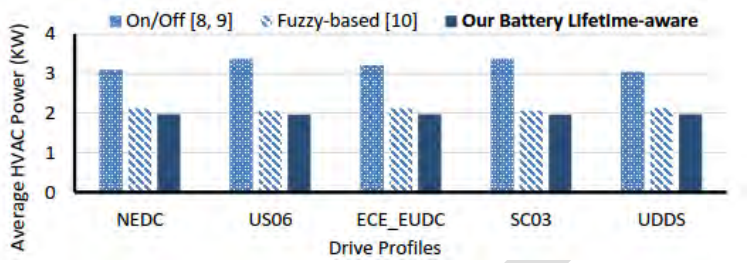

Figure 47 HVAC Power Consumption Analysis for Different Drive Profiles **[45]**

Yuksel & Michalek [46] also studied thermal management methods as they relate to battery life in a PHEV. The battery chemistry which formed the focus of the study was $LiFePO_4$/graphite. Drive cycles used are UDDS and US06, with a fan On/Off control strategy wherein ambient or cabin air is used to cool the battery. Climates considered for the study are Phoenix and Miami.

Conclusions drawn suggested that thermal management increases life by 5% to 53%, depending on the scenario. Variation in driving conditions from the UDDS cycle to the US06 cycle has a dramatic effect on battery life if there is no thermal management, reducing life by about 60%. With air cooling, US06 decreases life by only 20%. Thus, driving conditions are important for battery longevity, and thermal management mitigates the effects of aggressive driving. One observation was that batteries have a 20% shorter life in Phoenix than in Miami (reduced to 11% with thermal management) due to higher summer peak temperatures in Phoenix even though Miami has higher average temperatures, demonstrating the impact of sustaining high temperatures for a time. Use of ambient inlet air vs. pre-conditioned cabin air for battery cooling has a minor effect on degradation for the base control strategy. However, variation in control parameters (fan on-off temperatures) can increase battery life by 53% or more [46].

A study conducted by Smith, Earleywine, Wood, and Pesaran performed a study for the evaluation of PHEV10 (16km AER) and PHEV40 (64km AER) vehicles using a lithium ion graphite / nickel-cobalt-aluminum battery model. The analysis of battery lifetime was conducted using 782 different duty cycles obtained from travel survey data, using climate and geographic data as well. The term BTM is used for “battery thermal model”

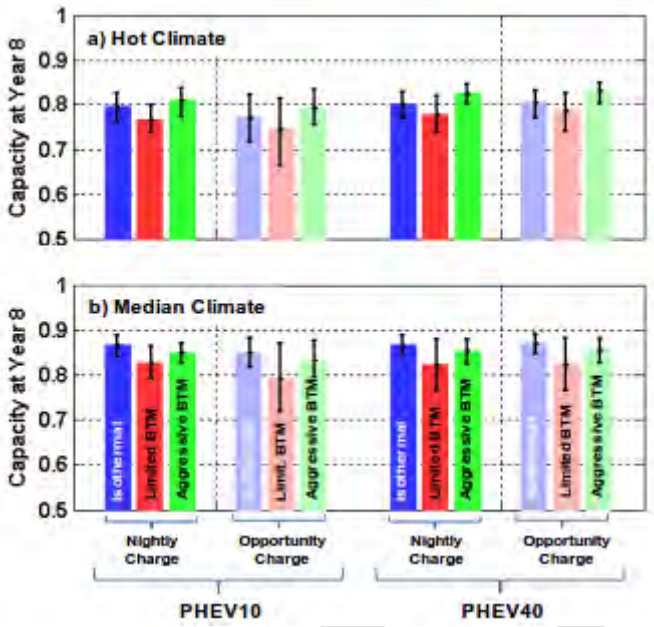

Figure 48 Remaining capacity at the end of 8 years for various BTM and charging scenarios. Colored bars show average result for all 782 drive cycles. Error bars show result for 5th and 95th percentile drive cycles. **[47]**

The drive cycle distribution in the study presented in [47] is identical to that of [40], namely, that the experiment's drive cycles are derived from 782 individual light-duty drive cycles.

Battery aging is caused by multiple phenomena related to both cycling and time. Battery degradation is accelerated with the DOD and frequency of cycling, elevated temperature, and elevated voltage exposure, among other factors. At the battery terminals, the observable effects of degradation are an increase in resistance and a reduction in capacity. These two effects can be correlated with power and energy losses that cause battery end-of-life in an application. Mechanisms for resistance growth include loss of electrical conduction paths in the electrodes, fracture and isolation of electrode sites, growth of film layers at the electrode surface, and degradation of electrolyte. Mechanisms for capacity loss include fracture, isolation, and chemical degradation of electrode material, as well as permanent loss of cyclable lithium from the system as a byproduct of side reactions.

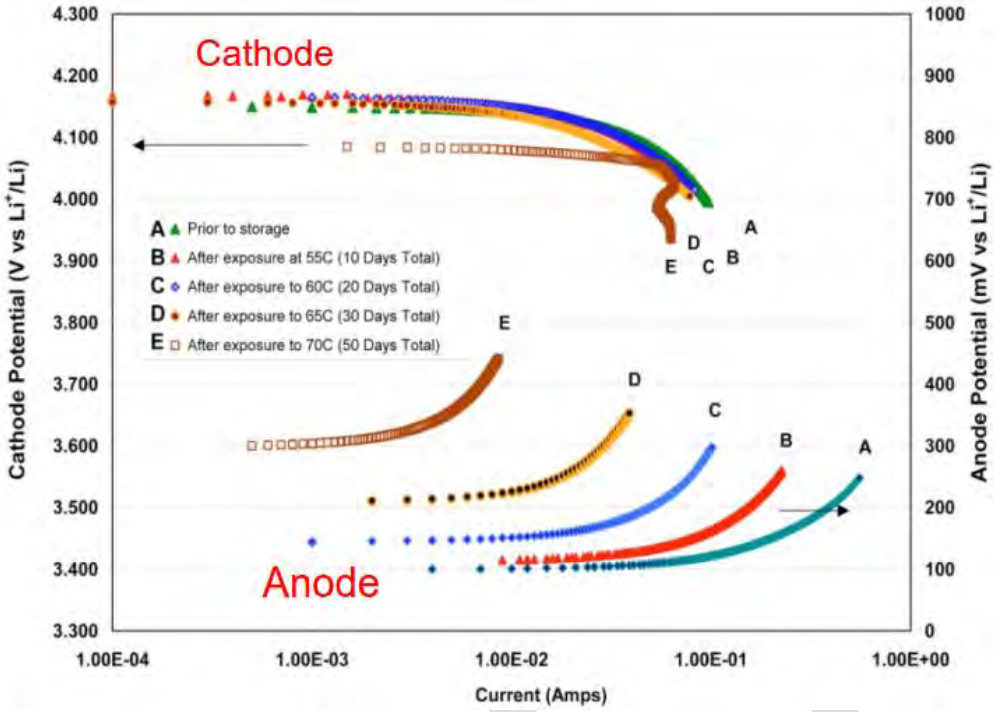

Figure 49 Half-cell Potentials from cells subjected to aging at different temperatures: Side reactions happen faster on the electrode surface with increase in the temperature – resulting in faster build-up of the resistance at the electrode surface **[51]**

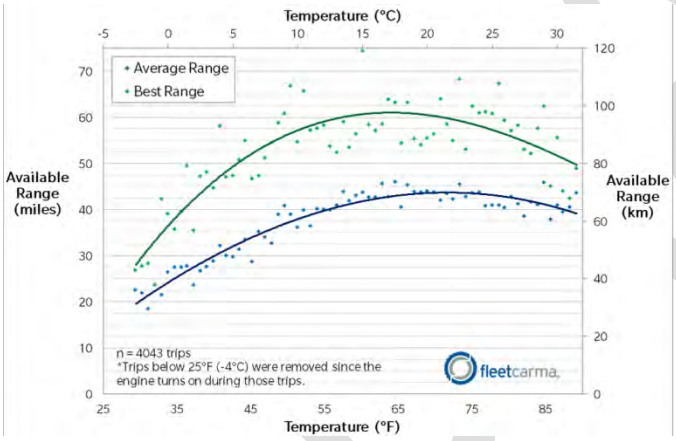

Figure 50 Chevrolet Volt: Electric Range vs. Temperature spanning all model years in the FleetCarma database [49]

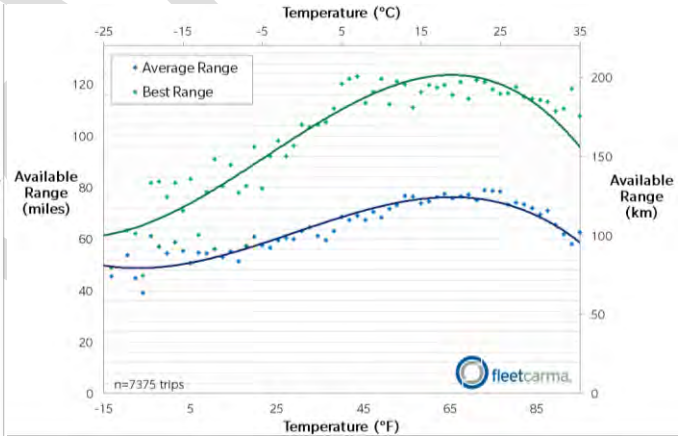

Figure 51 Nissan Leaf: Range vs. Temperature spanning all model years in the FleetCarma database **[49]**

From Figure 50 and Figure 51 we see that optimal range characteristics for the Volt and Leaf lie between 15°C and 25°C. It should be noted however as per Figure 50 that performance below -4°C is not shown for the Chevrolet Volt as the ICE is activated at this temperature. Nevertheless, we see a clear trend as far as decreases in range at concerned at these temperatures. The same can be said of both vehicles as ambient temperatures approach 30°C. A further comparison between the two vehicles is presented in Figure 52.

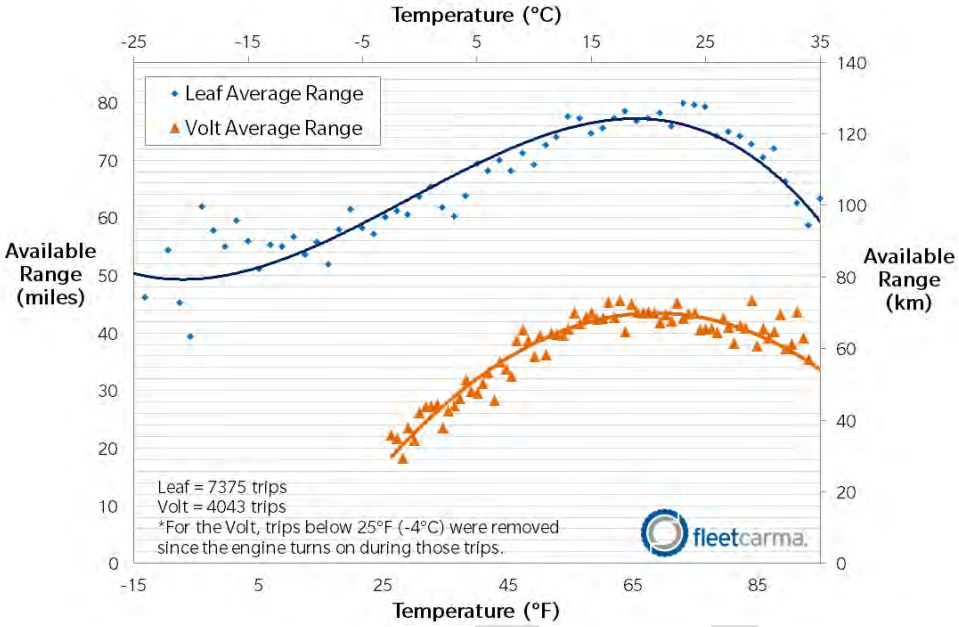

Figure 52 Nissan Leaf & Chevrolet Volt: Range vs. Temperature **[49]**

A study under taken by Santhanagopalan et. al [50] sought to create life models of lithium-ion cells based on obtained experimental data. Specifically, the study investigated capacity fade in cells (and related cell degradation) for cycling at different temperatures (5°C, 15°C, 25°C, 35°C, and 45°C). Each cycle consisted of a constant current charging at the C/2 rate (where in this case C-rate = 1.656A) until the voltage reached 4.1V, followed by constant charging at 4.1V until the current reduced to 50mA, and then a constant discharge at the C/2 rate until the cells reached a cutoff of 3.3V. Additionally, rate capability tests were performed before cycling and at the end of every 100 cycles. These rate capability tests consisted of measuring the charge-discharge capacity of the cell at different rates, with these being C/33, C/2, and C, in that order. [50]

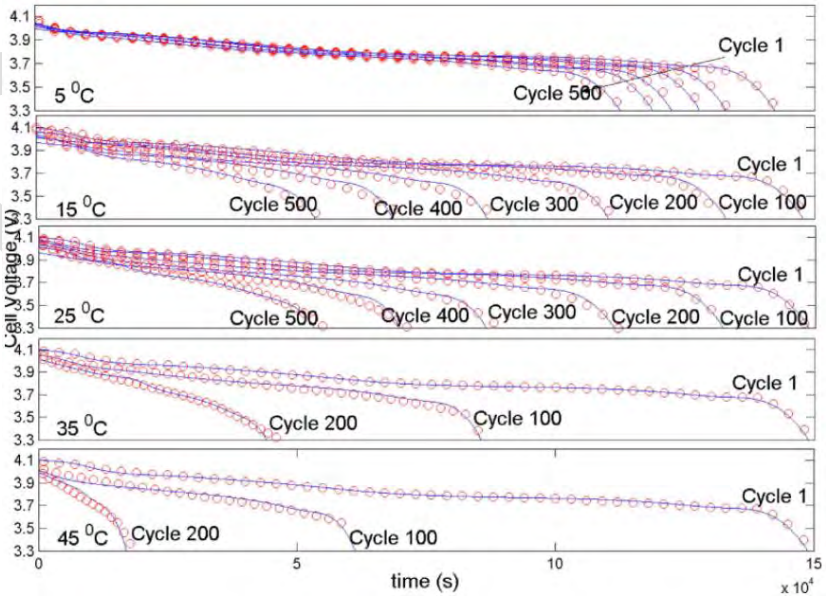

Figure 53: Degradation of cell voltage for increasing cycles at various temperatures [50]

Comparison of the predictions from the single particle model to the experimental data at the C/33 rate. Solid lines indicate experimental data and the symbols indicate the model predictions. At 35 and 45°C, the cycling was stopped after 200 cycles since the remaining capacity was very low.

	Fresh	Cycle 100	Cycle 200	Cycle 300	Cycle 400	Cycle 500
5°C	1.8867	1.7454	1.6723	1.6031	1.5522	1.4705
15°C	1.9870	1.7891	1.6094	1.4227	1.2143	0.9730
25°C	1.9667	1.7367	1.4567	1.1867	0.9467	0.7367
35°C	1.9667	1.3466	0.6667	--	--	--
45°C	1.9667	0.8667	0.2467	--	--	--

Table 13. Experimental capacities (Ah) measured after every 100 cycles for five different cells cycled at 5, 15, 25, 35, and 45°C [50]

From the data shown in Figure 53 and Table 13 we are able to see the evident loss of capacity as a result of the combination of both temperature and cycling, with temperature here as the main variable in the experimentation. Beyond 25°C we see significant degradation, as is also corroborated by Figure 50 and Figure 51, for example.

Battery Test Procedures in Japan

Since 2007, JARI, CRIEPI and National Institute of Advanced Industrial Science and Technology (AIST) have been developing a cycle-life test (CLT) procedure for lithium-battery technology, which accounts for actual usage conditions [7]. This development was conducted as part of the "Development of High-performance Battery System for Next-generation Vehicles (Li-EAD)" project [8] undertaken by New Energy and Industrial Technology Development Organization (NEDO) in Japan. This section discusses the rationale behind the more-recent CLT profile development in Japan. [52]

	JC08	UDDS	NEDC	Integrated
Test time [s]	1204	1371	1180	3755
Driving distance [km]	8.172	11.989	11.013	31.175
No. of trips	11	18	13	42
Average of (trip + idle) time [s]	109.5	76.2	90.8	89.4
Average trip time [s]	77.0	61.7	68.2	67.7
Average speed [km/h]	24.43	31.48	33.60	29.89

Table 14 Average of three driving cycles [52]

Spagnol et al. [53] conducted a study wherein they sought to develop an HEV-specific duty cycle for the aging and characterization of Li-Ion batteries for lifetime estimation.

Takei et al. [54] performed an experimental investigation into commercial 1.25Ah 18650 $LiCoO_2$/hard carbon cells for an accelerated aging study. The operating conditions were set as

Cycling and Depth-of-Discharge

Wood et al. [55] performed a study which sought to improve understanding of battery wear in xEVs by implementing a predictive battery wear model (developed by the National Renewable Energy Laboratory) that is capable of capturing the effects of multiple cycling and storage conditions in a representative lithium chemistry. In particular, Wood et al. explored the sensitivity of battery wear rates to ambient conditions, maximum allowable depth of discharge, and vehicle miles traveled. The analysis focuses on two midsize vehicle platforms: a battery electric vehicle (BEV) with a nominal range of 75 mi (121 km) and a plug-in hybrid electric vehicle (PHEV) with 40 mi (64 km) of nominal charge-depleting range.

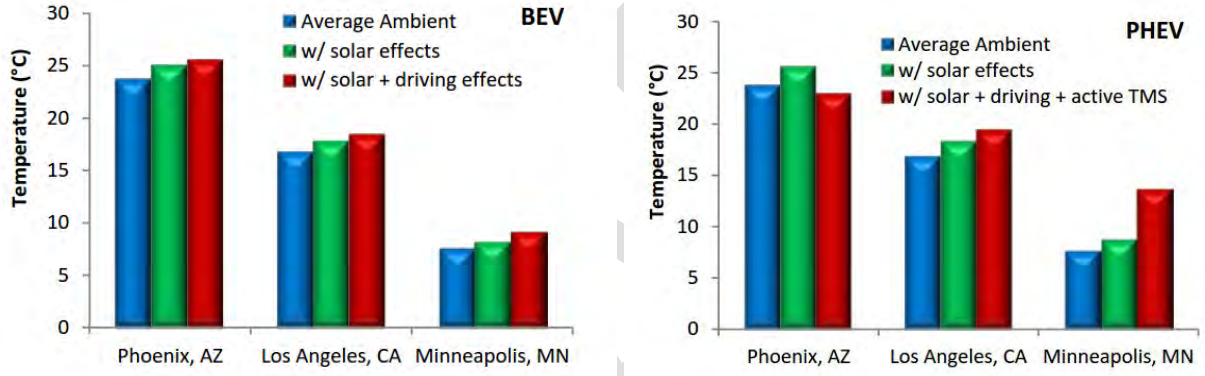

Figure 54 Average yearly battery temperature contributions from ambient, solar loading, and internal heat generation for simulated (a) BEV and (b) PHEV. **[55]**

The effect of maximum allowable DoD on battery wear is explored for both the BEV and the PHEV. Each vehicle was assigned a nominal value for maximum allowable DoD and maximum state of charge (SOC). These values are adjusted over a feasible range for both the BEV and PHEV to explore the effect on wear (80%–94% and 55%–87% maximum allowed DoD, respectively). The SOC window of the pack is adjusted relative to total energy to ensure that the available energy in the pack remains constant for all maximum allowable DoDs. By adjusting the maximum allowable DoD and maximum SOC, the life model will capture the wear effects of deep cycling and operation at high voltages [55].

In the case of the BEV, increasing the maximum allowable DoD of the pack from 80% to 94% causes 8-year resistance growth and capacity fade values to increase by 6% and 8% respectively. For the PHEV, increasing the maximum allowable DoD window of the PHEV from 55% to 87% increased resistance growth by 18% while capacity loss increased by 8% over the same range. [55]

Adjusting pack energy has an impact on vehicle mass (and cost) and is subsequently related to CD range, efficiency, and acceleration.

It was determined that maximum allowable DoD was found to significantly impact battery wear. Reductions to the maximum allowable DOD leads to a subsequent reduction in resistance growth rates and capacity fade. However, the tradeoff which allows a reduced DOD window to physically occur means that a larger overall battery pack will be required. The authors of [55] estimate that the extra battery capacity required for n 80% vs.

94% DOD window will lead to a $2800 increase in pack cost. Similarly, for the PHEV, adjusting the DOD for a 55% vs. 87% DOD window represents roughly a $4900 increase in pack cost.

Y. Zhang et al. [23] performed a study on the degradation of $LiFePO_4$ cells at various temperatures.

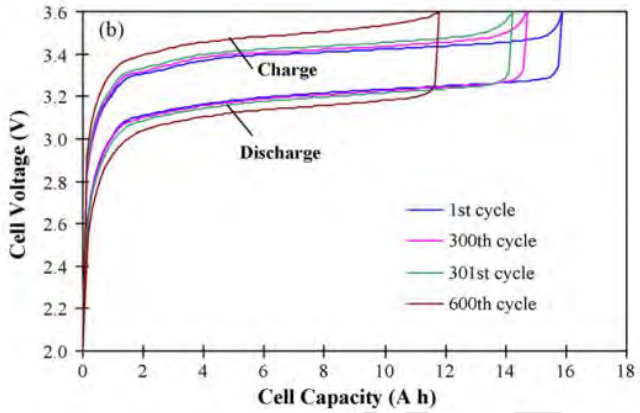

Figure 55 Cycling performance at 3C rate between 3.6 and 2.0 V at 50°C: charge–discharge loops for the beginning and last cycles of the 1st 300 cycles (1st and 300th cycles) and the 2nd 300 cycles (301st and 600th cycles). **[23]**

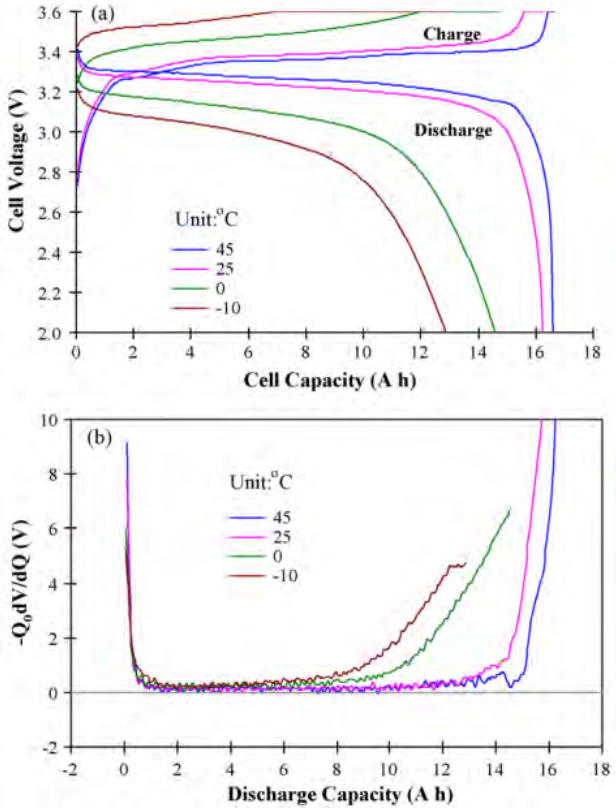

Figure 56 (a) Charge–discharge curves at 1C rate measured at different temperatures for a fresh cell and (b) the corresponding differential voltage ($-Q_o dV/dQ$) versus discharge capacity. [23]

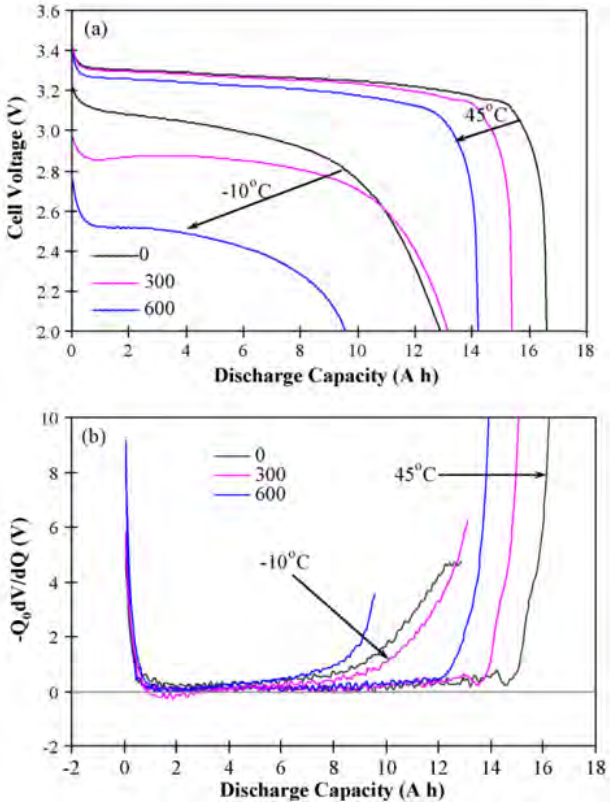

Figure 57 (a) Discharge curves at 1C rate measured at 45 and −10°C after different cycles and (b) the corresponding differential voltage ($-Q_o dV/dQ$) with respect to discharge capacity. [23]

An interesting result from [23] is that for testing temperatures of 25°C and 45°C, discharge capacity decreases linearly over the range of cycles 0 to 600. In the case of cycling at 0°C and -10°C, however, capacity fade is linear up to cycle 300, however, at 600 cycles, this has fallen drastically such at in the case of -10°C, a capacity fade of 25.8% at 600 cycles is noted [23].

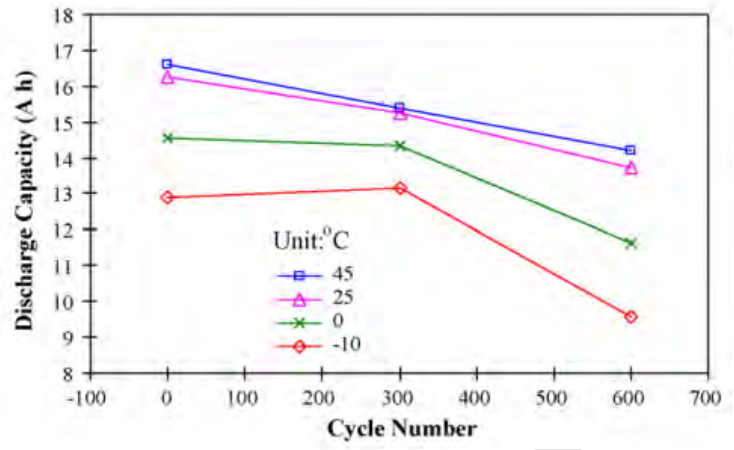

Testing for power fade in [23] is done with an HEV focus, specifically evaluating using discharge resistance and discharge pulse power capability as derived from [56].

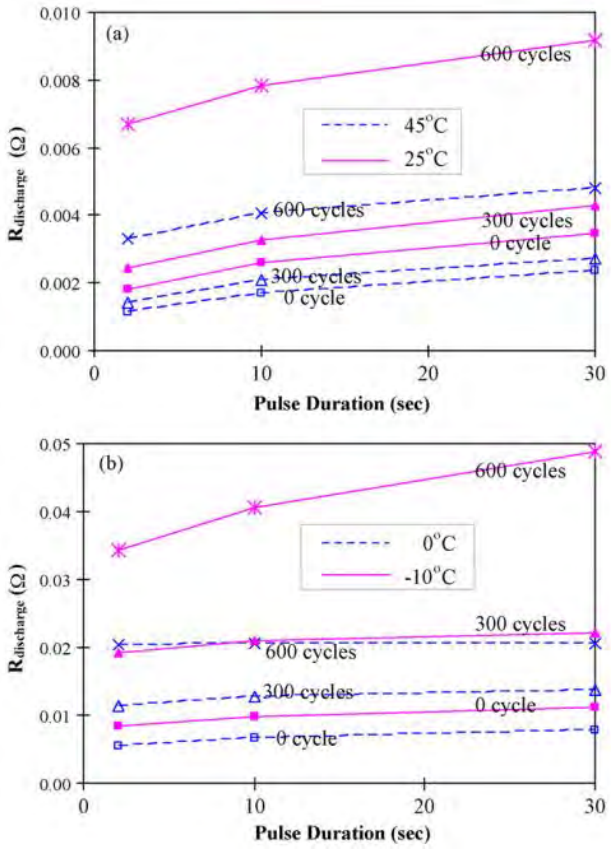

Conclusions [23]

Degradation of a high capacity $LiFePO_4$ cell with deep cycling at elevated temperature of 50°C is studied by characterizing capacity fade, power fade and impedance rise at different test temperatures (45, 25, 0 and −10 °C). Capacity fade after 600 cycles is 14.3% at 45°C and 25.8% at −10°C. The capacity and power fade evidently becomes more severe at lower temperature. In particular, the power fade at low temperatures (e.g., 0 and −10°C) rather than capacity loss is a major limitation of the $LiFePO_4$ cell.

It is found from the variation of the impedance spectra that ohmic resistance (Ro) clearly rises with lowering temperature and upon cycling. The activation energy from the relationship of lg(1/Ro) with 1/T remarkably increases from 4.3 kJ mol−1 for a fresh cell to 20.9 kJ mol−1 after 300 cycles, which suggests that the

electronic resistance of electrode particles is dominant in Ro for a fresh cell and increasing electrolyte resistance has become dominant in Ro after 300 cycles. Accordingly, the increase of ohmic resistance (Ro) with cycling comes mainly from increase in electrolyte resistance resulting from the lithium loss within the electrolyte due to lithium-consuming SEI layer growth and side reactions that also lead to loss of cyclable lithium. Mid-frequency arc width (Rw) evidently increases (2.5–6 times) from 300 to 600 cycles due to SEI layer growth on the graphite anode with a catalytic effect from iron impurities that deposit from the dissolved iron on the LiFePO4 cathode, but does not greatly increase (0.9–1.5 times) from 0 to 300 cycles because there is no catalytic effect of iron deposition in this period. Consequently, the increased interfacial resistance (Rw) due to the catalytic growth of SEI layer on the anode and increased electrolyte resistance in Ro are the main sources for power fade, leading to very poor discharge pulse power capability at low temperatures (0 and −10°C) after cycling and even very small electric-only range due to power capability too low to surmount a high discharge peak power under the UDDS driving schedule. [23]

Anseán et al. [5] subjected $LiFePO_4$ (LFP) cells from five different manufacturers to a series of tests for evaluating cycle life, energy efficiency, power capability, and internal resistance. The results were compared against the USABC targets for xEV applications. The various cells are described in Table 15.

	Cell 1	Cell 2	Cell 3	Cell 4	Cell 5
Nominal capacity	2.3Ah	16 Ah	42 Ah	60 Ah	100 Ah
Maximum continuous discharge	70A (30C)	160A (10C)	126A (3C)	180A (3C)	300A (3C)
Maximum continuous charge	10A (4C)	80A (5C)	42A (2C)	180A (3C)	300A (3C)
Cell weight	70g	500g	1000g	2000g	3200g
Cell geometry	Cylindrical	Cylindrical	Pouch	Prismatic	Prismatic
DC internal resistance	8 mΩ	< 8 mΩ	N/A	< 2 mΩ	< 0.9 mΩ
Country of Origin	USA	China	Finland	China	China

Table 15 Summary of the main characteristics of the batteries tested in [5]

The above cells were tested in accordance with USABC guidelines.

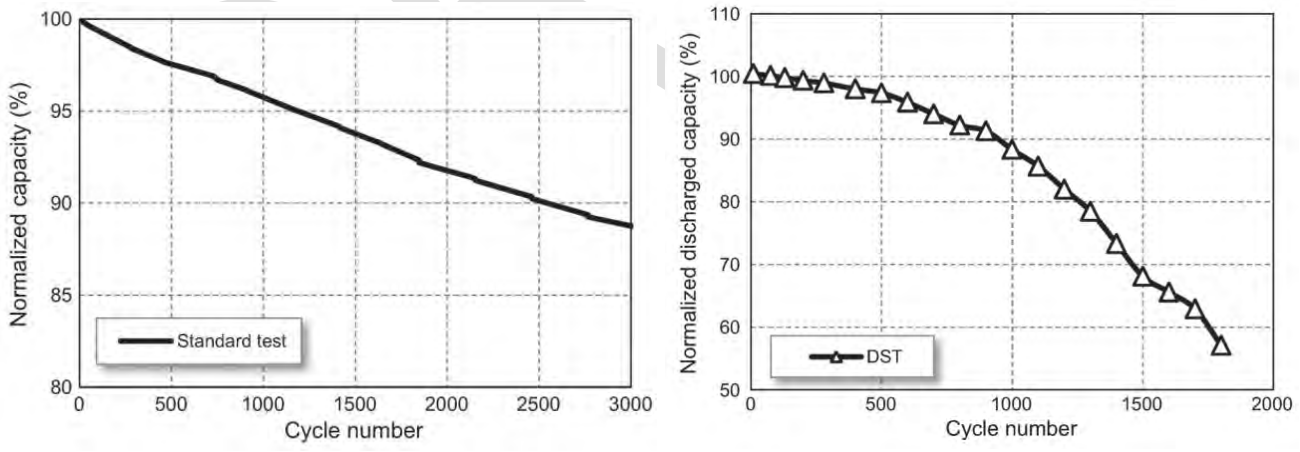

Figure 58 Cell 1 from [5] subjected to standard tests and USABC DST tests

The results of cycling tests for Cell 1 from Table 15 are shown in Figure 58. Under nominal conditions, the battery was tested for 3000 cycles, which corresponds to roughly 13 months of continuous testing. Under these conditions, 11% of capacity was lost. When subjected to more stressful testing, namely USABC DST tests, the cell was shown to meet EOL goals, losing 20% of capacity after approximately 1200 cycles [5].

The authors of [5] concluded that although the USABC long-term goal for cycling is achieved on both the nominal and the fast charge/DST, there are important differences in terms of capacity fade and power

capability. Testing under standard conditions is usually well tolerated by the batteries. On the other hand, stressful conditions, as the ones that can be found on an actual EV, are more detrimental to the battery life. This helps to understand the importance of developing an adequate set of testing protocols and diagnosis tools that can simulate and predict the battery performance in real-life EV applications.

In terms of performance, the LFP cells tested by [5] fail to meet the long-term goals set by the USABC in terms of specific energy. All cells were able to meet the requirements for cycle life as specified.

[57]

This test profile was adapted by Southern California Edison (SCE) to the test equipment at their Electric Vehicle Technical Center (EVTC) (see Table 2). The 7.3 h cycle was applied to 3 PHEV modules (see Table 3 for specifications) continuously from March 2005 to August 2009 for a total of 4323 cycles. Reference Performance Tests (RPTs) were conducted before the start of the life cycle test, and at periodic intervals every 240 test cycles (equivalent to approximately 2 months of testing) to characterize the performance of the battery. The following tests are included in each RPT:

• A constant current discharge at a rate of C/1.

• A constant current discharge at a rate of C/3.

• A peak power test.

• A Hybrid Pulse Power Characterization (HPPC) Test (performed in the dual mode configuration).

The first three tests were performed using the methods of the USABC Electric Vehicle Test Procedure Manual [8]; the HPPC test was performed using the methods the PNGV Battery Test Manual [16]. A preliminary cycle, including a discharge at a constant current rate of C/3 down to 60% DOD and a full recharge, was performed prior to each RPT. A 30 min rest was included in between each charge and discharge.

The authors of [57] examine both SOC and t-SOC, where t-SOC is defined as being the thermodynamic state of charge. This is defined as a characterization of the battery with respect to its instantaneous chemical composition. An example of how this relates to the capacity of the battery is shown in Figure 59.

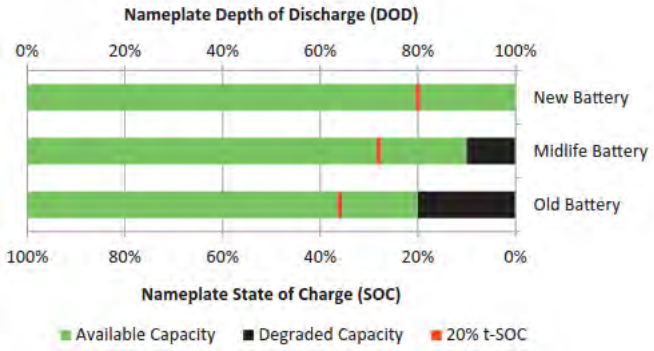

Figure 59 Variation of t-SOC as a result of capacity degradation. As the battery degrades, the degraded capacity occupies a greater fraction of nameplate SOC, whereas t-SOC is normalized to the available capacity. **[57]**

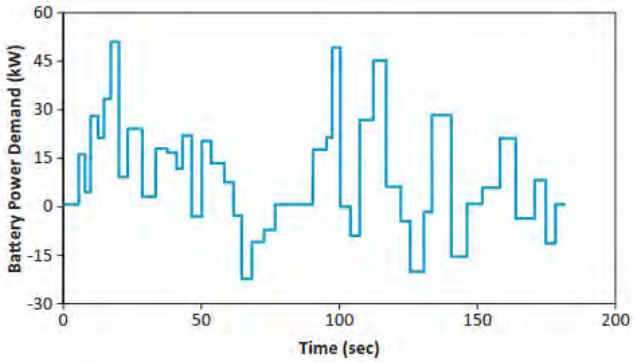

Fig. 2. PHEV CD test profile used to define PHEV-specific battery degradation test procedure.

[57]

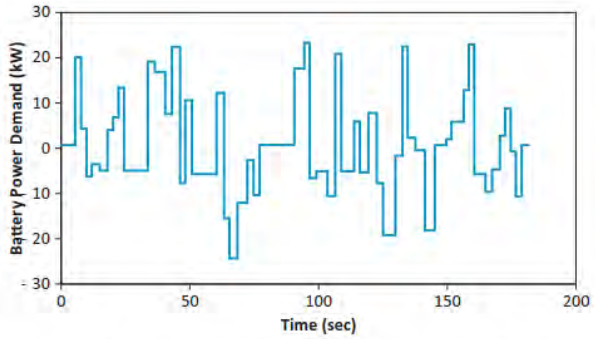

Fig. 3. PHEV CS test profile used to define PHEV-specific battery degradation test procedure.

[57]

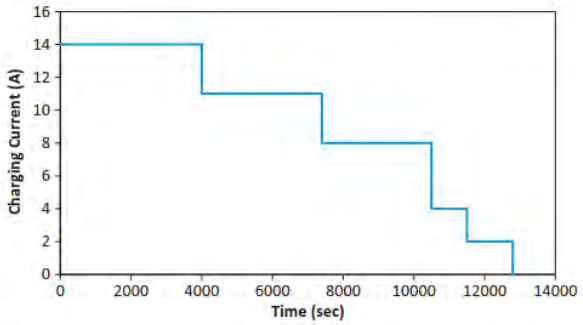

Fig. 4. PHEV charging profile used to define PHEV-specific battery degradation test procedure.

[57]

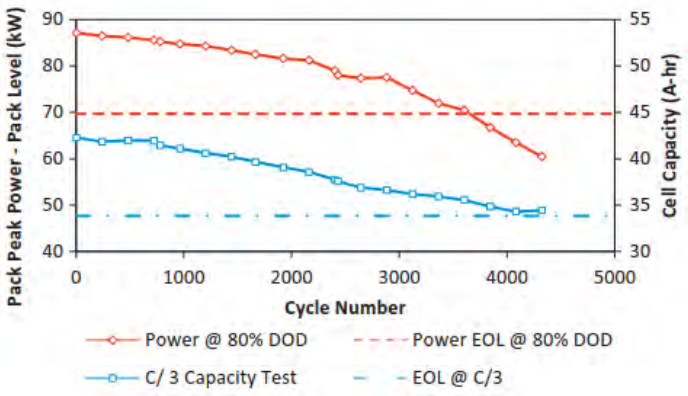

Figure 60 Energy and power measurements as a function of cycle number (fig5) **[57]**

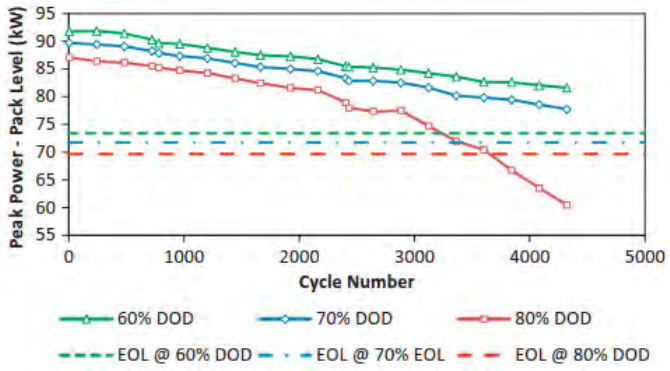

Figure 61 Power degradation at various levels of capacity based DOD as a function of cycle number (fig6) **[57]**

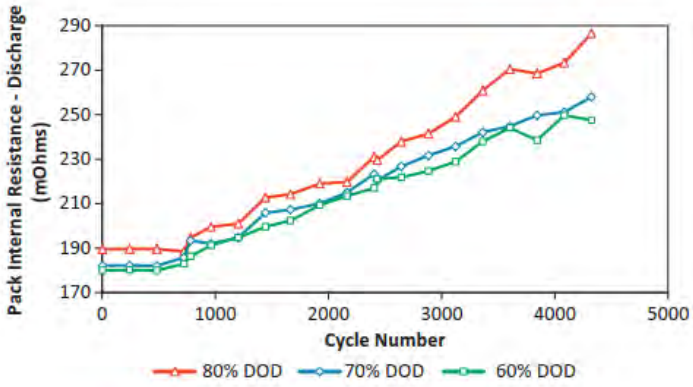

Figure 62 Pack internal discharge resistance as a function of cycle number **[57]**

A study presented by Wood et al. was conducted to ascertain the validity of USABC battery testing standards when applied to modern PHEVs.

These results indicate that USABC test procedure underestimates the cycle life capability of battery systems which can compromise on the requirement to discharge to a capacity-based SOC.

The results of the experimental battery degradation tests show that PHEVs can increase their battery cycle life and power capability by implementing a DCS which allows the battery to reduce its maximum capacity-based DOD during operation so as to maintain a constant minimum t-SOC. These changes to the battery DCS should minimize increases in fuel consumption, performance and lifecycle cost of the PHEV. To determine the effects of battery degradation and DCS on these PHEV attributes, a light commercial vehicle was modeled and simulated as a blended-mode capable, parallel PHEV20. A Modelica-based vehicle simulation environment representing the LFM vehicle model presented in [17] was used to relate battery degradation to changes in vehicle performance. These simulations assume that calendar life degradation in practice is insignificantly different from calendar life degradation in the laboratory, that module-level performance degradation dominates over pack level effects such as module imbalance, and that the rate of battery degradation is independent of control strategy.

Simulations were performed using two DCSs: a “Static DCS” and a “Dynamic DCS”. The Static DCS maintained the SOC window in the battery such that the energy available for discharge remained constant over the battery’s life (equivalent to maintaining a constant, minimum capacity-based SOC over the lifetime of the vehicle). The

Dynamic DCS allowed for a constant percentage of thermodynamic capacity to be utilized in CD mode such that the energy available for discharge was a function of the actual energy available in the battery instead of rated capacity (equivalent to measuring and recalibrating the minimum t-SOC continuously over the lifetime of the vehicle). The Dynamic DCS ensured that the vehicle entered charge sustaining mode at 25% t-SOC.

The vehicle model employed in these simulations represents a limited-production vehicle which was designed so that the battery was not oversized in terms of its power output, thereby minimizing incremental costs. As such, any loss of battery power from original specifications would be immediately visible at the vehicle level. Modern PHEVs are designed with some battery power margin to allow for battery degradation without affecting the electrical power capability of the drivetrain. As such, these degradation simulations represent a worst-case scenario.

Degradation Control Strategy (DCS) [57]

The work presented by [57] was a critique of the USABC manuals which were present at the time of [57]'s publication (2011). At the time, the work conducted was with respect to the 1996 USABC standards, whereas today there is a June 2015 revision (Rev. 3) of these USABC documents [58].

The question of charge patterns is specifically addressed in [35] and [33] [8] [60] [36]

Hoke et al. [60]performed a study using a simplified lithium-ion battery lifetime model (which includes effects due to temperature, state of charge profile, and daily depth of discharge) with the goal of developing an optimized charge pattern which would account for electricity cost and degradation. The chemistry utilized for this study was that of nickel-cobalt-aluminum (NCA) cathode and graphite anode. The optimized charging algorithm as described in [60] was run simultaneously for three vehicles with different plug-in times, initial SOCs, and charge target times. Each vehicle had a 30-kWh battery pack with a minimum SOC of 20% and a maximum SOC of 90%. Ambient temperature for this experiment was set at 25°C.

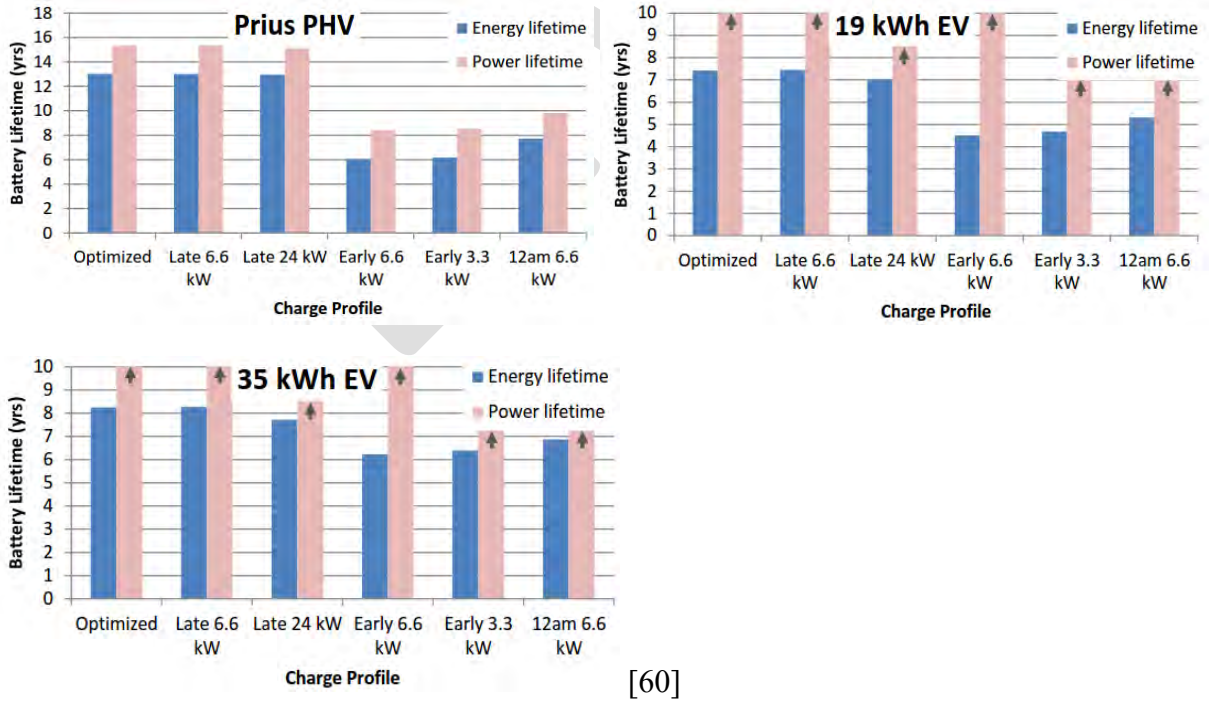

[60]

Niikuni et al. [61] sought to construct a test method for the evaluation of battery degradation, using load conditions that reflect the situation of an actual vehicle. In this study, the degrees of influence of two load terms, both a specific charge/discharge load (corresponding to the cycle life) and a thermal load (corresponding to the calendar life), in the capacity reduction were compared and a condition for an accelerated test was also discussed [61]. Four sets of three batteries each were tested at temperatures of 25°C, 40°C, 55°C, and 70°C.

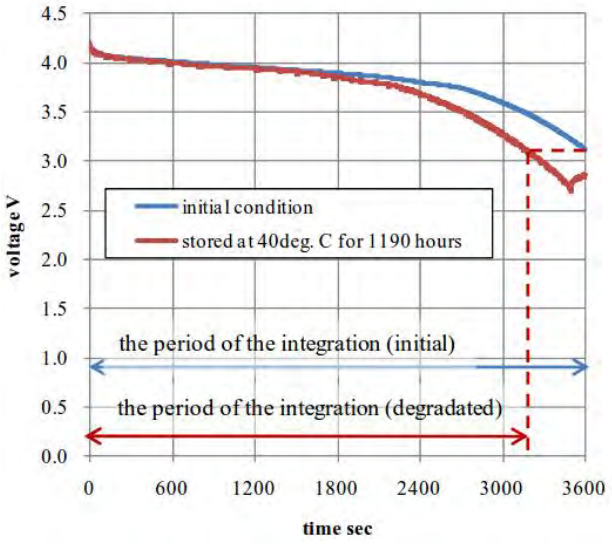

Figure 63 Comparison of the discharge characteristics of a battery which was initially not stored at 40°C at beginning of testing and after 1190 hours of storage at 40°C **[61]**.

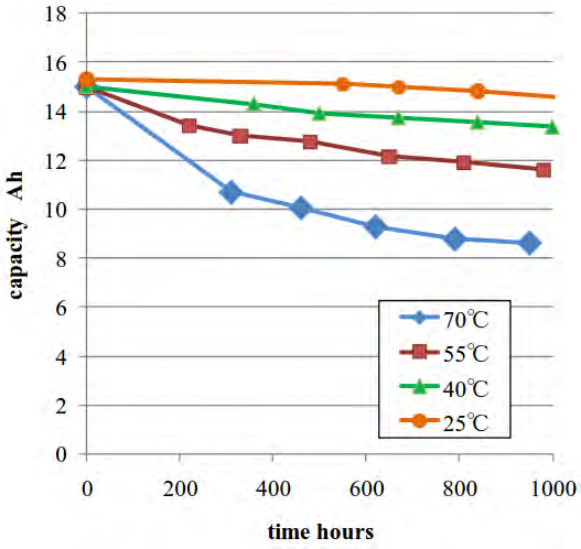

Figure 64 decrease of Ah capacity in each of the temperature conditions **[61]**

Capacity under a strictly thermal load was examined. The results showed that for ambient temperatures below 55°C, the capacity loss of test battery cells was proportional to the square root of days. Although the test battery cells had relatively short lifetime, the characteristic of the capacity loss against thermal load was same as that of other typical lithium ion batteries. Only the variation of the capacity loss under the condition of 70°C was not proportional against the square root of days and it suggested that other degradation processes, for example the degradation in the electrolyte, might be influenced.

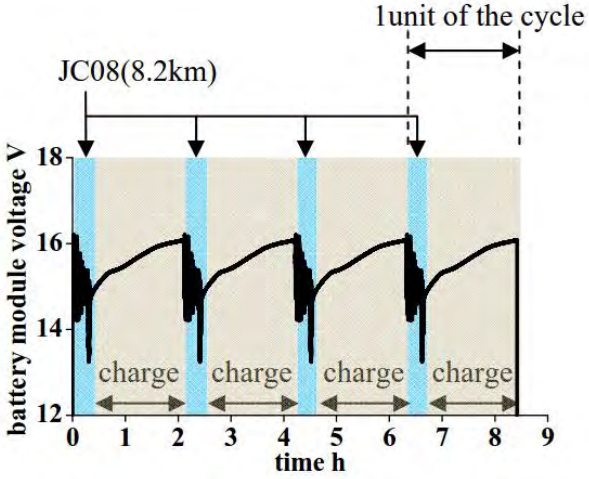

Figure 65 Voltage variation of the test battery module with the JC08 charge/discharge patterns [67]

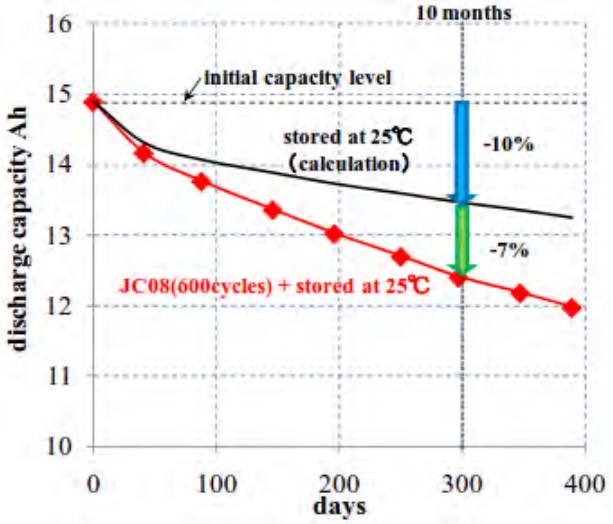

Figure 66 Variation of the discharge capacity against time in days [67]

The degree of influence of two load terms both the JC08 pattern cycle (corresponding to the cycle life) and the thermal load (corresponding to the calendar life) on the capacity reduction was compared. From the results, it was observed that there was a 7% difference in the capacity reduction between the specific pattern and the thermal-only load. In addition, the potential of a thermally accelerated test under the condition that consists of both the JC08 charge/discharge load and thermal load was shown. This methodology will contribute to evaluate battery degradation in a short period.

Niikuni et al. also offer an accelerated testing solution as part of their study in [67]. Coupling the JC08 cycling with an increase in temperature to +39°C (as opposed to +25°C as depicted in Figure 66), they were able to achieve the 17% loss from the initial level in 1.7 months as opposed to 10 months of testing.

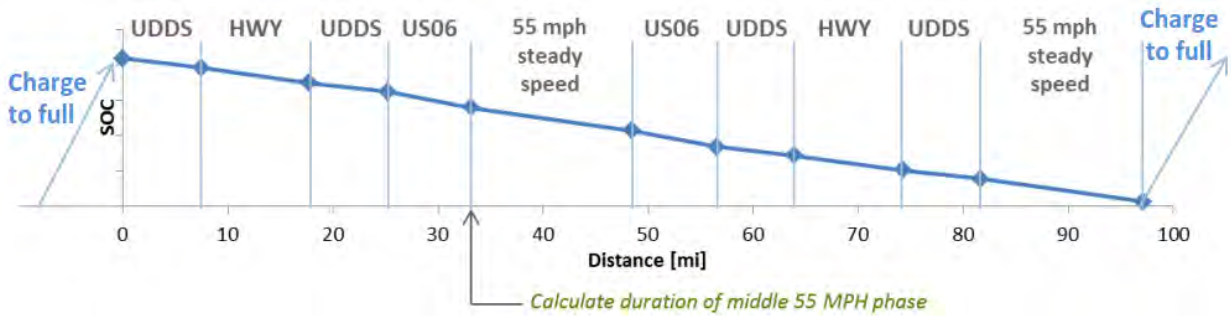

Figure 67 Multi-Cycle Test for BEV used by Argonne National Laboratory (Simplified) **[63]**

Duoba [63]

Fleet & On-Road Testing Activities

The Advanced Vehicle Testing Activity (AVTA) of the Idaho National Laboratory has the stated purpose of providing benchmark data for technology modeling, and research and development programs, by benchmarking and validating the performance of light-, medium-, and heavy-duty vehicles that feature one or more advanced technologies. Published on their website one is able to find test reports for a number of xEVs, with many models of vehicles having multiple unique vehicles (given by VIN) evaluated.

Vehicle models for which battery testing information is available is shown in below in Table 16.

Battery Electric Vehicles (BEVs)	Hybrid Electric Vehicles (HEVs)	Plug-In Hybrid Electric Vehicles (PHEVs)
• 2015 Chevrolet Spark • 2015 KIA Soul • 2014 BMW i3 • 2014 Smart Electric Drive Coupe • 2013 Ford Focus • 2013 Nissan Leaf • 2012 Mitsubishi i-MiEV • 2012 Nissan Leaf • 2011 Nissan Leaf	• 2015 Honda Accord • 2014 Volkswagen Jetta • 2013 Ford C-Max • 2013 Chevrolet Malibu • 2013 Honda Civic • 2011 Hyundai Sonata • 2011 Honda CRZ • 2010 Toyota Prius Gen III • 2010 Ford Fusion	• 2014 BMW i3 REx • 2013 Ford Fusion Energi • 2013 Ford C-Max Energi • 2013 Toyota Prius PHEV • 2013 Chevrolet Volt • 2011 Chevrolet Volt • 2011 Chrysler Town & Country

	• 2010 Honda Insight • 2008 Chevrolet Tahoe • 2007 Nissan Altima • 2007 Saturn Vue • 2007 Toyota Camry • 2006 Honda Civic • 2006 Lexus RX400H • 2005 Ford Escape • 2005 Honda Accord • 2004 Chevrolet Silverado • 2004 Toyota Prius • 2003 Honda Civic • 2002 Toyota Prius • 2001 Honda Insight	

Table 16 Vehicle Models with Battery Testing Results from INL [68] [69] [70]

For testing the vehicles in **Table 16**, they are operated on-road for a minimum mileage accumulation of 160,000 miles. Vehicle characteristics are then weighed against the existing DOE End of Life criteria using tests for acceleration, hybrid pulse power characterization, and static capacity. Degradation values are evaluated at initial laboratory and final laboratory tests. It should be noted that some of the later models in **Table 16** have only undergone their initial tests, and degradation figures are not yet available.

Some remarks regarding the fleet testing of vehicles:

On-road fleet testing was conducted for the 2010 Ford Fusion (160,000 miles) [71], 2010 Honda Insight (160,000 miles) [72],

Selected Case: 2012 Chevrolet Volt (PHEV)

On-road testing of a 2012 Chevrolet Volt was performed during the winter and spring months to determine the impact of cold temperature on driving and charging efficiency. A single test vehicle was parked and charged overnight in an unsheltered parking stall and driven by a single driver in the morning along a specified route. The route included a mix of rural, city, and highway roads in the Idaho Falls, Idaho area. Both the vehicle and the charging equipment were instrumented to record energy consumption and other usage parameters during driving and charging. [64]

Procedure

The testing regime specified that a single driver repeatedly drive a single 2012 Chevrolet Volt on a prescribed route on numerous days with varying ambient temperature. Each night, the vehicle was parked in an unsheltered parking stall, plugged in, and the battery pack fully charged. Each day, the driver completed two or more tests (where one test is defined as one lap around the prescribed route) to fully deplete the battery pack. Data were collected to quantify vehicle efficiency on a per-mile basis, distance driven in EV mode, and the distance driven until the vehicle transitioned from CD to CS mode (referred to as CD range). The vehicle and charging equipment were instrumented to record energy consumption, distance driven, engine state, and other parameters. Ambient temperature was logged by a measurement device located at the vehicle's parking location. The driver also recorded data provided by the Volt's instrument panel and center console display.

A route was selected on public roads in the Idaho Falls, Idaho area that includes a mix of city, rural, and highway driving. The route was 16.9 miles, starting and ending at the Volt's overnight parking location.

The route was not intended to mimic any standardized test cycle. The posted speed limit along this route ranged from 25 to 65 mph. Figure 1 shows a speed trace from a single test, chosen at random.

To reduce variation in efficiency due to changing driving style or aggressiveness, the driver was instructed to accelerate mildly to the posted speed limit and cruise within 2 mph above or below the posted speed limit. Occasionally, traffic required the driver to slow his speed below this tolerance. The driver was instructed to brake mildly and, to the extent possible, maximize the potential for regenerative braking by following the guide on the Volt's instrument panel.

Interim Conclusions

Not only do extreme ambient temperatures have direct effects on the internal chemistry of xEV batteries, but the demands on the HVAC systems of xEVs place further strain on battery systems by consuming energy in order to provide heating or cooling.

Fast charging is shown to accelerate degradation of xEV batteries. This effect is enhanced by operation in extreme temperature conditions, with fast charging in cold environments being particularly damaging to battery lifetime.

Fully charging and discharging batteries (deep discharges) also impacts battery lifetime. Maintaining a mid-range SOC offers improved longevity.

Existing Test Standards & Procedures

FEV GmbH has a facility intended solely for durability testing located in Brehna, Germany. The FEV Durability Test Center (Ger: *FEV Dauerlaufprüfzentrum*) [66]. The second and third expansions of the Durability Test Center (DLP-II and III) are fully capable of supporting hybrid and fully electric vehicles. In total, there are 58 engine test cells (of which 10 are equipped for deep freeze and thermal shock). Additionally, there are 8 powertrain test cells (2WD and 4WD) along with 10 dummy test benches. Each of the 76 test benches mentioned support battery simulation environments, with FEV able to provide high voltage capabilities of 400 to 600V.

In its PHEV Battery Test Manual, the Idaho National Laboratory (INL) identifies three phases of testing, with those being characterization, life, and reference performance testing. As part of the scope of this review, we shall focus on both life and reference performance testing as it is derived from the INL PHEV Battery Test Manual. Characterization testing establishes the baseline performance and includes static capacity, hybrid pulse power characterization, self-discharge, cold cranking, thermal performance, and efficiency tests. Life testing establishes behavior over time at various temperatures, states of charge and other stress conditions and includes both cycle life and calendar life testing. Reference Performance Tests establish changes in the baseline performance and are performed periodically during life testing, as well as at the start- and end-of-life testing.

Comparison of Standard Test Procedures from SAE, USABC, IEC, and ISO

Abuse tests are intended to emulate abnormal conditions or environments or when a battery pack is used in a manner outside the design parameters or beyond useful life. Abuse tests can be grouped into three major categories:

1. Thermal Abuse (includes thermal stability, simulated fuel fire, elevated temperature storage, rapid charge/discharge, and thermal shock cycling)

2. Electrical Abuse (includes overcharge/overvoltage, short circuit, overdischarge/voltage reversal, and partial short circuit)
3. Mechanical Abuse (includes controlled crush, penetration, drop, immersion, roll-over simulation, vibration, and mechanical shock)

International Standards & Procedures

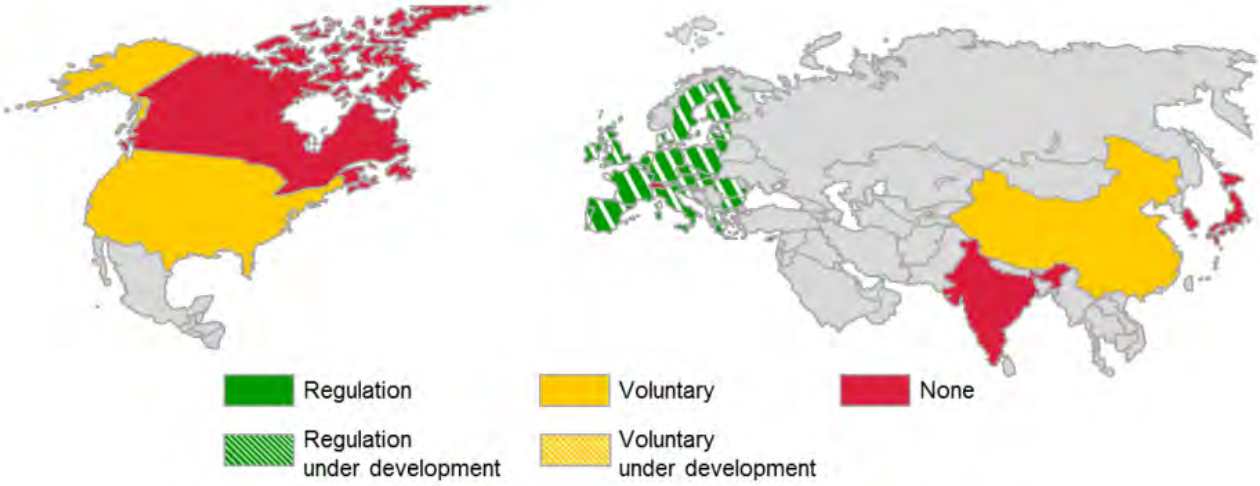

Figure 68 Battery durability requirements, world-wide view [80]

According to EVE-IWG [80] battery durability is somewhat unaddressed by present standards, with some exceptions being partial coverage in US and Canadian laws and optional Automotive Industry Standards in China. The activity level is expected to increase however with plans to develop battery durability requirements within the framework of the WLTP, which will be subsequently adopted into EC law (2015/2016). These requirements will not only address battery lifecycle determination, but the impact of partially deteriorated batteries on CO_2 emissions / fuel economy. [80]

The US EPA/NHTSA specifies a procedure for measuring the deterioration of PHEV batteries. This is to ensure that the CO_2 emissions from the vehicle do not increase excessively over the useful life of the vehicle. The regulation requires that CO_2 deterioration not exceed 10% of a vehicles certified value at full useful life. There are no regulations in place to address the durability of battery packs in BEVs, but the USABC has voluntary test procedures that can be followed for testing these so-called rechargeable energy storage devices (RESSs) [9]. There also exist voluntary SAE standards for battery module life cycle testing (J2288) and vibration testing (J2380). It should be noted that SAE J2288 is functionally identical [81] is the USABC Baseline Life Cycle Test Procedure. The California Air Resources Board (ARB) stipulates a durability requirement for HEVs and PHEVs that is required in order to earn credits under the California ZEV regulation. This requirement is enforced through a 10 year, 150,000 mile warranty of "zero-emission energy storage device used for traction power" that automakers must provide in conjunction with the sale of these vehicles. Canada has adopted into Federal law the US procedure for PHEVs, and does not presently have anything in place with regard to battery electric vehicles (BEVs). China has established voluntary guidelines for the determination of battery reliability and durability through the QC/T 743-2006 Automotive Industry Standard. The EC does not presently have battery durability requirements, but will adopt into law durability test requirements that are planned to be developed within the framework of the WLPT. Voluntary standards ISO 12405-1:2011 (International Standards Organization) and IEC 62660-

2 (International Electrotechnical Commission) both address durability testing of Lithium Ion batteries. Japan, India, South Korea, and Switzerland do not presently have requirements relating to battery durability. [80]

Some of the existing standards and test procedure manuals that we shall investigate are SAEJ2464 [82], ISO 12405-1/2 [83] [84], UN38.3 [85], FreedomCAR Battery Test Manual For Power-Assist Hybrid Electric Vehicles , Battery Technology Life Verification Test Manual [9]

As we consider durability to relate battery lifetime, from a combination of calendar life and cycle life standpoints, we shall examine components of standards and test procedures which specifically target these factors, with an emphasis on State of Health. Certain abuse and safety tests, such as penetration, shock, crush, etc. are not considered as part of the scope encompassing durability.

Life Testing Procedures

Per the U.S. Department of Energy and Idaho National Laboratory [58] [56], life testing consists of cycle-life and calendar-life aging to ensure the device can meet EOL targets. Cycle-life testing consists of repeating a test profile continuously for a sustained period of time until the appropriate amount of energy has been depleted specified by EOL. Cycle life testing as defined per ISO 12405-1

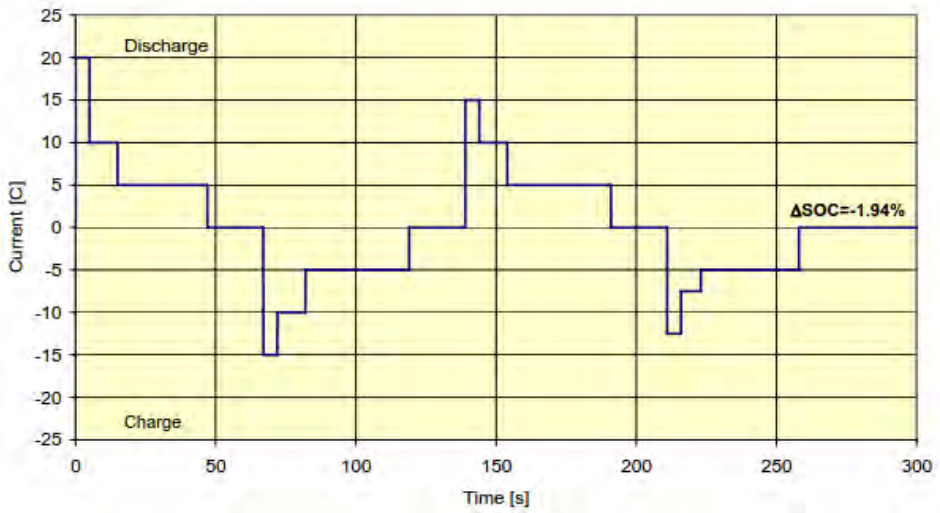

Figure 69 ISO 12405-1 — Current profile for cycle life test — Discharge-rich profile [83]

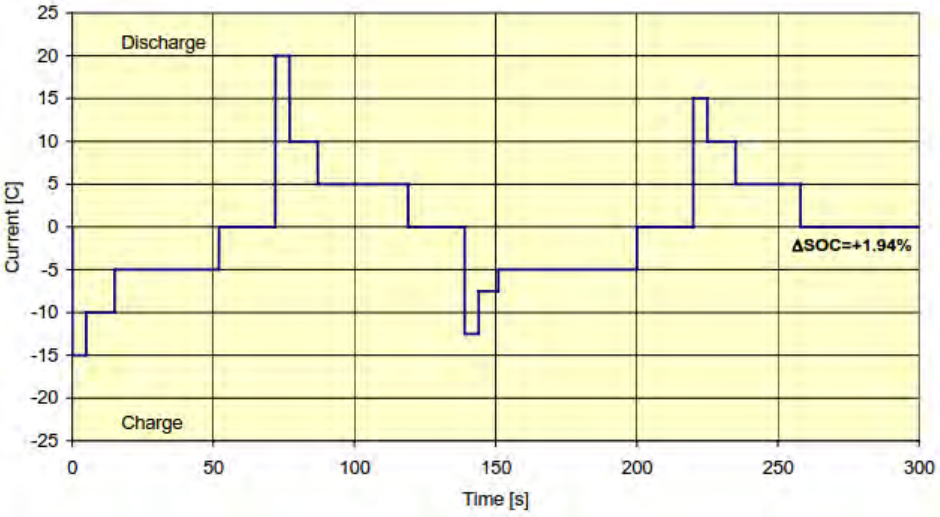

Figure 70 12405-1 — Current profile for cycle life test — Charge-rich profile [83]

As shown in Figure 69 and Figure 70, ΔSOC is -1.94% and +1.94%, respectively, over a period of 300 seconds. These cycles are combined in Figure 71 to present a cycle wherein the battery SOC goes from 80% to 30% and is then charged back up to 80%. Operating within this SOC range is a good way to ensure battery longevity, as deep-discharges from 100%-0% are shown to negatively impact battery SOH.

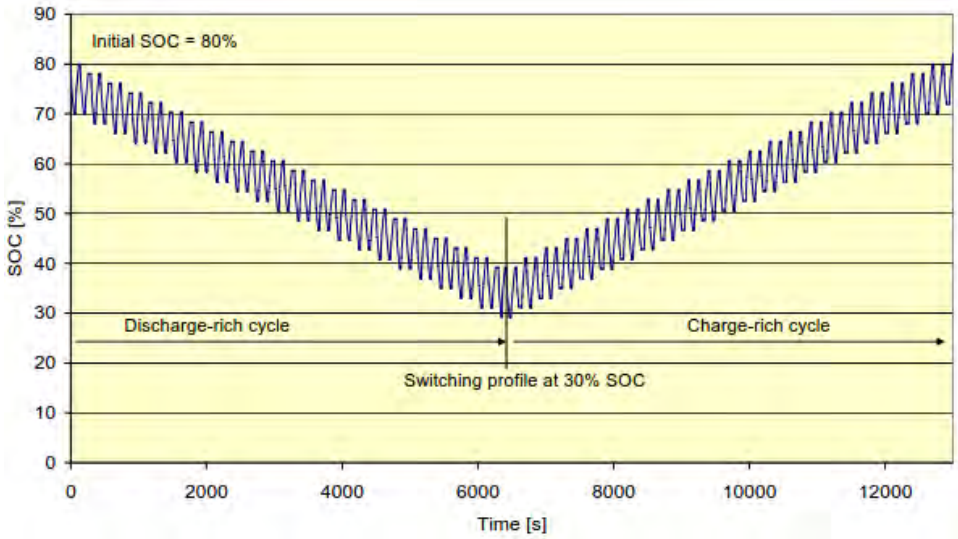

Figure 71 12405-1 — Typical SOC swing for combined cycles in Figure 69 and Figure 70 [83]

In the case of ISO 12405-2, SOC swing is from 100% to 20%. As above, there are two procedures which are combined to form a full cycle, and in this instance these are

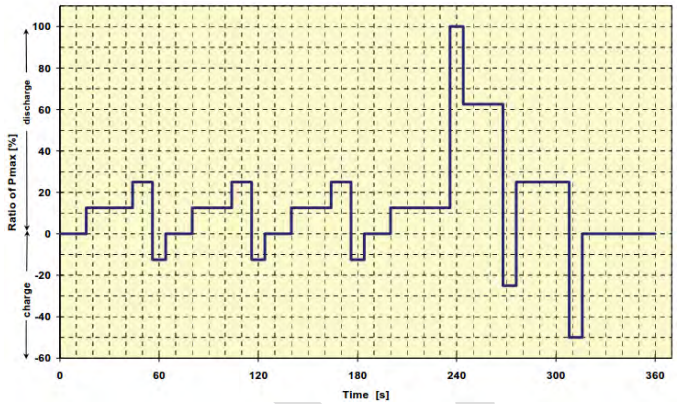

Figure 72 ISO 12405-2 Profile for cycle life test — Dynamic discharge power profile A [84]

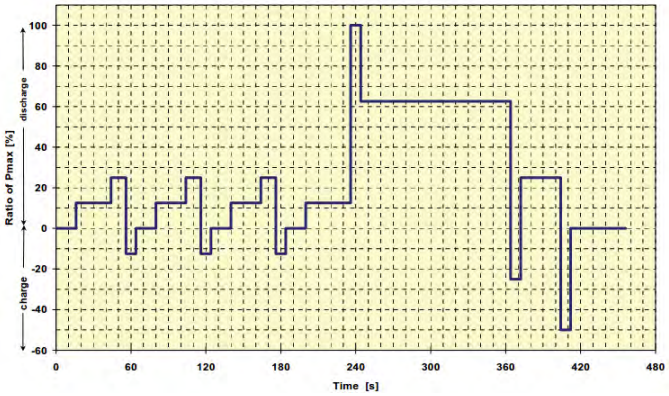

Figure 73 ISO 12405-2 Profile for cycle life test — Dynamic discharge power profile B [84]

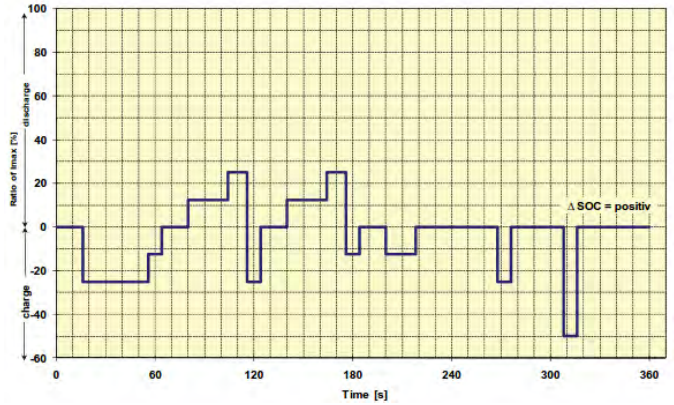

Figure 74 ISO 12405-2 Profile for cycle life test — Plug-in charge-rich current profile [84]

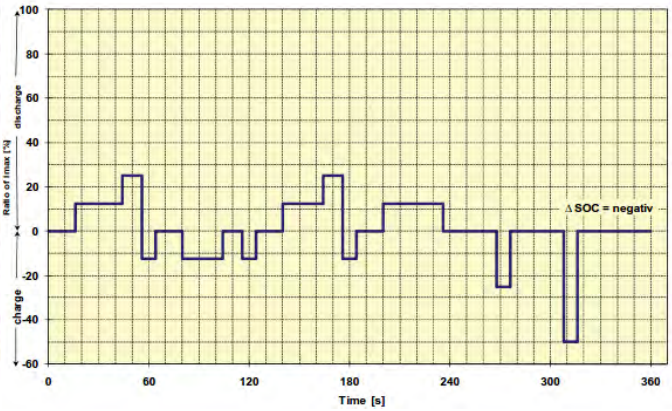

Figure 75 ISO 12405-2 Profile for cycle life test — Plug-in discharge-rich current profile [84]

Calendar-life testing generally consists of resting the device under test at OCV using elevated test temperatures with a pulse profile applied once per day. Calendar life tests are therefore more of an evaluation of degradation due to the passage of time. The specification for calendar life has the battery being charged and stored at 30°C. This provides an adequately high temperature when compared to some of the findings for average temperature as determined by the climate data used in [55], [43], [41], [40], **and** [37].

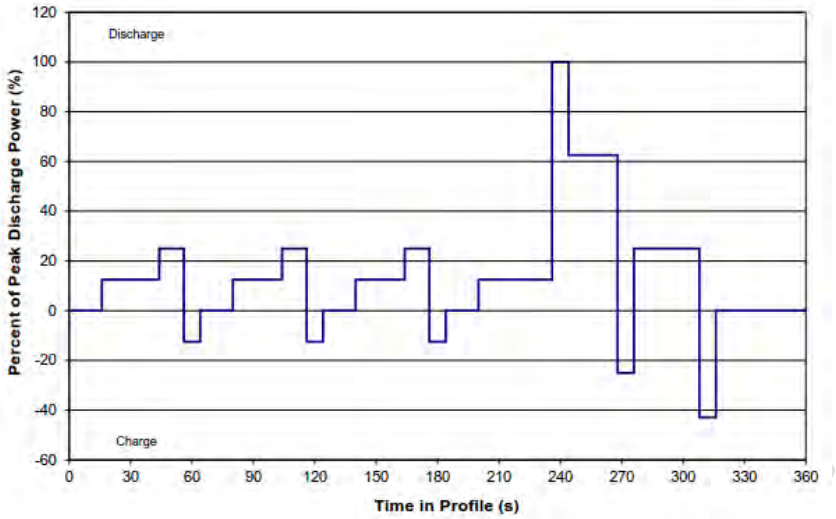

Figure 76 Charge-Depleting Cycle Life Test Profile for the BEV Battery [58]

One set of standards which may not have been considered for commercial electric vehicle applications are those from the United States Department of Defense [86], specifically for Group 31 and Group 34 lithium-ion batteries. These feature a range of performance and environmental tests which may be useful for determining some standards for xEV testing. Some of these specified tests are:

1. **Deep Cycle Life**: The batteries shall maintain at least 80% capacity rating after >1000 100% depth of discharge cycles at 35°C. Each cycle shall consist of a 1C rate charge and 1C rate discharge.
2. **High Temperature Cycle Life Test**: The batteries shall maintain at least 80% capacity rating after 250 100% depth of discharge cycles at 60°C. Each cycle shall consist of a 1C rate charge and 1C rate discharge.
3. **Battery Storage and Charge Retention (capacity fade)**: The batteries shall have a capacity fade of no more than 10% over a 90 day period at 40°C. The battery shall have a shelf life of at least 30 months. Shelf life is defined as the battery stored at 100% state of charge and not dropping below 20% state of charge at 25°C.
4. **Calendar Life**: The batteries' calendar life shall be at least 5 years when properly maintained in storage and when not exceeding cycle life.

SAE J2464 [82]

Mechanical Abuse Tests

- Shock Tests
- Drop Test

- Penetration Test
- Roll-over Test
- Immersion Test
- Crush Test

Thermal Abuse Tests

- High Temperature Hazard Test
- Thermal Stability Test
- Cycling without Thermal Management
- Thermal Shock Cycling
- Passive Propagation Resistance Test

Electrical Abuse Tests

- Short Circuit Tests
- Overcharge Test
- Overdischarge Test
- Separator Shutdown Integrity Test

MIL-STD-810G [85]

- Humidity
- Salt Fog
- Sand and Dust
- Fluid Susceptibility

INL / Department of Energy BEV [58]

- Static Capacity Test
- High Rate Charge
- Hybrid Pulse Power Characterization Test
- Peak Power Test
- Self-Discharge Test
- Thermal Performance Test
- Life Testing
- Cycle Life Dynamic Stress Tests
- Calendar Life Test

INL / Department of Energy PHEV [56]

- Static Capacity Test
- Constant Power Discharge Tests
- Hybrid Pulse Power Characterization Test
- Self-Discharge Test

- Cold Cranking Test
- Thermal Performance Test
- Energy Efficiency Test
- Life Testing
- Charge-Sustaining Cycle Life Tests
- Charge-Depleting Cycle Life Tests
- Calendar Life Test

FreedomCAR 42V [87]

FreedomCAR Power-Assist HEV [88]

UN 38.3 [89]

- Altitude Simulation
- Thermal Test
- Vibration
- Shock
- External Short Circuit
- Impact / Crush
- Overcharge
- Forced Discharge

ISO 12405-1/2 **[83] [84]**

Performance Tests

- Energy and capacity at RT
- Energy and capacity at different temperatures and discharge rates
- Power and internal resistance
- No load SOC loss
- SOC loss at storage
- Cranking power at low temperature
- Cranking power at high temperature
- Energy efficiency
- Cycle life

Reliability Tests

- Dewing (temperature change
- Thermal shock cycling
- Vibration
- Mechanical shock

Abuse tests

- Short circuit protection
- Overcharge protection
- Overdischarge protection

Recommendations and Future Work

Having examined the literature related to battery degradation & durability, testing procedures & methodologies, and existing international standards, FEV has identified several areas which the EVE-IWG may consider for investigation in developing standards for battery durability as part of its drive to establish harmonized testing programs for Electrified Vehicles. Ultimately, the decision to implement these recommendations, and the means by which they may be integrated into or utilized with the WLTP, are the sole discretion of the EVE-IWG and associated international regulatory bodies.

The key figure when determining the End of Life of an Electrified Vehicle is the capacity of the battery as a percentage of the initial or nameplate capacity. Upon reaching 80% of the initial state of charge, the battery is said to have reached its End of Life. Consequently, the combination of factors which lead to this figure must be considered as part of a whole when evaluating battery durability. Specifically, we shall look to improvements in Cycle Life and Calendar Life, along with environmental factors.

Cycle Life Testing

The number of cycles specified for PHEV and BEV EOL is 1000 [11] [10]. Some battery chemistries, such as $LiFePO_4$ have shown good cycle life performance as per the studies in [5], [8], and [23]. Temperature and the ΔSOC window / DOD in operation are, in addition to chemical considerations, large contributors to the degradation of batteries when combined with cycling. FEV recommends as part of cycle life testing a procedure which involves the following:

- Temperatures intended to indicate seasonal changes over the useful life of the vehicle. Testing should therefore allow for approximately three temperature grades: hot, average, and cold. Preliminary recommendations can be on the order of 35°C, 25°C, and -10°C for hot, average, and cold temperatures. Furthermore, one quarter of each year equivalent of cycling shall be hot, one quarter shall be cold, and one half shall be average.
- In instances where ambient temperature deviates sufficiently enough from room temperature values, cabin climate control functionality should become engaged.
- Inclusion of a mixture of fast and slow charging such that approximately four of every five cycles are charged using slow charging and the remainder is fast charged. This will give an idea of how the vehicle will react to the charging infrastructure.
- Determination of drive cycle duration and which of the stages of the WLTP shall be applied throughout should be derived from consumer patterns, indicating, for example, daily morning and evening commutes throughout a typical work-week, with the potential for longer duration, higher speed drive cycles reserved for a lesser part of the overall cycle pattern.

Calendar Life Testing

- Vehicles at rest undergo passive degradation as a function of temperature, time, and state of charge. Worst-case combinations of these factors should be considered alongside ideal cases (very high or low temperatures coupled with very high or low SOC as opposed to room temperature & mid-range SOC).

Additional Environmental Considerations for Testing

- In seeking to develop a Worldwide harmonized Light vehicle Testing Procedure, it may be prudent to seek to develop test conditions which may mimic future markets for xEVs. It may be worthwhile to adapt some of the environmental MIL standards for commercial usage (humidity [90] [91], salt spray, sand/dust, etc.)

References

[1] S. E. de Lucena, "A Survey on Electric and Hybrid Electric Vehicle Technology".

[2] C. C. Chan, A. Bouscayrol and K. Chen, "Electric, Hybrid, and Fuel-Cell Vehicles: Architectures and Modeling," *IEEE Transactions on Vehicular Technology,* vol. 59, no. 2, 2010.

[3] MIT Electric Vehicle Team, "Electric Powertrains," 2008.

[4] M. A. Kromer and J. B. Heywood, "Electric Powertrains: Opportunities and Challenges in the U.S. Light-Duty Vehicle Fleet," Laboratory for Energy and the Environment, Cambridge, MA, 2007.

[5] D. Ansean, M. Gonzalez, V. M. Garcia, J. C. Viera, J. C. Anton and C. Blanco, "Evaluation of LiFePO4 Batteries for Electric Vehicle Applications," *IEEE Transactions on Industry Applications,* vol. 51, no. 2, pp. 1855-1863, 2015.

[6] National Petroleum Council, "Advancing Technology for America's Transportation," 2012.

[7] S. J. Gerssen-Gondelach and A. Faaij, "Performance of batteries for electric vehicles on short and longer term," *Journal of Power Sources,* vol. 212, pp. 111-129, 2012.

[8] E. M. Krieger, "Effects of Variability and Rate on Battery Charge Storage and Lifespan," Princeton University, 2013.

[9] Idaho National Laboratory, "Battery Technology Life Verification Test Manual," 2012.

[10] "USABC Goals for Advanced Batteries for EVs - CY 2020 Commercialization," 2014.

[11] "USABC Goals for Advanced Batteries for PHEVs for FY 2018 to 2020 Commercialization," 2014.

[12] "USABC Goals for Advanced Batteries for 48V Hybrid Electric Vehicle Applications," 2014.

[13] A. Millner, "Modeling Lithium Ion Battery Degradation in Electric Vehicles," Lexington, MA.

[14] G. M. Ehrlich, "Lithium-Ion Batteries," in *Handbook of Batteries, 3rd Edition*, McGraw-Hill, 2001, pp. 1074-1167.

[15] V. Agubra and J. Fergus, "Lithium Ion Battery Anode Aging Mechanisms," *Materials,* no. 6, pp. 1310-1325, 2013.

[16] J. Morales, R. Trócoli, S. Franger and J. Santos-Pena, "Cycling-induced stress in lithium ion negative electrodes: LiAl/LiFePO4 and and Li4Ti5O12/LiFePO4 cells," *Electrochimica Acta,* vol. 55, pp. 3075-3082, 2010.

[17] V. Etacheri, R. Marom, R. Elazari, G. Salitra and D. Aurbach, "Challenges in the development of advanced

Li-ion batteries: a review," *The Royal Society of Chemistry,* 2011.

[18] J. Vetter, P. Novák, M. Wagner, C. Veit, K.-C. Möller, J. O. Besenhard, M. Winter, M. Wohlfahrt-Mehrens, C. Vogler and A. Hammouche, "Aging mechanisms in lithium-ion batteries," *Journal of Power Sources,* vol. 147, pp. 269-281, 2005.

[19] SECONDARYSOURCE, J. Vetter, P. Novák, M. Wagner, C. Veit, K.-C. Möller, J. O. Besenhard, M. Winter, M. Wohlfahrt-Mehrens, C. Vogler and A. Hammouche, "Aging mechanisms in lithium-ion batteries," *Journal of Power Sources,* vol. 147, pp. 269-281, 2005.

[20] P. Kubiak, M. Wolfahrt-Mehrens, K. Edström and M. Morcrette, "Review on aging mechanisms of different Li-ion batteries for automotive applications".

[21] T. Finley, "Battery Degradation Modeling for Vehicle Applications," 2015.

[22] M. Koltypin, D. Aurbach, L. Nazar and B. Ellis, "More on the performance of LiFePO4 electrodes—The effect of synthesis route, solution composition, aging, and temperature," *Journal of Power Sources,* vol. 174, p. 1241–1250, 2007.

[23] Y. Zhang, C.-Y. Wang and X. Tang, "Cycling degradation of an automotive LiFePO4 lithium-ion battery," *Journal of Power Sources,* vol. 196, pp. 1513-1520, 2011.

[24] J. Shim, R. Kostecki, T. Richardson, X. Song and K. Striebel, "Electrochemical analysis for cycle performance and capacity fading of a lithium-ion battery cycled at elevated temperature," *Journal of Power Sources,* vol. 112, pp. 222-230, 2002.

[25] Argonne National Laboratory, "Diagnostic Examination of Generation 2 Lithium-Ion Cells and Assessment of Performance Degradation Mechanisms," 2005.

[26] L. Kanevskii and V. Dubasova, "Degradation of Lithium-Ion Batteries and How to Fight It: A Review," *Russian Journal of Electrochemistry,* vol. 41, no. 1, pp. 1-16, 2005.

[27] SECONDARYSOURCE, D. Aurbach, B. Markovsky, A. Rodkin, E. Levi and Y. Cohen, "On the capacity fading of LiCoO2 intercalation electrodes: the effect of cycling, storage, temperature, and surface film forming additives," *Electrochimica Acta,* vol. 47, no. 27, p. 4291–4306, 2002.

[28] M. Broussely, S. Herreyre, P. Biensan, P. Kasztejna, K. Nechev and R. Staniewicz, "Aging mechanism in Li ion cells and calendar life predictions," *Journal of Power Sources,* Vols. 97-98, pp. 13-21, 2001.

[29] R. G. Jungst, G. Nagasubramanian, C. C. Crafts, D. Ingersoll and D. H. Doughty, "Analysis of Lithium-Ion Battery Degradation During Thermal Aging," Sandia National Laboratories, 2010.

[30] J. P. Sullivan, K. R. Fenton, F. E. G. Marquez, C. T. Harris, C. C. Hayden, N. S. Hudak, K. L. Jungjohann, C. J. Kliewer, K. Leung, K. McCarty, A. H. McDaniel, G. Nagasubramanian and J. D. Sugar, "The Science of Battery Degradation," Sandia National Laboratories, 2015.

[31] S. S. Zhang, "The effect of the charging protocol on the cycle life of a Li-ion battery," *Journal of Power Sources 161,* vol. 161, pp. 1385-1391, 2006.

[32] J. Groot, "State-of-Health Estimation of Li-ion Batteries: Cycle Life Test Methods," Chalmers University of Technology, Göteborg, Sweden, 2012.

[33] A. Bandyopadhyay, L. Wang, V. K. Devabhaktuni, R. Yang and R. C. G. II, "Assessing the Effect of Fast Charging on the Battery Health of Plug-in Hybrid Electric Vehicles," IEEE, Toledo, OH, 2012.

[34] G. Lacey, T. Jiang, G. Putrus and R. Kotter, "The Effect of Cycling on the State of Health of the Electric Vehicle Battery," in *Power Engineering Conference (UPEC), 2013 48th International Universities*, 2013.

[35] S. Bashash, S. J. Moura and H. K. F. Joel C. Forman, "Plug-in hybrid electric vehicle charge pattern optimization for energy cost and battery longevity," Ann Arbor, MI, 2010.

[36] A. Hoke, A. Brissette, D. Maksimovic, D. Kelly, D. Boundy and A. Pratt, "Maximizing Lithium Ion Vehicle Battery Life Through Optimized Partial Charging".

[37] J. Neubauer, E. Wood, E. Burton, K. Smith and A. Pesaran, "FY14 Milestone: Simulated Impacts of Life-Like Fast Charging on BEV Batteries," 2014.

[38] J. Neubauer and E. Wood, "Will Your Battery Survive a World With Fast Chargers?," 2015.

[39] L. Serrao, Z. Chehab, Y. Guezennec and G. Rizzoni, "An Aging Model of Ni-MH Batteries for Hybrid Electric Vehicles," 2005.

[40] K. Smith, M. Earleywine, E. Wood, J. Neubauer and A. Pesaran, "Comparison of Plug-In Hybrid Electric Vehicle Battery Life Across Geographies and Drive Cycles," 2012.

[41] H. Lohse-Busch, M. Duoba, E. Rask and M. Meyer, "Advanced Powertrain Research Facility AVTA Nissan Leaf Testing and Analysis," 2012.

[42] H.-S. Song, J.-B. Jeong, B.-H. Lee, D.-H. Shin, B.-H. Kim, T.-H. Kim and H. Heo, "Experimental Study on the Effects of Pre-Heating a Battery in a Low-Temperature Environment," in *IEEE Vehicle Power and Propulsion Conference*, Seoul, Korea, 2012.

[43] R. A. Barnitt, A. D. Brooker, L. Ramroth, J. Rugh and K. Smith, "Analysis of Off-Board Powered Thermal Preconditioning in Electric Drive Vehicles," 2010.

[44] J. P. Rugh, A. Pesaran and K. Smith, "Electric Vehicle Battery Thermal Issues and Thermal Management Techniques," 2013.

[45] K. Vatanparvar and M. A. Al-Faruque, "Battery Lifetime-Aware Automotive Climate Control for Electric Vehicles," San Fransisco, CA, 2015.

[46] T. Yuksel and J. Michalek, "Evaluation of the Effects of Thermal Management on Battery Life in Plug-in Hybrid Electric Vehicles".

[47] K. Smith, M. W. E. Earleywine and A. Pesaran, "Battery Wear from Disparate Duty-Cycles: Opportunities for Electric-Drive Vehicle Battery Health Management," 2012.

[48] A. Pesaran, S. Santhanagopalan and G. H. Kim, "Addressing the Impact of Temperature Extremes on Large Format Li-Ion Batteries for Vehicle Applications," 2013.

[49] M. Allen, "Electric Range for the Nissan Leaf & Chevrolet Volt in Cold Weather," fleetcarma, [Online]. Available: http://www.fleetcarma.com/nissan-leaf-chevrolet-volt-cold-weather-range-loss-electric-vehicle/. [Accessed 27 July 2015].

[50] S. Santhanagopalan, Q. Zhang, K. Kumaresan and R. E. White, "Parameter Estimation and Life Modeling of Lithium-Ion Cells," *Journal of the Electrochemical Society,* vol. 155, no. 4, pp. A345-A353, 2008.

[51] M. C. Smart, B. V. Ratnakumar, J. F. Whitacre, L. D. Whitcanack, K. B. Chin, M. D. Rodriguez, D. Zhao, S. G. Greenbaum and S. Surampudi, "Effect of Electrolyte Type upon the High-Temperature Resilience of Lithium-Ion Cells," *Journal of the Electrochemical Society,* vol. 152, no. 6, pp. A1096-A1104, 2005.

[52] M. Conte, F. V. Conte, I. D. Bloom, K. Morita, T. Ikeya and J. R. Belt, "Aging Testing Procedures on Lithium Batteries in an International Collaboration Context," in *25th World Battery, Hybrid, and Fuel Cell Electric Vehicle Symposium & Exhibition*, 2010.

[53] P. Spagnol, S. Onori, N. Madella, Y. Guezennec and J. Neal, "Aging and Characterization of Li-Ion Batteries in a HEV Application for Lifetime Estimation".

[54] K. Takei, K. Kumai, Y. Kobayashi, H. Miyashiro, N. Terada, T. Iwahori and T. Tanaka, "Cycle life estimation of lithium secondary battery by extrapolation method and accelerated aging test," *Journal of Power Sources,* vol. 97, pp. 697-701, 2001.

[55] E. Wood, J. Neubauer, A. D. Brooker, J. Gonder and K. A. Smith, "Variability of Battery Wear in Light Duty Plug-In Electric Vehicles Subject to Ambient Temperature, Battery Size, and Consumer Usage," in *International Battery, Hybrid and Fuel Cell Electric Vehicle Symposium 26*, Los Angeles, California, 2012.

[56] Idaho National Laboratory, "Battery Test Manual For Plug-In Hybrid Electric Vehicles (Rev. 3)," United States Department of Energy, 2014.

[57] E. Wood, M. Alexander and T. H. Bradley, "Investigation of battery end-of-life conditions for plug-in hybrid electric vehicles," *Journal of Power Sources,* vol. 196, pp. 5147-5154, 2011.

[58] Idaho National Laboratory, "Battery Test Manual for Electric Vehicles, Rev. 3," 2015.

[59] D. H. Doughty and C. C. Crafts, "FreedomCAR Electrical Energy Storage System Abuse Test Manual for Electric and Hybrid Electric Vehicle Applications," Sandia National Laboratories, 2005.

[60] A. Hoke, A. Brissette, K. Smith, A. Pratt and D. Maksimovic, "Accounting for Lithium-Ion Battery Degradation in Electric Vehicle Charging Optimization," 2013.

[61] T. Niikuni, K. Koshika and T. Kawai, "Evaluation of the influence of JC08-based cycle stress on batteries in plug-in hybrid electric vehicle," 2010.

[62] M. Dubarry, N. Vuillaume, B. Y. Liaw and T. Quinn, "Vehicle Evaluation, Battery Modeling, and Fleet-testing Experiences in Hawaii: A Roadmap to Understanding Evaluation Data and Simulation," *Journal of Asian Electric Vehicles,* vol. 5, no. 2, pp. 1033-1042, 2007.

[63] M. Duoba, H. Lohse-Busch, K. Stutenberg and E. Rask, "HEV, PHEV, EV Testing Activities," 2013.

[64] J. Smart, "Advanced Vehicle Testing Activity Cold Weather On-road Testing of the Chevrolet Volt," 2015.

[65] J. P. Rugh, A. Pesaran and K. Smith, "Electric Vehicle Battery Thermal Issues and Thermal Management Techniques," in *Alternative Refrigerant and System Efficiency Symposium*, Scottsdale, Arizona USA, 2011.

[66] FEV GmbH, "The New FEV Durability Test Center in Brehna near Leipzig," 2009.

[67] D. H. Doughty and A. A. Pesaran, "Vehicle Battery Safety Roadmap Guidance," 2012.

[68] "Full Size Battery Electric Vehicles," Idaho National Laboratory, [Online]. Available: http://avt.inl.gov/fsev.shtml. [Accessed 23 July 2015].

[69] "Hybrid Electric Vehicles," Idaho National Laboratory, [Online]. Available: http://avt.inl.gov/hev.shtml. [Accessed 23 July 2015].

[70] "Plug-in Hybrid Electric Vehicles/Extended Range Electric Vehicles," Idaho National Laboratory, [Online]. Available: http://avt.inl.gov/phev.shtml. [Accessed 23 July 2015].

[71] T. Gray and M. Shirk, "2010 Ford Fusion VIN 4757 Hybrid Electric Vehicle Battery Test Results," 2013.

[72] T. Gray, "2010 Honda Insight VIN 0141 Hybrid Electric Vehicle Battery Test Results," 2013.

[73] T. Gray and M. Shirk, "2010 Toyota Prius VIN 0462 Hybrid Electric Vehicle Battery Test Results," 2013.

[74] T. Gray, M. Shirk and J. Wishart, "2010 Honda Civic Hybrid Ultra Battery Conversion 5577 - Hybrid Electric Vehicle Battery Test Results," 2013.

[75] T. Gray, M. Shirk and J. Wishart, "2010 Honda CR-Z VIN 4466 Hybrid Electric Vehicle Battery Test Results," 2014.

[76] T. Gray, M. Shirk and J. Wishart, "2011 Chevrolet Volt VIN 0815 Plug-In Hybrid Electric Vehicle Battery Test Results," 2013.

[77] T. Gray, M. Shirk and J. Wishart, "2011 Hyundai Sonata VIN 3539 Hybrid Electric Vehicle Battery Test Results," 2014.

[78] J. Francfort, D. Karner, R. Harkins and J. Tardiolo, "Hybrid Electric Vehicle End-Of-Life Testing On Honda Insights, Gen I Civics And Toyota Gen I Priuses," 2006.

[79] D. Skaggs, J. Smith and R. P. Hill, "The Electric Vehicle Fleet Experience at Southern California-Edison," *The World Electric Vehicle Journal,* vol. 2, no. 4, pp. 135-139, 2008.

[80] The United Nations Economic Commission for Europe, "Electric Vehicle Regulatory Reference Guide, First Draft".

[81] "J2288: Life Cycle Testing of Electric Vehicle Battery Modules," SAE International, [Online]. Available: http://standards.sae.org/j2288_200806/.

[82] SAE International, "SAE J2464 Surface Vehicle Recommended Practice: Electric and Hybrid Electric Vehicle Rechargeable Energy Storage System (RESS) Safety and Abuse Testing," SAE International, 2009.

[83] International Organization for Standardization, "ISO 12405-1: Electrically propelled road vehicles — Test specification for lithium-Ion traction battery systems — Part 1: High power applications," 2009.

[84] International Organization for Standardization, "ISO 12405-2: Electrically propelled road vehicles — Test specification for lithium-Ion traction battery systems — Part 2: High energy applications," 2010.

[85] United States Department of Defense, "MIL-STD-810G: Department of Defense Test Method Standard for Environmental Engineering Considerations and Laboratory Tests," 2008.

[86] L. Toomey, "Battery Specification for MATV, Group 31 and 34 Li-Ion Battery," U.S. Army TARDEC, Warren, MI, 2011.

[87] USABC, Idaho National Laboratory, "FreedomCAR 42V Battery Test Manual," 2003.

[88] USABC, Idaho National Laboratory, "FreedomCAR Battery Test Manual for Power-Assist Hybrid Electric Vehicles," U.S. Department of Energy, 2003.

[89] United Nations, "38.3 Lithium metal and lithium ion batteries," in *Recommendations on the Transport of Dangerous Goods: Manual of Tests and Criteria*.

[90] H. Horie, T. Abe, T. Kinoshita and Y. Shimoida, "A Study on an Advanced Lithium-ion Battery System for EVs," *The World Electric Vehicle Journal,* vol. 2, no. 2, pp. 25-31, 2008.

[91] M. Ebner, F. Marone, M. Stampanoni and V. Wood, "Visualization and Quantification of Electrochemical and Mechanical Degradation in Li Ion Batteries," *Science,* vol. 342, pp. 716-719, 2013.

[92] S. Zhang, K. Xu and T. Jow, "EIS study on the formation of solid electrolyte interface in Li-ion battery," *Electrochimica Acta,* vol. 51, pp. 1636-1640, 2006.

[93] S. J. Harris and P. Lu, "Effects of Inhomogeneities - Nanoscale to Mesoscale - on the Durability of Li-Ion Batteries," *Journal of Physical Chemistry C,* vol. 117, pp. 6481-6492, 2013.

[94] F.-M. Wang, M.-H. Yu, Y.-J. Hsiao, Y. Tsai, B.-J. Hwang, Y.-Y. Wang and C.-C. Wan, "Aging Effects to Solid Electrolyte Interface (SEI) Membrane Formation and the Performance Analysis of Lithium Ion Batteries," *International Journal of Electrochemical Science,* vol. 6, pp. 1014-1026, 2011.

[95] S. Han, H. Aki and S. Han, "A Practical Battery Wear Model for Electric Vehicle Charging Applications," 2013.

[96] L. Gaines and J. Sullivan, "A Review of Battery Life-Cycle Analysis: State of Knowledge and Critical Needs," October 1, 2010.

[97] S. Santhanagopalan, Q. Guo, P. Ramadass and R. E. White, "Review of models for predicting the cycling performance of lithium ion batteries," *Journal of Power Sources,* vol. 156, pp. 620-628, 2006.

[98] L. Gaillac, "Accelerated Testing of Advanced Battery Technologies in PHEV Applications," *The World Electric Vehicle Journal,* vol. 2, no. 2, pp. 83-92, 2008.

[99] Y. Xing, Q. Miao, K.-L. Tsui and M. Pecht, "Prognostics and Health Monitoring for Lithium-ion Battery," 2011.

[100] V. Marano, S. Onori, Y. Guezennec, G. Rizzoni and N. Madella, "Lithium-ion Batteries Life Estimation for Plug-in Hybrid Electric Vehicles," 2009.

[101] J. Zhang and J. Lee, "A review on prognostics and health monitoring of Li-ion battery," *Journal of Power Sciences,* vol. 196, pp. 6007-6014, 2011.

[102] B. Dickinson, J. Baer, O. A. Velev and D. Swan, "Performance, Management and Testing Requirements for Hybrid Electric Vehicle Batteries".

[103] SECONDARYSOURCE, M. Kassem, J. Bernard, R. Revel, S. Pelissier, F. Duclaud and C. Delacourt, "Calendar aging of a graphite LiFePO4 cell," *Journal of Power Sources,* vol. 208, pp. 296-305, 2012.

[104] SECONDARYSOURCE, A. Barré, B. Deguilhem, S. Grolleau, M. Gérard, F. Suard and D. Riu, "A review on lithium-ion battery aging mechanisms and estimations for automotive applications," *Journal of Power Sources,* vol. 241, pp. 680-689, 2013.

[105] SECONDARYSOURCE, P. B. M. Broussely, F. Bonhomme, P. Blanchard, S. Herreyre, K. Nechev and R. Staniewicz, "Main aging mechanisms in Li ion batteries," *Journal of Power Sources,* vol. 146, pp. 90-96, 2005.

[106] SECONDARYSOURCE, Q. Badey, G. Cherouvrier, Y. Reynier, J.-M. Duffault and S. Franger, "Aging forecast of lithium-ion batteries for electric and hybrid vehicles," *Current Topics in Electrochemistry,* vol. 16, pp. 65-79, 2011.

[107] M. B. Pinson and M. Z. Bazant, "Theory of SEI Formation in Rechargeable Batteries: Capacity Fade, Accelerated Aging and Lifetime Prediction".

[108] L. Gaines, J. Sullivan, A. Burnham and I. Belharouak, "Life Cycle Analysis for Lithium-Ion Battery Production and Recycling," in *90th Annual Meeting of the Transportation Research Board*, Washington, D.C, 2011.

[109] B. Price, E. Dietz and J. Richardson, "Life Cycle Costs of Electric and Hybrid Electric Vehicle Batteries and End-of-Life Uses".

[110] J. Smart, J. Francfort, D. Karner, M. Kirkpatrick and S. White, "Advanced Vehicle Testing Activity: Plug-In Hybrid Electric Vehicle Testing and Demonstration Activities," 2009.

[111] C. H. Park, J. H. Yoon and J. D. Choi, "A Quantitative Study for Critical Factors of Automotive Battery Durability," SAE International, 2007.

[112] Idaho National Laboratory, "Battery Test Manual," 2010.

[113] A. A. Pesaran, T. Markel, H. S. Tataria and D. Howell, "Battery Requirements for Plug-In Hybrid Vehicles - Analysis and Rationale".

[114] J. C. Forman, S. J. Moura, J. L. Stein and H. K. Fathy, "Optimal Experimental Design for Modeling Battery Degradation," in *ASME 2012 5th Annual Dynamic Systems and Control Conference*, Fort Lauderdale, FL, 2012.

[115] C.-S. N. Shiau, N. Kaushal, C. T. Hendrickson, S. B. Peterson, J. F. Whitacre and J. J. Michalek, "Optimal Plug-In Hybrid Electric Vehicle Design and Allocation for Minimum Life Cycle Cost, Petroleum Consumption, and Greenhouse Gas Emissions," *Journal of Mechanical Design,* vol. 132, 2010.

[116] L. Kang, X. Zhao and J. Ma, "A new neural network model for the state-of-charge estimation in the battery degradation process," *Applied Energy,* vol. 121, pp. 20-27, 2014.

[117] Tesla Motors, Inc., "Tesla Model S Range," 2014. [Online]. Available: www.teslamotors.com.

[118] L. Knibbs, R. D. Dear and S. Atkinson, "Field study of air change and flow rate in six automobiles," *Indoor Air,* vol. 19, no. 4, pp. 303-313, 2009.

[119] S. Brown, "Diagnosis of the Lifetime Performance Degradation of Lithium-Ion Batteries: ocus on Power-Assist Hybrid Electric Vehicle and Low-Earth-Orbit Satellite Applications," Universitetsservice US-AB, Stockholm, 2008.

[120] K. N. Genikomakis, C. S. Ioakimidis, A. Murillo, A. Trifonova and D. Simic, "A Life Cycle Assessment of a Li-ion urban electric vehicle battery," in *EVS27*, Barcelona, 2013.

[121] M. Zackrisson, L. Avellán and J. Orlenius, "Life cycle assessment of lithium-ion batteries for plug-in hybrid electric vehicles -- Critical issues," *Journal of Cleaner Production,* vol. 18, pp. 1519-1529, 2010.

[122] M. Contestabile, G. Offer, R. North, M. Akhurst and J. Woods, "Electric Vehicles: A Synthesis of the Current Literature with a Focus on Economic and Environmental Viability," LCAworks, 2012.

[123] M. Dubarry, "Test Plan to Assess Electric Vehicle Cell Degradation under Electric Utility Grid Operations," 2015.

[124] R. Graham, "Comparing the Benefits and Impacts of Hybrid Electric Vehicle Options," 2001.

[125] J. D. Graham, "Electromobility: Comparing Public Policies in Europe, the United States, and China".

[126] Y. S. Jung, A. S. Cavanagh, L. A. Riley, S.-H. Kang, A. C. Dillon, M. D. Groner, S. M. George and S.-H. Lee, "Ultrathin Direct Atomic Layer Deposition on Composite Electrodes for Highly Durable and Safe Li-Ion Batteries," *Advanced Materials,* vol. 22, pp. 2172-2176, 2010.

[127] O. Karabasoglu and J. Michalek, "Influence of driving patterns on life cycle cost and emissions of hybrid and plug-in electric vehicle powertrains," *Energy Policy,* 2013.

[128] D. Karner and J. Francfort, "Hybrid and plug-in hybrid electric vehicle performance testing by the US Department of Energy Advanced Vehicle Testing Activity," *Journal of Power Sources,* vol. 174, pp. 69-75, 2007.

[129] T.-H. Kim, J.-S. Park, S. K. Chang, S. Choi, J. H. Ryu and H.-K. Song, "The Current Move of Lithium Ion Batteries Towards the Next Phase," *Advanced Energy Materials,* pp. 1-13, 2012.

[130] M. T. Lawder, P. W. Northrop and V. R. Subramanian, "Model-Based SEI Layer Growth and Capacity Fade Analysis for EV and PHEV Batteries and Drive Cycles," *Journal of The Electrochemical Society,* vol. 161, no. 14, pp. A2099-A2108, 161.

[131] D. Liu, Y. Luo, Y. Peng, X. Peng and M. Pecht, "Lithium-ion Battery Remaining Useful Life Estimation Based on Nonlinear AR Model Combined with Degradation Feature," in *Annual Conference of Prognostics and Health Management Society*, 2012.

[132] S. Renganathan, G. Sikha, S. Santhanagopalan and R. E. White, "Theoretical Analysis of Stresses in a Lithium Ion Cell," *Journal of The Electrochemical Society,* vol. 157, no. 2, pp. A155-A163, 2010.

[133] S. M. Rezvanizaniani, Z. Liu, Y. Chen and J. Lee, "Review and recent advances in battery health monitoring and prognostics technologies for electric vehicle (EV) safety and mobility," *Journal of Power Sources,* vol. 256, pp. 110-124, 2014.

[134] M. Safari, M. Morcrette, A. Teyssot and C. Delacourt, "Life Prediction Methods for Lithium-Ion Batteries Derived from a Fatigue Approach," *Journal of The Electrochemical Society,* vol. 157, no. 7, pp. A892-A898, 2010.

[135] E. Samadani, "Modeling of Lithium-ion Battery Performance and Thermal Behavior in Electrified Vehicles," University of Waterloo, 2015.

[136] H. Sattler, "Prüfanforderungen an Li-Batterien für Elektrofahrzeuge: Übersicht vorhandener Normen sowie zukünftige Standards".

[137] C. Wu, C. Zhu, Y. Ge and Y. Zhao, "A Review on Fault Mechanism and Diagnosis Approach for Li-Ion Batteries," Hindawi Publishing Corporation, 2015.

[138] M. Yilmaz and P. T. Krein, "Review of Battery Charger Topologies, Charging Power Levels, and Infrastructure for Plug-In Electric and Hybrid Vehicles," *IEEE Transactions on Power Electronics,* vol. 28,

no. 5, pp. 2151-2169, 2013.

[139] T. Yuksel and J. Michalek, "Development of a Simulation Model to Analyze the Effect of Thermal Management on Battery Life," SAE International, 2012.

[140] Q. Zhang and R. E. White, "Calendar life study of Li-ion pouch cells," *Journal of Power Sources,* vol. 173, pp. 990-997, 2007.

[141] FEV GmbH, "FEV Dauerlaufprüfzentrum in Brehna / Leipzig," [Online]. Available: http://www.fev-dlp.de/en/fev-dauerlaufpruefzentrum-in-brehnaleipzig.html.

[142] M. Tutuianu, A. Marotta, H. Steven, E. Ericsson, T. Haniu, N. Ichikawa and H. Ishii, "Development of a World-wide Worldwide harmonized Light duty driving Test Cycle (WLTC)," 2013.

[143] N. Omar, M. Daowd, P. v. d. Bossche, O. Hegazy, J. Smekens, T. Coosemans and J. v. Mierlo, "Rechargeable Energy Storage Systems for Plug-in Hybrid Electric Vehicles - Assessment of Electrical Characteristics," *Energies,* vol. 5, pp. 2952-2988, 2012.

Appendix

Characteristics	Units	Target
Peak Pulse Discharge Power (10 sec)	kW	9
Peak Pulse Discharge Power (1 sec)	kW	11
Peak Regen Pulse Power (5 sec)	kW	11
Available Energy for Cycling	Wh	105
Minimum Round-trip Energy Efficiency	%	95
Cold cranking power at -30 °C (three 4.5-s pulses, 10s rests between pulses at min SOC)	kW	6kW for 0.5s followed by 4kW for 4s
Accessory Load (2.5 minute duration)	kW	5
CS 48V HEV Cycle Life	Cycles / MWh	75000 / 21
Calendar Life, 30°C	Year	15
Maximum System Weight	kg	≤ 8
Maximum System Volume	Liter	≤ 8
Maximum Operating Voltage	Vdc	52
Minimum Operating Voltage	Vdc	38
Minimum Voltage during Cold Crank	Vdc	26
Maximum Self-discharge	Wh/day	1
Unassisted Operating Temp Range (Power available to allow 5s charge and 1s discharge pulse) at min. and max. operating SOC and Voltage	°C	-30 to +52
30 °C - 52 °C	kW	11
0 °C	kW	5.5
-10 °C	kW	3.3
-20 °C	kW	1.7
-30 °C	kW	1.1
Survival Temperature Range	°C	-46 to +66
Max System Production Price @ 250k units/yr	$	275

Table 17 USABC Requirements of Energy Storage Systems for 48V HEVs at EOL [12]

End of Life Characteristics at 30°C	Units	System Level	Cell Level
Peak Discharge Power Density, 30 sec pulse	W/L	1000	1500
Peak Specific Discharge Power, 30 sec pulse	W/kg	470	700
Peak Specific Regen Power, 10 sec pulse	W/kg	200	300
Useable Energy Density @ C/3 Discharge Rate	Wh/L	500	750
Useable Specific Energy @ C/3 Discharge Rate	Wh/kg	235	350
Useable Energy @ C/3 Discharge Rate	kWh	45	N/A
Calendar Life	Years	15	15
DST Cycle Life	Cycles	1000	1000
Selling Price @ 100K units	$/kWh	125	100
Operating Environment	°C	-30 to +52	-30 to +52
Normal Recharge Time	Hours	< 7 Hours, J1772	< 7 Hours, J1772
High Rate Charge	Minutes	80% ΔSOC in 15 min	80% ΔSOC in 15 min
Minimum Operating Voltage	Vdc	420	N/A
Minimum Operating Voltage	Vdc	220	N/A
Peak Current, 30 seconds	A	400	400
Unassisted Operating at Low Temperature	%	> 70% Useable Energy @ C/3 Discharge rate at -20°C	> 70% Useable Energy @ C/3 Discharge rate at -20°C
Survival Temperature Range, 24 Hr	°C	-46 to +66	-46 to +66
Maximum Self-discharge	%/month	< 1	< 1

Table 18 USABC Goals for Advanced Batteries for BEVs – CY 2020 Commercialization [10]

Characteristics	Units	PHEV-20 Mile	PHEV-40 Mile	xEV-50 Mile
Commercialization Timeframe		2018	2018	2020
AER	Miles	20	40	50
Peak Pulse Discharge Power (10 sec)	kW	37	38	100
Peak Pulse Discharge Power (2 sec)	kW	45	46	110
Peak Regen Pulse Power (10 sec)	kW	25	25	60
Available Energy for CD Mode	kWh	5.8	11.6	14.5
Available Energy for CS Mode	kWh	0.3	0.3	0.3
Minimum Round-trip Energy Efficiency	%	90	90	90
Cold cranking power at -30 °C (3 2sec pulses)	kW	7	7	7
CD Life / Discharge Throughput	Cycles/MWh	5000/29	5000/58	5000/72.5
Calendar Life, 30°C	Year	15	15	15
Maximum System Weight	kg	70	120	150
Maximum System Volume	Liter	47	80	100
Maximum Operating Voltage	Vdc	420	420	420
Minimum Operating Voltage	Vdc	220	220	220
Maximum Self-discharge	%/month	< 1	< 1	< 1
Unassisted Operating Temp Range	°C	-30 to +52	-30 to +52	-30 to +52
30 °C - 52 °C	%	100	100	100
0 °C	%	50	50	50
-10 °C	%	30	30	30
-20 °C	%	15	15	15
-30 °C	%	10	10	10
Survival Temperature Range	°C	-46 to +66	-46 to +66	-46 to +66
Max System Production Price @ 250k units/yr	$	2200	3400	4250

Table 19 USABC Goals for Advanced Batteries for PHEVs for FY 2018 to 2020 Commercialization [11]